DESIGN OF MULTI-FUNCTIONAL HYDROGEL FOR CELL THERAPIES

BY

CHAENYUNG CHA

DISSERTATION

Submitted in partial fulfillment of the requirements
for the degree of Doctor of Philosophy in Chemistry
in the Graduate College of the
University of Illinois at Urbana-Champaign, 2011

Urbana, Illinois

Doctoral Committee:

Assistant Professor Hyunjoon Kong, Chair
Professor Rashid Bashir
Professor Martha U. Gillette
Professor Deborah E. Leckband

Abstract

Hydrogels are being actively investigated as encapsulation devices for cell transplantation therapies, as they provide structural stability and protection against harsh chemical and mechanical stimuli, and host immune system. In addition, chemical moieties, mechanical stiffness, and minerals presented in hydrogels act as insoluble signals to regulate a variety of cellular function. However, the conventional hydrogel design is plagued by complex dependencies between hydrogel properties; stiffness, permeability, density of cell adhesion molecules, and mineralization capacity. The objective of this research is to decouple or tune the intricate dependencies between these hydrogel properties, in order to better understand and regulate cellular activities in a 3D matrix. The hydrogel system is created by the assembly of three functional modules that contribute to the overall hydrogel properties: (1) The dependency between stiffness and permeability was tuned by incorporating pendant polymeric chains into a poly(ethylene glycol)-based hydrogel system; (2) Incorporation of alginate into a hydrogel system by co-polymerization allowed the control of hydrogel stiffness without affecting permeability; (3) The hydrogel was modified with cell adhesion proteins independent of other hydrogel properties using an amine-reactive polyaspartamide linker enabling single-step protein conjugation. Furthermore, mineralization capacity of the hydrogel was controlled independently by modulating hydrophobicity, charge density, and porosity. The efficacy of the hydrogel system developed in this research was evaluated by encapsulating two different cell types, fibroblasts and mesenchymal stem cells, and exploring the effects of hydrogel properties on the viability and growth factor expression of the encapsulated cells.

Acknowledgements

I wish to extend my deepest gratitude to my research advisor, Dr. Hyunjoon Kong, for his thoughtful guidance throughout my doctoral research. I appreciate many fruitful discussions and helpful advice from the members of the Kong research group. I would also like to thank my doctoral research committee members, Dr. Bashir, Dr. Gillette, and Dr. Leckband, for their support.

I could not have finished this project without the love and support from my family and friends, especially my wife, So Youn, who has been by my side supporting me throughout my graduate studies.

This research was funded by National Science Foundation (DMR-0847253, ECCS-1002165), National Science Foundation Science and Technology Center (EBICS), American Heart Association (0830468Z), US Army (W81XWH-08-1-0701), Korea Ministry of Knowledge Economy (KETEP Grant, 20104010100610), Amore Pacific Co. Korea (Gift Grant), and Harry G. Drickamer Graduate Fellowship (Department of Chemistry, University of Illinois at Urbana-Champaign).

Table of Contents

Chapter 1 Introduction

1.1 Background and Motivation

Delivery of therapeutic cells has garnered much attention in recent years as the next-generation treatment to cure various diseases, as it offers the possibility of significantly enhanced tissue regeneration.[1-3] For example, stem cells derived from a patient's own tissue, mostly from adipose tissue or bone marrow, have the potential to differentiate into a wide array of cell types that can incorporate into the host tissue and undergo regeneration, while bypassing the immunogenicity and ethical issues associated with using embryonic stem cells. The stem cells are also known to express various growth factors can also promote wound healing and regeneration via paracrine effect.[4,5] Fibroblasts have also been frequently utilized in several therapeutic applications, since they are intricately involved in inflammation and wound healing via expression of extracellular matrix (ECM) components and growth factors.

However, there are several challenges that cell therapies should overcome for their successful uses in clinical treatments. These challenges often result in limited therapeutic efficacy in vivo, whereas the cells evaluated in vitro display more powerful therapeutic potentials. For example, cells that are currently being tested in preclinical and clinical therapies are mostly administered via intramuscular or intravascular injection. Then, only a small fraction of the delivered cells are active for desired treatments at the transplanatation site, because cells are readily scattered by external tissue pressure. In addition, there is a lack of tools to regulate cellular phenotypic activities in a desired manner.

Therefore, biomaterial scaffolds are being actively investigated for their use as cell

encapsulation devices. Among those, hydrogel has been the most popular choice of biomaterial, as the polymeric network imbibing a large amount of water mimics the natural ECM and provides stability against external mechanical and chemical stimuli, as well as protection against host immune response.[6] The hydrogels are usually presented with moieties, such as cell adhesion proteins, peptides and growth factors, to provide insoluble signals to regulate diverse cell phenotypes.[7,8] For example, RGD peptides spatially organized at varied length scales for binding with specific cellular integrins, can tune the proliferation rates and differentiation levels of encapsulated cells. Thus, it would be important to develop a chemical linker, so the cell recognition moieties of choice can be efficiently conjugated to the hydrogel system.

The mechanical stiffness of the hydrogel acts as another important signal to regulate cellular activities, and ultimately affect therapeutic efficacy in clinical treatments.[9-12] Cells sense their mechanical environment, either the inherent matrix stiffness or external mechanical force, through the formation of focal adhesion, a complex mechanosensory machinery consisting of specific ECM domains, cellular integrins, and intracellular components. For example, tissue stiffness under normal physiological conditions range from softer neural tissue (<1 kPa), muscle tissue (≈ 10 kPa) to stiffer cartilage (≈ 30 kPa).[8] Matrix stiffness also has been shown to influence the differentiation fate of stem cells. These roles of hydrogel matrices in cell phenotypes have been largely studied using cells adherent to two dimensional (2D) hydrogel surfaces, even though cells in vivo are surrounded by three dimensional (3D) ECM.

Therefore, it is desirable to create hydrogel system with varying stiffness to provide suitable mechanical environment for different cell types. The hydrogel stiffness is usually controlled by varying the cross-linking density of the polymeric network. But this inversely affects the

hydrogel permeability that influences transport of oxygen, nutrients and other metabolites, which is a critical factor for cells in 3D environment. So it becomes necessary to create a hydrogel system which allows variation of stiffness, while minimizing the change in permeability which is also crucial for cellular functions.

In certain cases, hydrogel should be able to accommodate non-matrix factors in order to create a more suitable microenvironment. For example, bone tissue is extensively mineralized, mostly with carbonated hydroxyapatite, on the surface of ECM made up of type I collagen, osteopontin, osteocalcin, and bone sialoprotein.[13] It has been shown that osteoblast functions and osteogenic differentiation of stem cells improve significantly in the presence of biominerals.[14] So it would be beneficial to create a mineralized hydrogel for applications in bone tissue regeneration. There have been previous studies focused on inducing mineralization on hydrogel, by modulating charge density or hydrophobicity to promote mineral deposition.[15,16] However, these studies have been done mostly on 2D surface, and the mineralization in 3D has been proven difficult, because hydrophilic microenvironment within the hydrogel does not permit supersaturation of mineral ions, which is a critical step in mineral deposition.

Therefore, it is desirable to create a hydrogel system that allows one to control cell adhesion molecules density, stiffness, permeability and mineralization in an independent manner for better understanding and control of cellular phenotypic activities in a 3D matrix, as conventional hydrogel design strategies are often plagued by intricate dependencies between these hydrogel properties and lead to complicating accurate analyses.

1.2 Research Overview

In this research, multi-functional hydrogel was developed by assembling three modules designed to perform different functions (Figure 1.1). First, Chapter 2 describes a strategy of presenting hydrophilic pendant polymer chains in hydrogels to control the hydrogel stiffness, while limiting the change in permeability. Second, Chapter 3 describes methacrylic alginate which could be incorporated into a hydrogel system to control hydrogel stiffness, while facilitating water uptake, and ultimately improve permeability. Third, Chapter 4 describes the synthesis of amine-reactive polyaspartamide-based linker which allows efficient conjugation of a variety of cell responsive proteins to the hydrogel. Fourth, Chapter 5 describes the fabrication of hydrogel system by the assembly of three different modules described in Chapters 2, 3 and 4. The effects of hydrogel properties on the phenotypes of encapsulated cells are explored. Fifth, Chapter 6 describes a strategy of varying the physical properties of hydrogels: hydrophobicity, charge density and porosity. Then the mineralization was induced within the hydrogels to determine the hydrogel design criteria for 3D biomineralization for its applications in bone tissue engineering. Finally, conclusion and future studies are presented in Chapter 7.

1.3 Figures

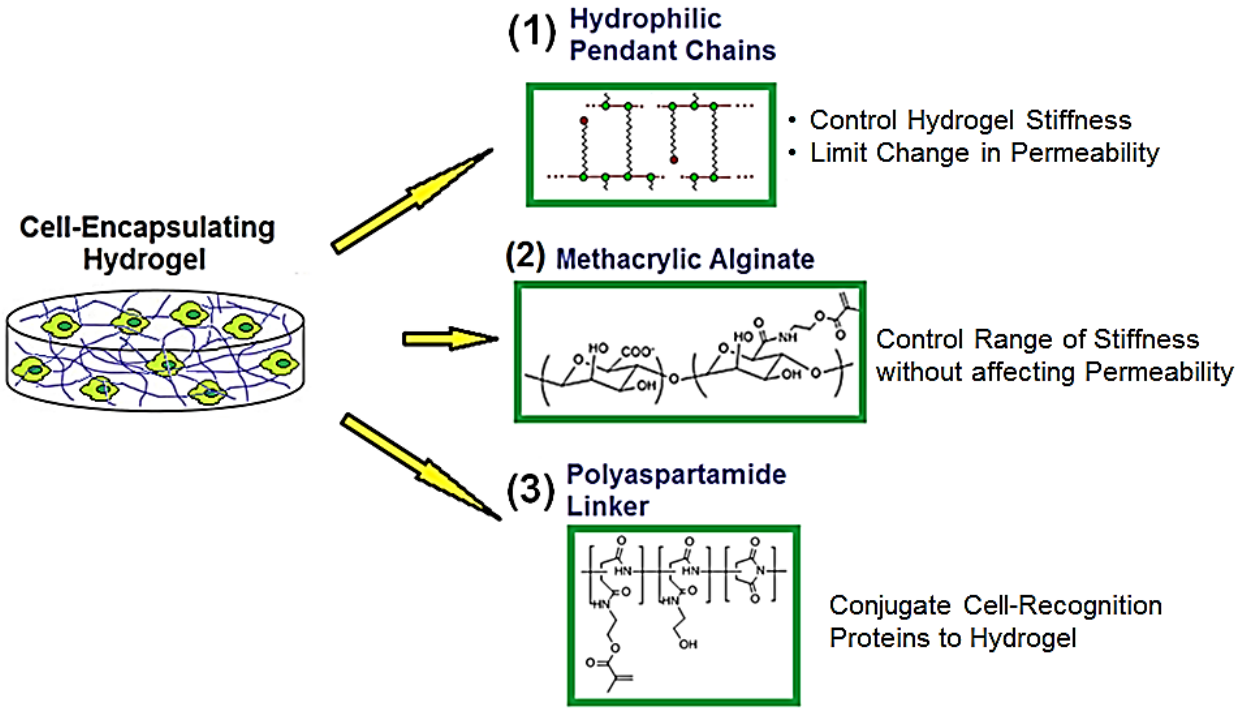

Figure 1.1 Schematic representation of the hydrogel system assembled with various functional modules: (1) Varying the number of hydrophilic pendant chains allows control of stiffness while limiting the change in permeability. (2) Incorporation of photo-polymerizable alginate (methacrylic alginate) promotes biomolecular diffusion, and allows control of mechanical properties with the concentration and the degree of methacrylic substitution. (3) Polyaspartamide-based linker allows conjugation of conjugation of cell adhesion molecules to the hydrogel.

Chapter 2 Tuning the Dependency between Stiffness and Permeability of Hydrogels with Hydrophilic Pendant Chains

2.1 Introduction

Hydrogels have been increasingly studied as in vitro cell culture platforms and cell transplantation devices because they are structurally similar to natural extracellular matrices (ECM) and provide insoluble signals to regulate diverse cell phenotypes.[17-20] For example, modifying hydrogels to present functional groups, oligopeptides, or proteins, spatially organized at varied length scales for binding with specific cellular integrins, can tune the proliferation rates and differentiation levels of embedded cells.[21-24] The mechanical stiffness of the gel matrix acts as another signal to regulate cellular activities and ultimately therapeutic efficacy in clinical treatments.[10,12,25] These roles of hydrogel matrices in cell phenotypes have been largely studied using cells adherent to two dimensional (2D) hydrogel surfaces, even though cells in vivo are surrounded by three dimensional (3D) ECM.

Therefore, extensive efforts are now being made to understand the role of 3D cellular microenvironments on cellular activities, usually by encapsulating cells in hydrogel matrices with varying chemical and mechanical properties.[12,19,22,25-29] However, these approaches are largely plagued by intricate dependencies between matrix properties. For example, most efforts to increase the mechanical stiffness of a hydrogel are accompanied by a decrease in the

permeability of the hydrogel.[29] Hydrogel stiffness is known to act as a signal to regulate a series of cellular activities including apoptosis, proliferation and differentiation by tuning cell adhesion and traction force. Matrix permeability also plays a critical role in maintaining viability and homeostasis of cells residing in a 3D matrix, because it controls transport properties of oxygen, nutrients and metabolites, as well as space within cellular microenvironment. Therefore, the dependency between stiffness and permeability of a hydrogel makes it difficult to examine individual and combined effects of matrix stiffness and permeability on cells cultured in a 3D matrix.[25,30-32]

This study presents an advanced strategy to independently modify the stiffness and permeability of cell-encapsulating hydrogels. We hypothesize that the incorporation of pendant hydrophilic polymers in cross-linked networks will allow us to control the stiffness via concentration of pendant polymers while limiting changes in permeability. This hydrogel system would enable us to address the individual and combined effects of matrix stiffness and permeability on viability, proliferation and gene expression levels of cells within a 3D matrix. This hypothesis was examined by cross-linking poly(ethylene glycol) diacrylate (PEGDA) and poly(ethylene glycol) monoacrylate (PEGMA) to form hydrogels, with PEGMA acting as a pendant polymer chain. The mass fraction, molecular weight, and end group of PEGMA were controlled to tune the inverse dependency between permeability and stiffness of the hydrogels and also to address the underlying mechanism. Hydrogels made only by cross-linking PEGDA of varying molecular weights (M_W), which exhibit a larger range of permeability with the same range of stiffness, were used as a control.[33,34] Mechanical stiffness of the hydrogels was evaluated by measuring the elastic modulus, and permeability of the hydrogels was evaluated by

measuring the swelling ratio and diffusion coefficient of biomacromolecules within each hydrogel. Finally, both PEGDA-PEGMA hydrogels and pure PEGDA hydrogels were used to uncover the effects of matrix stiffness and permeability on the viability, proliferation and endogenous vascular endothelial growth factor (VEGF) expression levels of encapsulated cells.

2.2 Results

2.2.1 Mechanical properties of poly(ethylene glycol) (PEG) hydrogels with varying numbers of pendant PEG chains

Hydrogels with varying numbers of cross-links and pendant PEG chains were prepared by chemically cross-linking a mixture of PEG diacrylate (PEGDA) and PEG monoacrylate (PEGMA) (Figure 2.1a). The mass percentage of PEGMA (Φ_{PEGMA}) in the PEGDA-PEGMA hydrogel was varied while keeping the total concentration constant at 20 wt %. Separately, pure PEGDA hydrogels with varying numbers of cross-links were prepared by cross-linking PEGDA with different molecular weights ($M_{W,PEGDA}$) while keeping the PEGDA concentration constant at 20 wt % (Figure 2.1b). Increasing both Φ_{PEGMA} of PEGDA-PEGMA hydrogels and $M_{W,PEGDA}$ of pure PEGDA hydrogels led to the exponential decrease of the elastic modulus from 41 to 3 kPa (Figure 2.2a-b). The ranges of the elastic moduli attained with the PEGDA-PEGMA hydrogels and pure PEGDA hydrogels were equivalent.

In contrast, Φ_{PEGMA} of PEGDA-PEGMA hydrogels and $M_{W,PEGDA}$ of PEGDA hydrogels influenced the swelling ratio of PEG hydrogels differently. Increasing Φ_{PEGMA} of the PEGDA-PEGMA hydrogels from 0 to 50 led to a 1.8-fold increase in the swelling ratio. However, increasing $M_{W,PEGDA}$ of pure PEGDA hydrogels from 3400 to 14000 g mol^{-1} resulted in a 2.8-fold increase in the swelling ratio (Figure 2.2a-b). These changes in the swelling ratio related to the elastic modulus were fitted to a power law, described by $(Q/Q_0) \propto (E/E_0)^{-m}$ (Figure 2.2c). The inverse dependency between the swelling ratio and the elastic modulus, represented by m, was smaller with the PEGDA-PEGMA hydrogel than with the pure PEGDA hydrogel (Figure 2.2d).

2.2.2 Measuring hydrogel permeability using fluorescence recovery after photobleaching (FRAP) assay

The swelling ratio quantified above represents the amount of fluid taken up by hydrogels at equilibrium. This property does not necessarily represent the rate of biomolecular transport through the hydrogels, which is also an important parameter for hydrogel permeability. Therefore, this study also quantified the diffusion coefficients of fluorescently labeled dextran ($D_{dextran}$) within the hydrogels with varying elastic modulus using FRAP. The FRAP technique is commonly used to quantify the diffusion coefficients of molecules within a 3D matrix by measuring the flux of fluorescently labeled molecules into a photobleached spot during a given time (Figure 2.3). As this assay utilizes a highly sensitive laser microscopy-based detection system to record a molecular diffusion in real time, it allows more accurate measurements of diffusion coefficient values, on the order of 10^{-10}~ 10^{-9} cm^2 s^{-1}, than conventional methods to evaluate the diffusivity with amount of analytes released from the hydrogel.

Increasing the Φ_{PEGMA} of PEGDA-PEGMA hydrogels from 0 to 40 % made only a minimal change in $D_{dextran}$. There was a 1.15-fold increase of $D_{dextran}$ when Φ_{PEGMA} increased from 40 to 50 % (Figure 2.4a). In contrast, increasing $M_{W,PEGDA}$ of pure PEGDA hydrogels resulted in a linear increase in $D_{dextran}$, leading to a 1.3-fold increase of $D_{dextran}$ (Figure 2.4b). These changes in $D_{dextran}$ with the elastic modulus of the hydrogel were fitted to a power law, described by $(D_{dextran}/D_{dextran,0}) \propto (E/E_0)^{-n}$ (Figure 2.4c). The inverse dependency between $D_{dextran}$ and E, represented by n, was smaller with the PEGDA-PEGMA hydrogel than with the pure PEGDA hydrogel (Figure 2.4d).

2.2.3 Effects of length and hydrophobicity of pendant PEG chains on hydrogel properties

The role of pendant PEG chains on the stiffness and permeability of PEGDA-PEGMA hydrogels was further explored by modulating the length and hydrophobicity of the pendant chains. First, the length of pendant PEG chains was modulated by varying the M_W of PEGMA from 750 to 5000 g mol^{-1}. The elastic moduli of the PEGDA-PEGMA hydrogels decreased with the mass percentage of PEGMA (Φ_{PEGMA}) regardless of M_W of PEGMA (Figure 2.5a). The inverse dependency of the elastic modulus (E) on Φ_{PEGMA} was fitted to the exponential decay model using the following equation, [35]

$$E = E_0 \exp(-k_E \Phi_{PEGMA}) \quad (1)$$

where E_0 is the elastic modulus when Φ_{PEGMA} is 0, and k_E is the decrease rate of the elastic modulus with respect to Φ_{PEGMA} (in units of Φ_{PEGMA}^{-1}). The k_E values increased with increasing M_W of pendant PEG chains (Figure 2.5b). In contrast, the swelling ratio of the hydrogels was only minimally influenced by the M_W of pendant PEG chains at any given Φ_{PEGMA} (Figure 2.5c). This result demonstrates that the chain length of the pendant PEG chain is another factor that can be used to broaden the controllable range of elastic moduli while limiting change in the swelling ratio.

Separately, the end groups of pendant PEG chains were modified with hydrophobic phenyl groups (PEG-Ph), in order to examine the role of the hydrophobicity of pendant chains on the dependency between the permeability and stiffness of the hydrogel (Figure 2.6). Interestingly, increasing the fraction of pendant PEG chains substituted with phenyl groups ($\phi_{PEG\text{-}Ph}$) while keeping the total number of pendant PEG chains constant (Φ_{PEGMA} at 50 %) resulted in an almost

ten-fold increase in the elastic modulus and a decrease in the swelling ratio of the hydrogel by a factor of two (Figure 2.7a).

The effect of hydrophobic end groups of pendant PEG chains on the stiffness and swelling ratio of hydrogels was studied using pyrene incorporated into PEGDA-PEGMA hydrogels. Pyrene monomers associate with hydrophobic domains in the surrounding environment and generate a fluorescent emission spectrum which includes five characteristic emission peaks (from I_1 to I_5, Figure 2.7b).[36-38] Specifically, the ratio of emission intensity at the wavelength of 385 nm (I_3) to that at 373 nm (I_1), denoted as I_3/I_1, correlates with the hydrophobicity of the surrounding environment. The I_3/I_1 values increased linearly with $\phi_{PEG\text{-}Ph}$ in PEGDA-PEGMA hydrogels (Figure 2.7c). The I_3/I_1 values were also linearly correlated with changes in the elastic modulus and swelling ratio (Figure 2.7d).

2.2.4 Effects of hydrogel properties on cell viability and proliferation

NIH3T3 fibroblasts were encapsulated in PEGDA-PEGMA hydrogels with varying Φ_{PEGMA}, and in PEGDA hydrogels with varying $M_{W,PEGDA}$ to study the effects of hydrogel stiffness on cell viability. Type I collagen was chemically linked to the hydrogels to promote cell adhesion to the gel matrices. The incorporation of collagen made only minimal changes in the elastic moduli and swelling ratios of the hydrogels.

The viability of cells encapsulated in the hydrogel was determined by staining the cells with MTT. After 24 hours, the PEGDA-PEGMA hydrogel displayed a biphasic dependency of cell viability on the elastic modulus. The cell viability became maximal at an elastic modulus of 26 kPa (Φ_{PEGMA} = 12.5) (Figure 2.8a-b). Above 10 kPa, the viability profile of pure PEGDA

hydrogels was similar to that of PEGDA-PEGMA hydrogels, with the maximal viability value at 20 kPa ($M_{W,PEGDA}$ = 6000 g mol^{-1}). However, below 10 kPa, cell viability increased significantly with decreasing elastic modulus (Figure 2.8b).

The quantified cell viability was then related to the change in swelling ratio to evaluate the role of hydrogel permeability on cell viability (Figure 2.8c). Smaller increase in swelling ratio of PEGDA-PEGMA hydrogels, as compared with pure PEGDA hydrogels, did not promote the viability of cells. In contrast, the viability of cells encapsulated in pure PEGDA hydrogels with varying $M_{W,PEGDA}$ increased significantly as the normalized swelling ratio increased from 1.5 to 2.8.

Cell viability was also examined separately in hydrogels free of collagen. Unlike in the hydrogels chemically linked with collagen, cell viability in the PEGDA-PEGMA hydrogel decreased with increasing elastic modulus (Figure 2.9a). Cell viability increased linearly with the swelling ratio for both PEGDA-PEGMA hydrogels and pure PEGDA hydrogels (Figure 2.9b).

Next, the cell proliferation rate was quantified by measuring an increase in the number of viable cells over seven days using MTT. The dependency of cell viability on time was fitted to the following equation,

$$N_t = N_0\, 2^{k_P \cdot t} \tag{2}$$

where N_0 is the initial cell viability, N_t is the cell viability at a given time, t, and k_P is the cell proliferation rate.[39] Both PEGDA-PEGMA hydrogels with varying Φ_{PEGMA} and pure PEGDA with varying $M_{W,PEGDA}$ displayed the decrease of k_P with increasing elastic modulus from 2 to 10 kPa (Figure 2.10a). However, the k_p became almost independent of the elastic modulus, as the

modulus became larger than 10 kPa. In contrast, the k_P was linearly related to the swelling ratio, for both two gels (Figure 2.10b). Specifically, cells cultured in hydrogels with swelling ratios larger than 1.5 formed clusters, because the matrix supported cell proliferation while limiting migration of daughter cells (Figure 2.10c). All cells in the cluster remained spherical within a 3D matrix.

2.2.5 Effects of hydrogel properties on vascular endothelial growth factor (VEGF) expression

Cellular expression of vascular endothelial growth factor (VEGF) within the hydrogel linked with collagen was examined by measuring the concentration of VEGF in the cell culture media. Fibroblasts are able to produce multiple angiogenic factors endogenously in response to soluble signals and subsequently promote neovascularization in vivo,[40,41] and those activities are known to be mediated by matrix stiffness.[11,42] In this study, the cells were stimulated to up-regulate VEGF by exposure to 12-O-tetradecanoylphorbol-13-acetate (TPA) for 24 hours, because TPA stimulates cellular expression of VEGF by activating protein kinase C (PKC) signaling.[43,44] The fibroblasts not exposed to TPA made minimal expression of VEGF.

In PEGDA-PEGMA hydrogels with varying Φ_{PEGMA}, the VEGF expression level displayed a biphasic curve, similar to the viability profile in Fig. 5. The VEGF expression level was maximal at the elastic modulus of 13 kPa (Φ_{PEGMA} = 25 %) (Figure 2.11). The VEGF expression level of cells encapsulated in pure PEGDA hydrogels with varying $M_{W,PEGDA}$ was also maximal when elastic modulus was 10 kPa ($M_{W,PEGDA}$ = 8000 g mol^{-1}). However, the biphasic dependency was much smaller than that of PEGDA-PEGMA hydrogels.

2.3 Discussion

Taken together, the results of these studies demonstrated a novel strategy to decouple the control of stiffness on permeability of a cell-encapsulating hydrogel, and also how matrix stiffness and permeability influence cellular viability, proliferation and endogenous angiogenic factor expression. Decreasing elastic modulus of the PEGDA-PEGMA hydrogels with increasing Φ_{PEGMA} clearly indicates that the replacement of PEGDA with PEGMA decreases the number of elastically responsive cross-links. However, the limited increases in the swelling ratios and biomolecular diffusion coefficients in PEGDA-PEGMA hydrogels as compared with pure PEGDA hydrogels suggest that PEGMA chains act as pendant chains that influence pore diameter and subsequent molecular transport.

This interpretation on the role of PEGMA is also supported by the smaller inverse dependency between swelling ratio and elastic modulus of the PEGDA-PEGMA hydrogel, fitted by a power law, as compared with the pure PEGDA hydrogel. According to the Flory-Rehner equation, the exponent of power law equation should be equal to 0.6 for an ideal elastic model solely consisting of interconnected network.[35] Therefore, the larger deviation of the power law constant from 0.6 for the PEGDA-PEGMA hydrogel implicates that pendant PEGMA chains influence solely swelling ratio of the hydrogel.

Modifying the length and hydrophobic end groups of pendant PEG chains further influenced the dependency between permeability and stiffness of the PEGDA-PEGMA hydrogels. The more rapid decrease in the elastic moduli of the hydrogels observed with longer PEGMA implies that larger pendant chains disturb chemical cross-linking reactions between PEGDA chains and decrease the number of effective cross-links. More significant changes of stiffness and

permeability resulted when hydrophobic pendant chains were incorporated into the hydrogel. The presence of hydrophobic pendant chains likely resulted in a physical cross-linking network, as evidenced by characteristic pyrene fluorescent emission. The physical network likely contributed to the elastic response of the hydrogel and also limited mass transport through the hydrogel pores. These results suggest that hydrophobic PEGMA chains do not act as pendant chains, but rather as a new source of cross-links to increase the elastic response of the hydrogel.[45,46] Therefore, we found that it is important to use hydrophilic pendant PEG chains to decrease the elastic modulus while limiting changes in the swelling ratio and diffusion of biomacromolecules.

A previously published study also reported a strategy to control the inverse dependency between permeability and stiffness of PEG hydrogel, by introducing hydrophobic moieties [47]. Another study also introduced the use of hydrophobic nanoparticles into PEG hydrogels in order to modulate the permeability.[48] However, the hydrophobic moieties within the matrix have been shown to mediate cellular response via non-specific interactions, thus clouding the effects of other matrix variables.[21] Therefore, the use of hydrophilic pendant polymer chains to decrease the inverse dependency between permeability and stiffness of the hydrogel may assist in exploring the effects of matrix stiffness on cell functions more precisely.

This reduced inverse dependency of the hydrogel permeability on stiffness enabled us to amplify the effects of mechanical signal on the cellular activities in a 3D matrix, specifically the one chemically linked with cell adhesion proteins. The viability and growth factor expression of fibroblasts encapsulated in PEGDA-PEGMA hydrogels showed biphasic dependence on the matrix stiffness. This result therefore identifies an elastic modulus which optimally activates

intracellular signaling pathways involved in the growth factor expression, while likely limiting the activation of signaling pathways involved in cell apoptosis.[49,50]

The important role of stiffness on the cellular functions in PEGDA-PEGMA hydrogels was confirmed by comparing the results with those obtained from pure PEGDA hydrogels. As compared with PEGDA-PEGMA hydrogels, the larger increase in permeability of pure PEGDA hydrogels outweighed the effect of stiffness, as demonstrated by the significant increase in viability with decreasing elastic modulus and the insignificant biphasic dependence of VEGF expression level on elastic modulus. This control condition therefore signifies the importance of decoupled control of stiffness and permeability of cell encapsulating hydrogel.

This study also demonstrated that cell proliferation in a 3D hydrogel was more dependent on the permeability than stiffness of the hydrogel, as the cell proliferation rate was proportional to the swelling ratio for both two hydrogel systems. This result is in accordance with previous studies which reported that increased permeability induced by matrix degradation enhanced cell proliferation.[29,51] Thus, we propose that increase of gel permeability should facilitate diffusion of soluble factors and increase available space within gel matrix, and subsequently promote the cell division.

The range of elastic modulus proper to support cellular activities in this study is similar to that of soft connective tissue where the fibroblasts are found,[8] which suggests that the matrix used for 3D cell culture should present a similar mechanical environment to the specific tissue where the cells reside. In addition, the inverse dependency of cell viability on the elastic modulus in the collagen-free PEGDA-PEGMA hydrogels indicates that the specific bonds between integrins and cell adhesion proteins of the matrix act as transducers of mechanical

signals from the matrix to the cells. This result also shows that, without these mechanical signals, the permeability of a hydrogel becomes the dominant influence on cell viability.

The dependency of cell viability on permeability of the pure PEGDA hydrogel may also be related to significant changes in the diffusion coefficients of bioactive macromolecules within the hydrogel. As confirmed with FRAP assay, changes in diffusion coefficients were well correlated with changes in swelling ratios. In future studies, it will be necessary to further examine which factor, swelling ratio or biomolecular diffusivity, has a more significant influence on cell viability.

2.4 Materials and Methods

2.4.1 Synthesis of acrylated poly(ethylene glycol)

Poly(ethylene glycol) (PEG, Sigma Aldrich) or methyl ether poly(ethylene glycol) (mPEG, Sigma Aldrich) of various molecular weights (3400, 6000, 8000, 10000, and 14000 g mol^{-1} for PEG, 750, 2000, and 5000 g mol^{-1} for mPEG) was dissolved in dichloromethane at a concentration of 20 wt %, along with triethylamine (TEA, Fisher Chemical). The mixture was placed under dry N_2 gas for 30 minutes to completely dry the mixture. Acryloyl chloride (Sigma Aldrich) was added dropwise into the mixture and stirred for 24 hours under dry N_2 gas. The molar ratio of PEG, acryloyl chloride, and TEA was kept constant at 1:4:4, and the molar ratio of mPEG, acryloyl chloride, and TEA was 1:2.5:2.5 (mPEG has only one hydroxyl group). After the reaction, the insoluble salt (TEA-HCl) was removed by filtering, and the filtrate was concentrated by rotary evaporator. Next, ice-cold ether was used to precipitate the product. The product collected by filtration was washed with dry diethyl ether several times, and then dried under vacuum. Diacrylated PEG and monoacrylated PEG are referred to as PEGDA and PEGMA, respectively.

2.4.2 Hydrogel preparation

Pre-gel solutions were prepared by mixing 20 wt % PEGDA (M_W 3400 g mol^{-1}) and 20 wt % PEGMA (M_W 750, 2000 or 5000 g mol^{-1}) at varied ratios, together with 0.01 wt% Irgacure 2959 (Ciba) as a photoinitiator. The total polymer concentration was kept constant at 20 wt %. Each pre-gel solution was placed between two glass plates with a 1 mm thick spacer, and then irradiated with UV for 10 minutes to form a hydrogel. Subsequently, hydrogel disks with

diameters of 5 and 10 mm were punched out and incubated in phosphate buffered saline (PBS, pH 7.4) at 37 ℃ for 24 hours before characterization. For control experiments, hydrogels were prepared by cross-linking PEGDA with varying M_W (3400, 6000, 8000, 10000, and 14000 g mol^{-1}) while keeping the concentration constant at 20 wt %.

2.4.3 Characterization of stiffness and swelling ratios of hydrogels

Hydrogel stiffness was evaluated by measuring the elastic modulus. Following the incubation of hydrogel disks in PBS for 24 hours at 37 ℃, the disks were uniaxially compressed at a rate of 1 mm min^{-1} using a mechanical testing system (Insight, MTS Systems).[52,53] The elastic modulus was calculated from the slope of a stress (σ) vs. strain (λ) curve at the first 10 % strain. The hydrogel swelling ratio was calculated as the weight ratio of a swollen hydrogel incubated in PBS for 24 hours at 37 ℃ to a dried gel.

2.4.4 Characterization of hydrogel permeability using fluorescence recovery after photobleaching (FRAP) assay

Diffusion coefficients of dextran molecules within the gel matrices were measured using the FRAP assay to evaluate hydrogel permeability.[54-56] The hydrogel disks were fabricated as mentioned above, except the thickness of the hydrogel was reduced to 0.3 mm in order to allow effective photobleaching. In addition, 2 mg ml^{-1} of fluorescein isothiocyanate conjugated dextran (FITC-dextran, M_W ~ 40000 g mol^{-1}, Sigma Aldrich), which was used as a fluorescent probe, was incorporated in the pre-gel solution. The FRAP assay was performed using a multi-photon confocal microscope equipped with a FRAP module (LSM 710 NLO, Zeiss) and

controlled with control/analysis software (Zen 2009, Zeiss). The 488 nm laser was used for both imaging and photobleaching. The fluorescent surface of the hydrogel was first visualized and fine-focused to give the best quality image. A circular spot (radius of 85 μm) for photobleaching was randomly designated, and photobleaching time was adjusted so that the resulting fluorescence was approximately 40 % of the original fluorescence. After the photobleaching, the fluorescence image and intensity were recorded every 2 seconds for 3 minutes.

The fluorescence intensity (F) over time (t) was plotted, and the curve was fitted using the following equation,[62,63]

$$F = A_1 + A_2 \exp\left(-\frac{2T}{t}\right) \tag{3}$$

where A_1 represents the initial fluorescence intensity, A_2 represent a modified Bessel function,[54] and T represents the recovery time constant. The diffusion coefficient (D) was then calculated using the following equation,

$$D = \frac{R^2}{4T} \tag{4}$$

where R represents the radius of the photobleached spot (85 μm for all experiments).

2.4.5 Characterization of hydrophobic domains in hydrogels with pyrene

Hydrophobic interactions within the hydrogels containing phenyl-capped pendant PEG chains were assessed by the emission of pyrene (Sigma Aldrich) encapsulated in the hydrogels.[36-38] 1 μL of stock solution of pyrene (100 μg mL^{-1} in cyclohexane) was added to 1 mL of pre-gel

solution containing 10 wt % PEGDA and 10 wt % of the mixture of PEGMA and phenyl-capped PEGMA. The fraction of PEGMA that is phenyl-capped was varied from 0 to 1. The pre-gel solution was sonicated for 1 minute to completely dissolve the pyrene, then photo-crosslinked to form the hydrogels, as described above. Next, the hydrogel was incubated in deionized (DI) water for 1 day, while changing the DI water twice to remove the pyrene molecules not associated with hydrophobic domains. The hydrogel was excited at a wavelength of 330 nm, and the resulting emission spectrum of pyrene in each hydrogel was acquired using a spectrofluorometer (FluoroMax® -4, HORIBA Jobin Yvon).

2.4.6 Analysis of viability and proliferation of cells encapsulated in hydrogels

NIH3T3 fibroblasts (purchased from American Type Culture Collection (ATCC)) were suspended in the pre-gel solution at a density of 1×10^6 cells mL^{-1}. To promote cell adhesion to the hydrogel, 1.2 mg mL^{-1} of type I collagen conjugated with PEGMA was added to the pre-gel solution (see Supporting Information for the detailed PEGMA conjugation procedure). The cell-encapsulated hydrogel disks with 5 mm diameter were fabricated as described in Section 3.4.2, except that mixture of cells and pre-gel solution were exposed to UV light. The hydrogel disks were incubated in growth medium (Dulbecco's Modified Eagle Medium supplemented with 10 % fetal bovine serum and 1 % penicillin/streptomycin, all purchased from Gibco) at 37 ℃ under 5% CO_2.

Cell-encapsulating hydrogels were exposed to MTT (3-(4,5-dimethylthiazol-2-yl)-2,5-diphenyltetrazolium bromide) at various time points to assess the number of viable cells.[53] MTT is taken up and enzymatically reduced by viable cells to become MTT formazan which has

a maximum absorbance at 570 nm. Briefly, each hydrogel disk was placed in one well of a 96-well plate with 0.1 mL of growth medium. 10 μL of MTT Reagent (ATCC) was added to each well and incubated for 4 hours at 37 ℃. Then, 0.1 mL of stop solution (20 % sodium dodecyl sulfate in water/dimethylformamide (50:50)) was added to the well and incubated overnight to let the product diffuse out of the hydrogel and completely dissolve. The absorbance of the surrounding medium at 570 nm, which represents the number of viable cells positively stained with MTT, was measured using a spectrophotometer (Synergy HT, BioTek). The absorbance was normalized by that of a pure medium, due to color variations of growth medium over time. The normalized absorbance was divided by that measured right after cell encapsulation, in order to quantify the cell viability as percentage of cells that remained viable. The normalized absorbance was measured daily for 7 days to quantify the cell proliferation rate with an increase of the absorbance over time. In addition, the extent of cell spreading and the cell division were observed using an inverted microscope (Leica DMIL).

2.4.7 Analysis of vascular endothelial growth factor (VEGF) expression of cells encapsulated in hydrogels

Hydrogels encapsulated with NIH3T3 fibroblasts were incubated in DMEM supplemented with 100 nM 12-O-tetradecanoylphorbol-13-acetate (TPA, Sigma Aldrich) for 24 hours.[43,44] Subsequently, the cell culture medium was collected and the amount of VEGF released from the cell-encapsulating hydrogel was quantified with an enzyme-linked immunosorbent assay (Quantikine Mouse VEGF ELISA, R&D systems). The medium incubated with cell-free hydrogel disks was assayed as a negative control. The amount of VEGF released from each

hydrogel disk was normalized with the number of viable cells measured at the same time point to represent VEGF expression level by each viable cell.

2.5 Figures

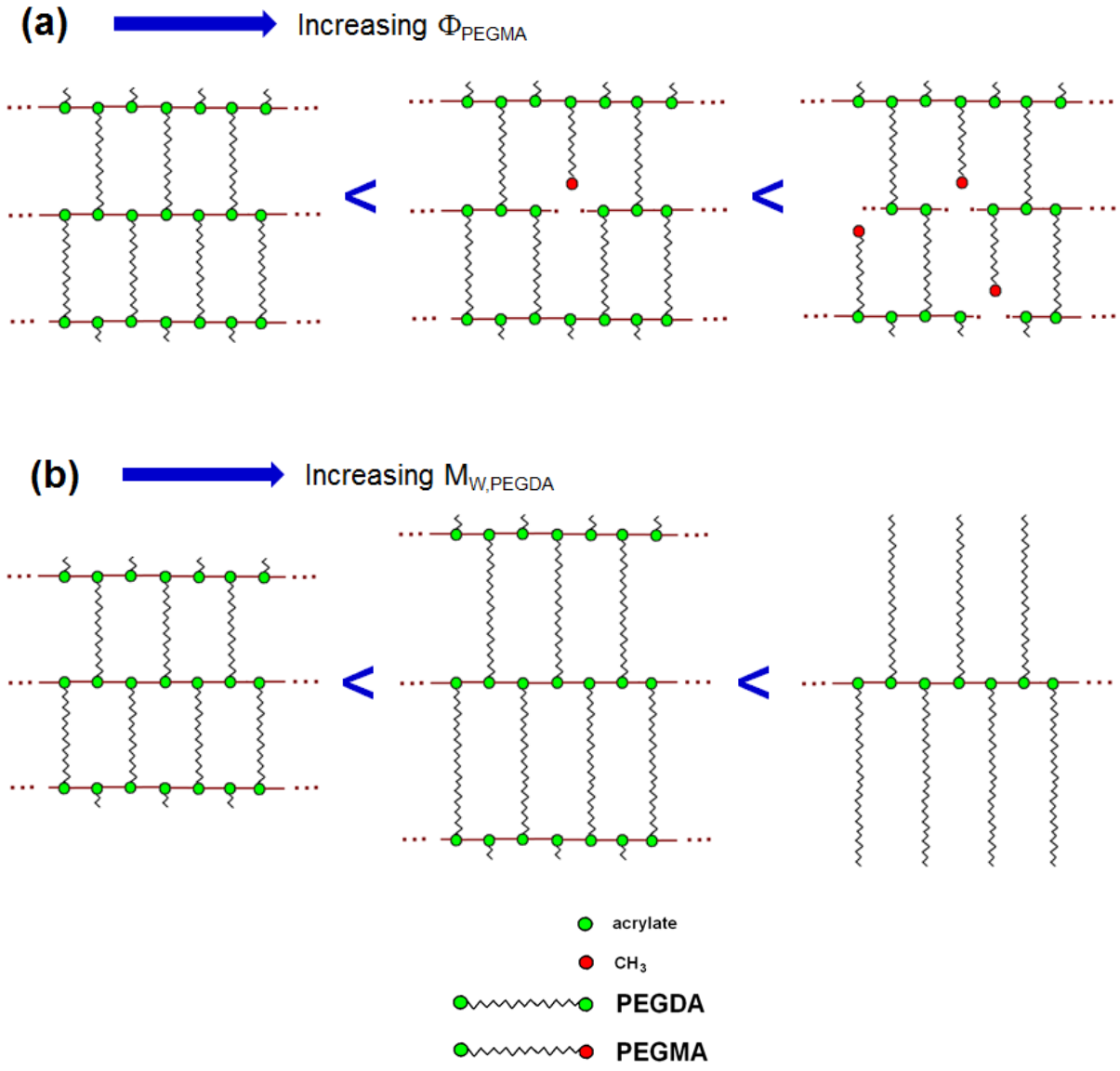

Figure 2.1 Schematic description of (a) PEGDA-PEGMA hydrogels with varying mass percentage of PEGMA (Φ_{PEGMA}), and (b) PEGDA hydrogels with varying M_W of PEGDA ($M_{W,PEGDA}$). In (a), increasing Φ_{PEGMA} of PEGDA-PEGMA hydrogels (from left to right) was expected to increase the number of pendant PEGMA chains, while reducing the number of cross-links. In (b), increasing $M_{W,PEGDA}$ of PEGDA hydrogels (from left to right) was expected to decrease the number of cross-links and increase the pore diameter.

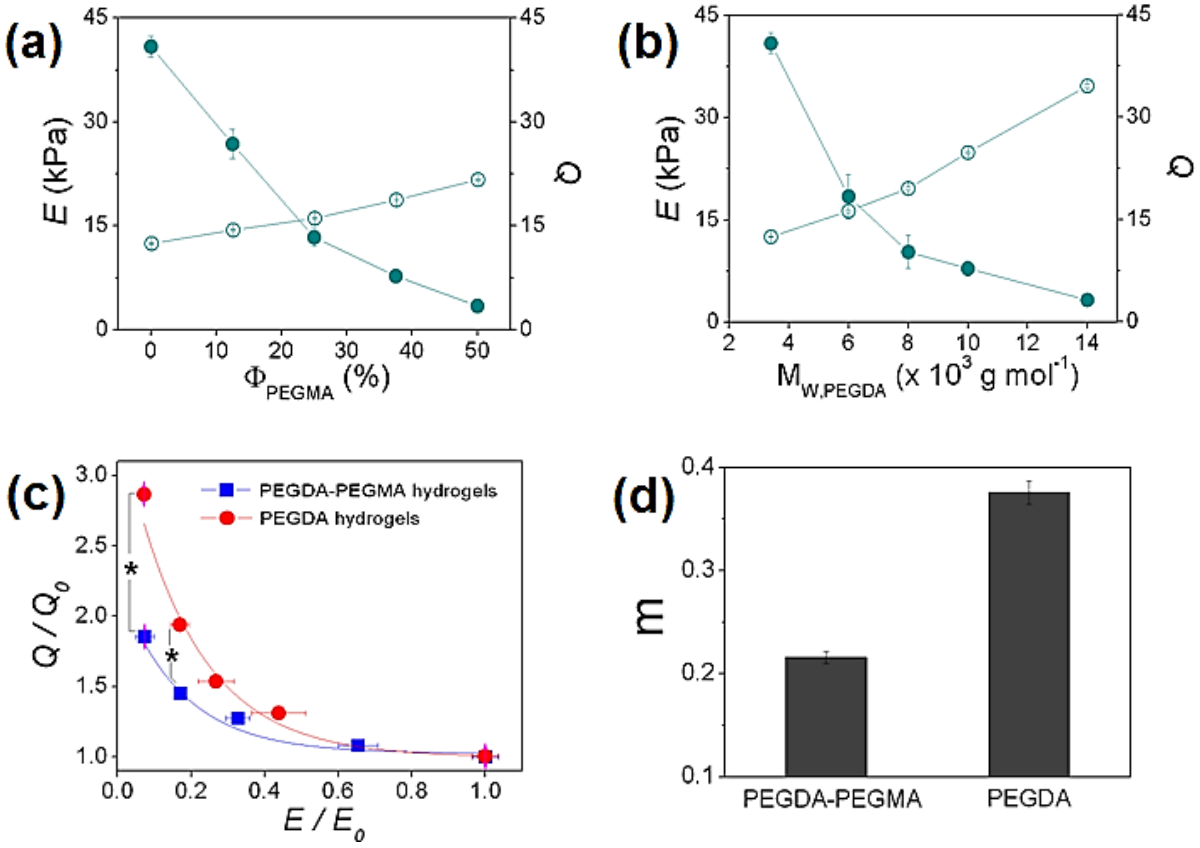

Figure 2.2 (a) Increasing Φ_{PEGMA} of the PEGDA-PEGMA hydrogels led to the significant decrease of the elastic modulus (E, ●), but limited increase of the swelling ratio (Q, ○). (b) Increasing $M_{W,PEGDA}$ of the pure PEGDA hydrogels resulted in the significant decrease of E (●) and increase of Q (○). In (a) and (b), E of the hydrogels were controlled in the same range. (c) The inverse dependency of normalized swelling ratios (Q/Q_0) on the normalized elastic moduli (E/E_0) was fitted to the power law, $(Q/Q_0) \propto (E/E_0)^{-m}$, for PEGDA-PEGMA hydrogels (■) and pure PEGDA hydrogels (●). E_0 and Q_0 represent E and Q of PEGDA hydrogels with $M_{W,PEGDA}$ of 3400 g mol^{-1}.(*$p<0.05$) (d) The exponent, m, of the fitted power law was smaller for PEGDA-PEGMA hydrogels than pure PEGDA hydrogels.

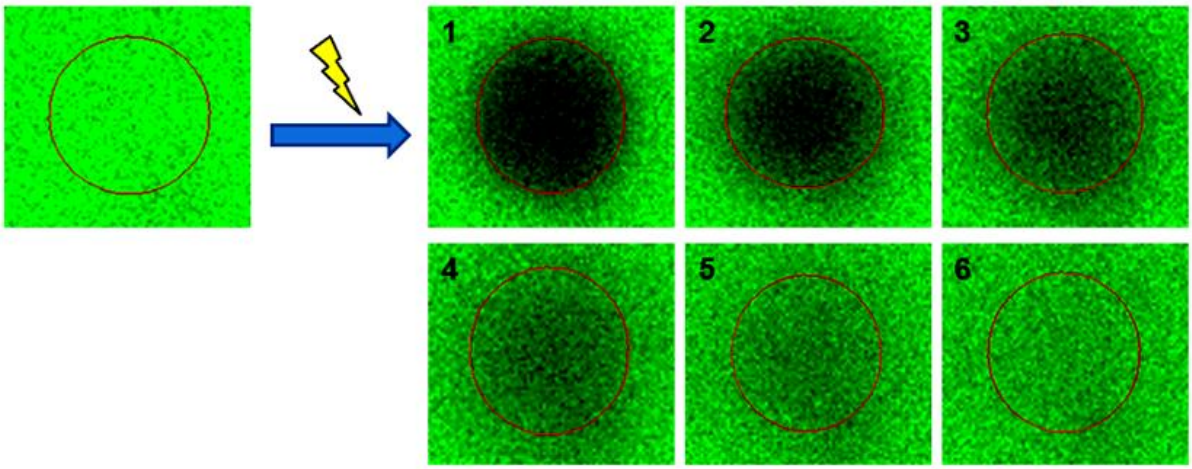

Figure 2.3 Schematic representation of fluorescence recovery after photobleaching (FRAP) assay. A small spot in a hydrogel containing fluorescent probe is photobleached, and the increase of fluorescence in the photobleached area was measured over time (from 1 to 6).

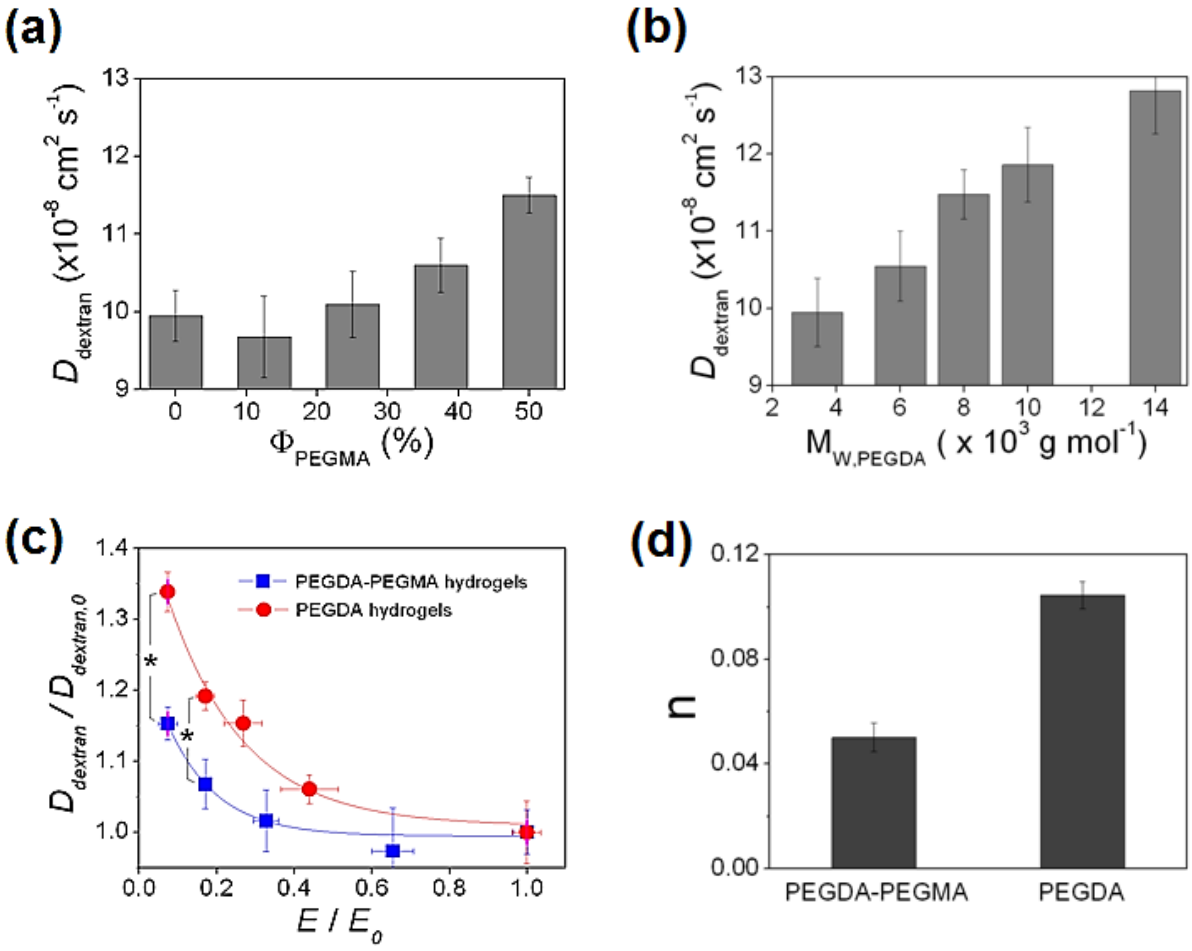

Figure 2.4 Diffusion coefficient ($D_{dextran}$) values of fluorescently labeled dextran, quantified with the FRAP assay, increased with increasing (a) Φ_{PEGMA} of PEGDA-PEGMA hydrogels and (b) $M_{W,PEGDA}$ of PEGDA hydrogels. (c) The inverse dependency of the normalized $D_{dextran}$ ($D_{dextran}/D_{dextran,0}$) on the normalized elastic modulus (E/E_0) of the hydrogel was fitted to the power law, ($D_{dextran}/D_{dextran,0}$) $\propto$ $(E/E_0)^{-n}$, for the PEGDA-PEGMA hydrogels (■) and pure PEGDA hydrogels (●). $D_{dextran,0}$ and E_0 represents $D_{dextran}$ and E of PEGDA hydrogels with $M_{W,PEGDA}$ of 3400 g mol^{-1}. (*$p<0.05$) (d) The exponent, n, of the fitted power law was smaller for PEGDA-PEGMA hydrogels than pure PEGDA hydrogels.

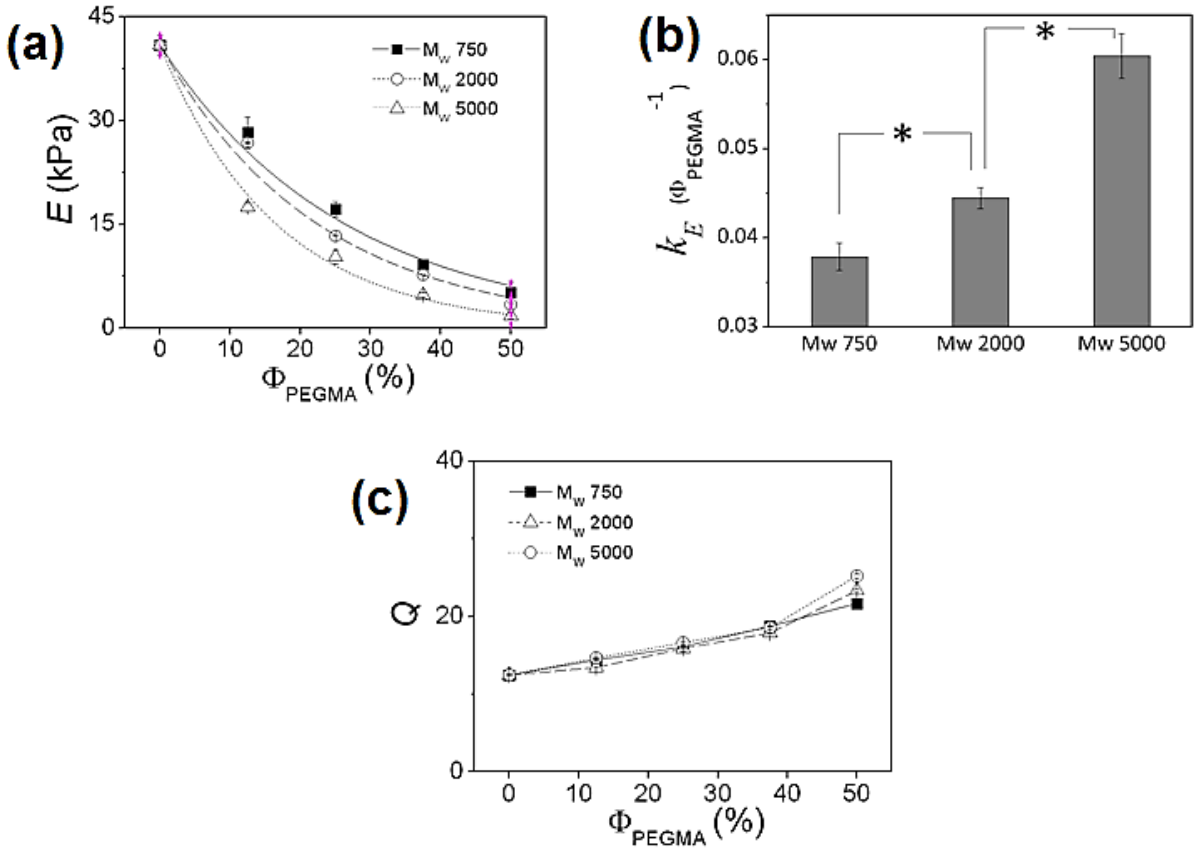

Figure 2.5 The inverse dependency of (a) elastic modulus (E) of the PEGDA-PEGMA hydrogel on Φ_{PEGMA} was tuned with M_W of the PEGMA, which was varied from 750 to 5000 g mol^{-1}. (b) The rate of decrease in elastic modulus (k_E), calculated from Eq. (1), increased with M_W of pendant PEGMA. (*$p<0.05$)

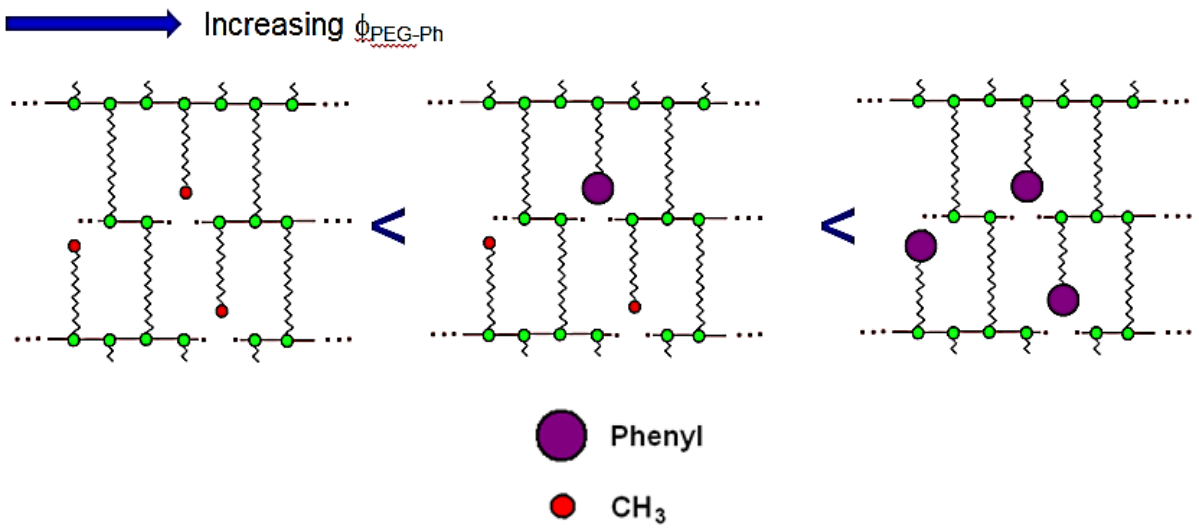

Figure 2.6 Schematic description of PEGDA-PEGMA hydrogels with increasing hydrophobicity of pendant PEG chains (left to right), by modifying the end groups of pendant PEG chains to present hydrophobic phenyl groups. The total number of pendant PEG chains were fixed (Φ_{PEGMA} at 50), while changing the fraction of pendant PEG chains with phenyl end groups (ϕ_{PEG-Ph}).

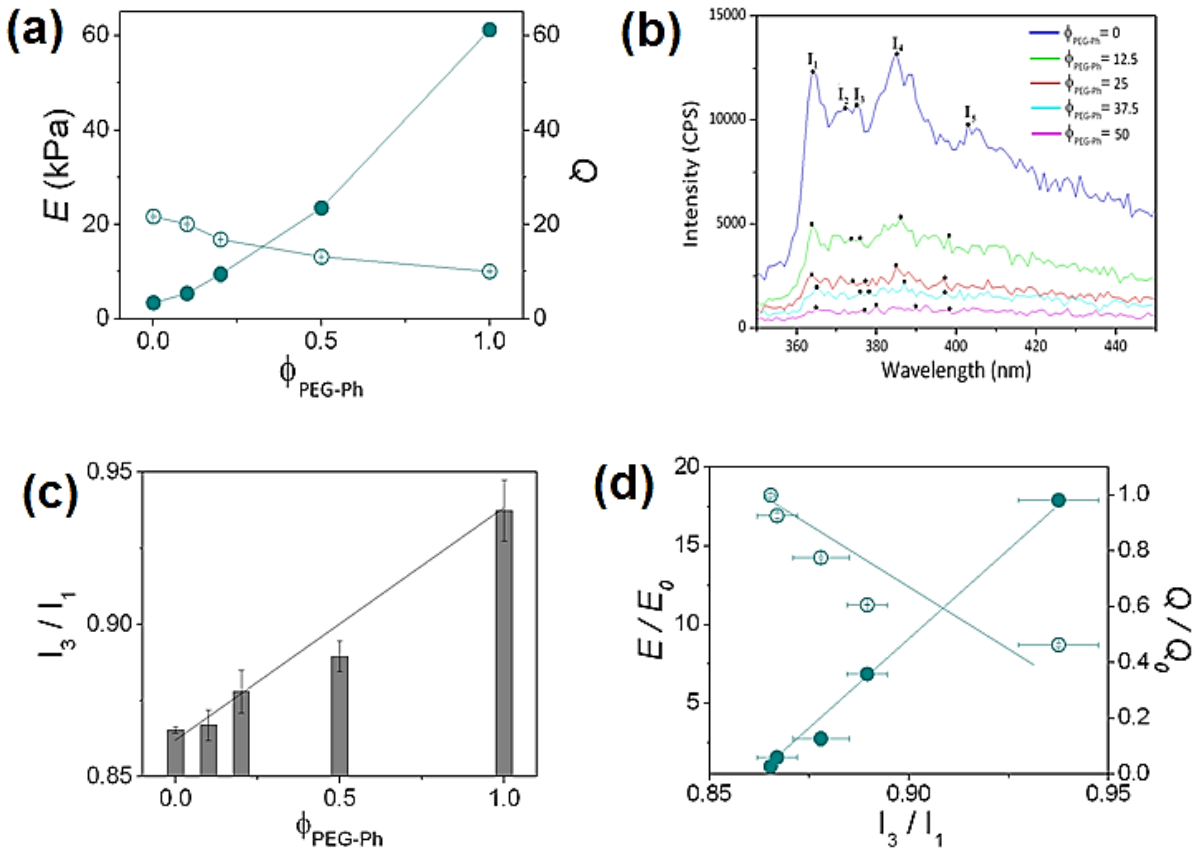

Figure 2.7 (a) Increasing $\phi_{PEG\text{-}Ph}$ led to the increase of elastic modulus (E,●) and decrease of the swelling ratio (Q,○). (b) The emission spectra of pyrene in hydrogels were measured with varying $\phi_{PEG\text{-}Ph}$. The characteristic peaks of pyrene (from I_1 to I_5) were designated. (c) The ratio of I_3 to I_1 (I_3/I_1) was increased with $\phi_{PEG\text{-}Ph}$. (d) The change in elastic modulus (E/E_0,●) and swelling ratio (Q/Q_0,○) was related to I_3/I_1. E_0 and Q_0 represent E and Q of the hydrogel at the lowest $\phi_{PEG\text{-}Ph}$ of 0.

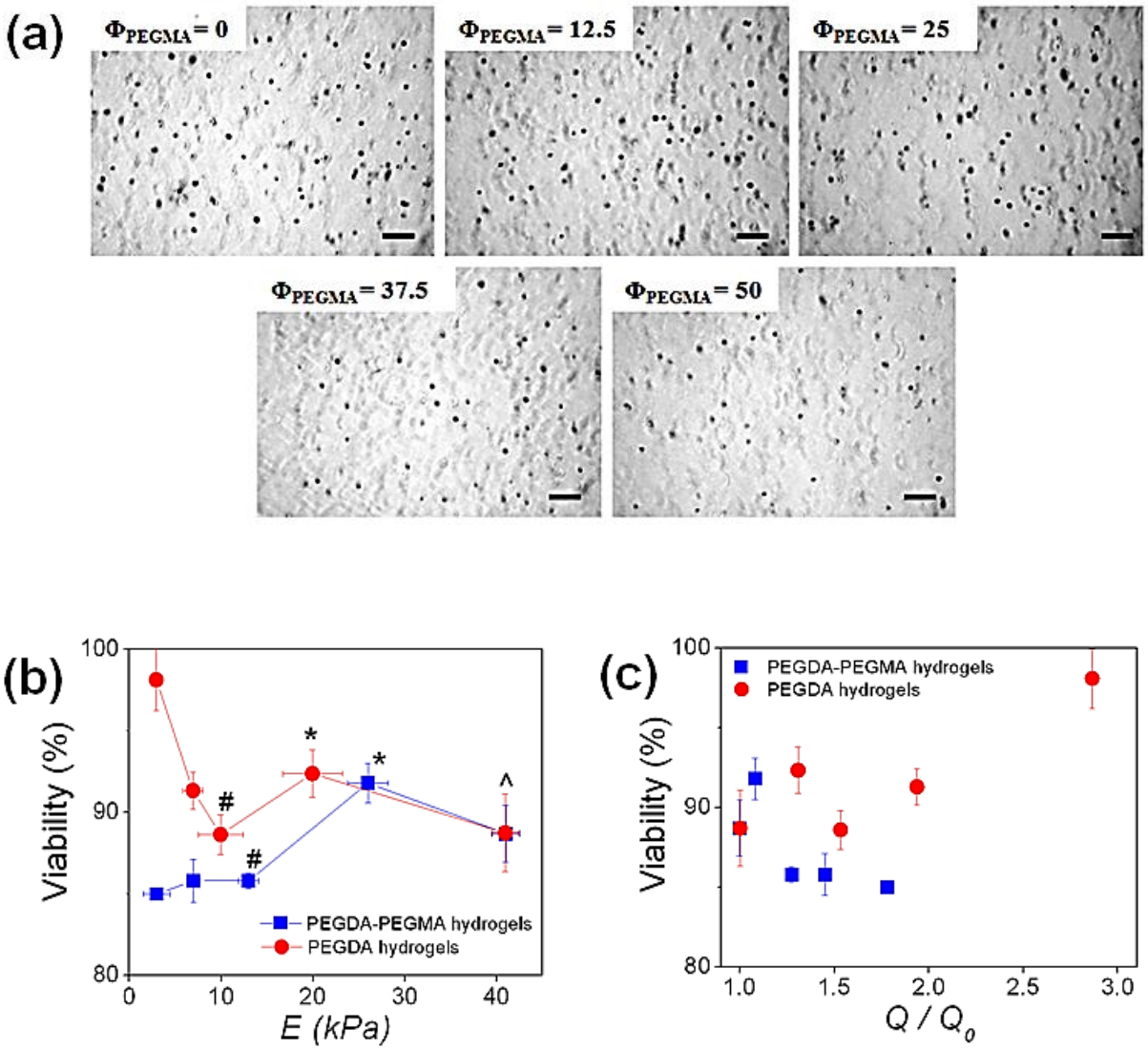

Figure 2.8 (a) Phase-contrast microscopic images of cells taken 24 hours after encapsulation in PEGDA-PEGMA hydrogels with Φ_{PEGMA}. The viable cells were positively stained with MTT (dark purple).(Scale bar: 100 μm) The viability of cells was related to (b) elastic modulus (E) and (c) the normalized swelling ratio (Q/Q_0) of the PEGDA-PEGMA hydrogels with varying Φ_{PEGMA} (■) and pure PEGDA hydrogels with varying $M_{W,PEGDA}$ (●). ($p<0.05$ between * and ^, and also between * and #) Q_0 represents the swelling ratio of the PEGDA hydrogel with $M_{W,PEGDA}$ of 3400 g mol^{-1}.

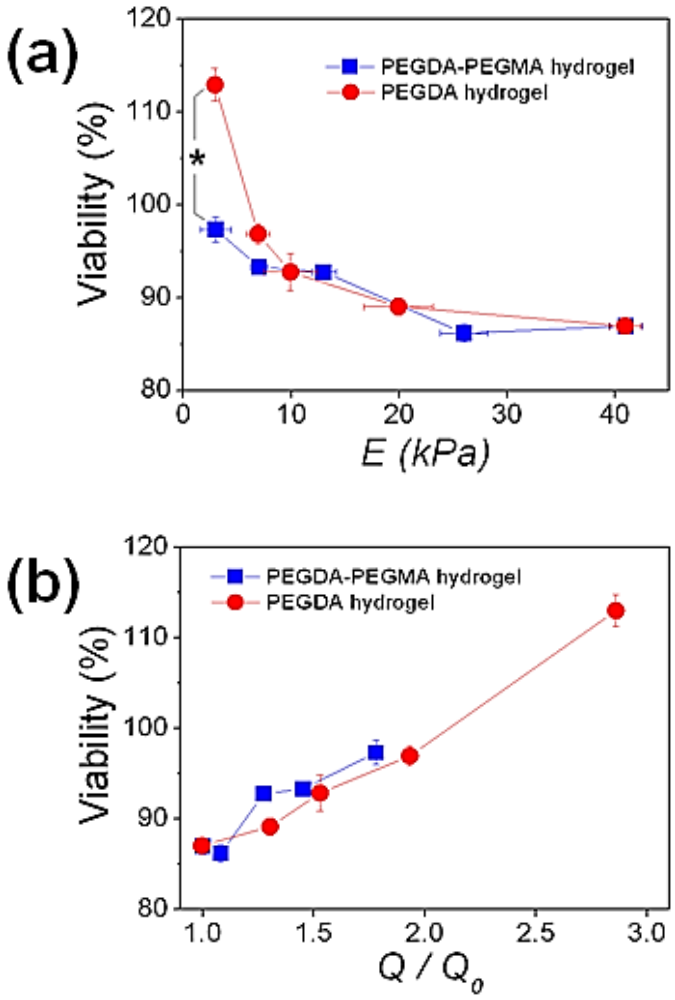

Figure 2.9 The viability of NIH3T3 fibroblasts encapsulated in collagen-free PEGDA-PEGMA hydrogels with varying Φ_{PEGMA} (■) and collagen-free PEGDA hydrogels with varying $M_{W,PEGDA}$ (●) were related to (a) elastic modulus (E) and (b) swelling ratio (Q/Q_0). (*$p<0.05$) Swelling ratio was normalized with that of PEGDA hydrogel with $M_{W,PEGDA}$ of 3400 g mol^{-1}(Q_0). The viability was measured 24 hours after encapsulation.

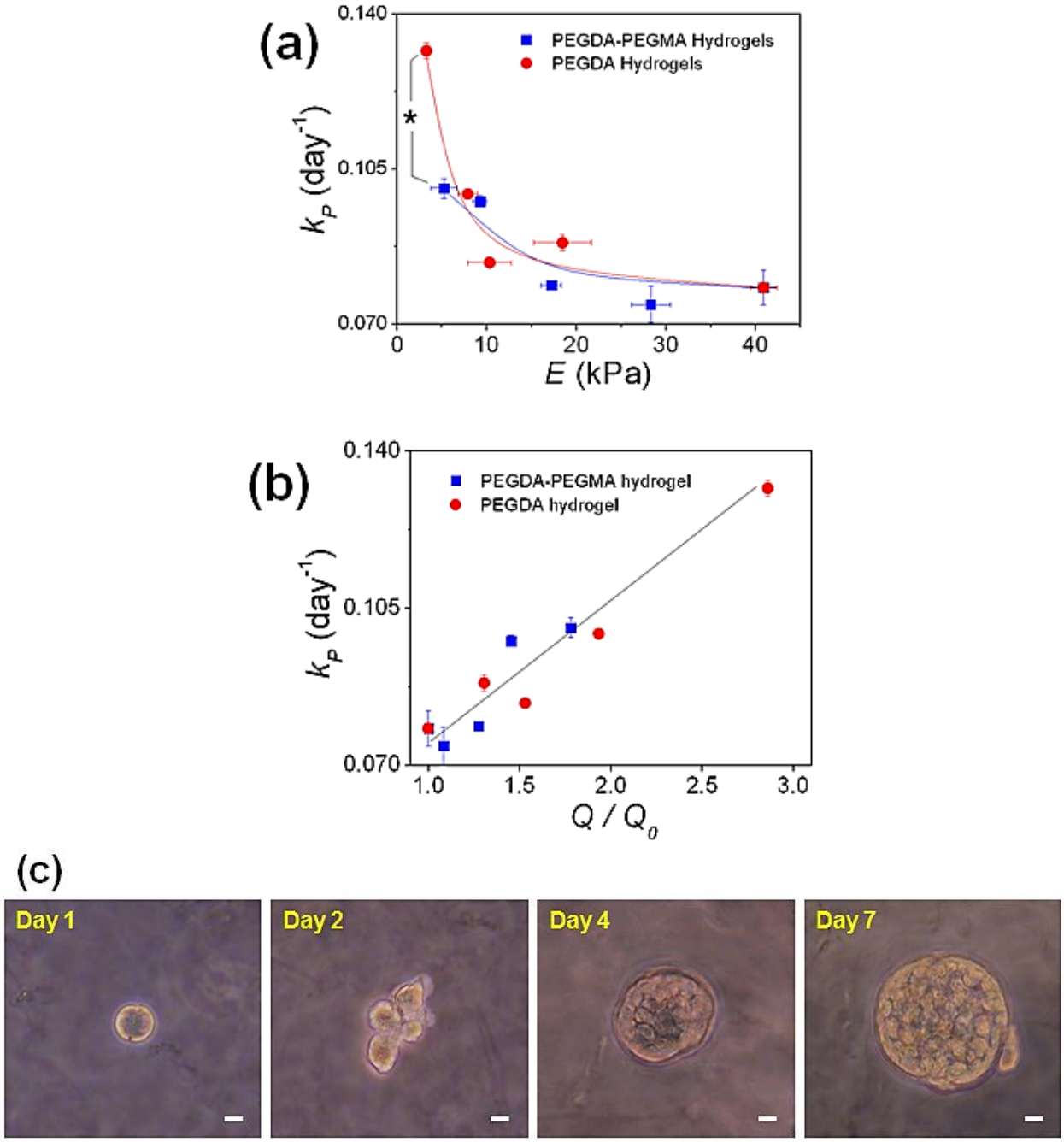

Figure 2.10 Proliferation rates (k_P) were related to (a) elastic modulus (E) and (b) normalized swelling ratio (Q/Q_0) of PEGDA-PEGMA hydrogels with varying Φ_{PEGMA} (■) and pure PEGDA hydrogels with varying $M_{W,PEGDA}$ (●).(*p<0.05) Q_0 represents the swelling ratio of the PEGDA hydrogel with $M_{W,PEGDA}$ of 3400 g mol^{-1}. (c) Phase-contrast microscopic images of cells undergoing proliferation over time.(Scale bar: 10 μm)

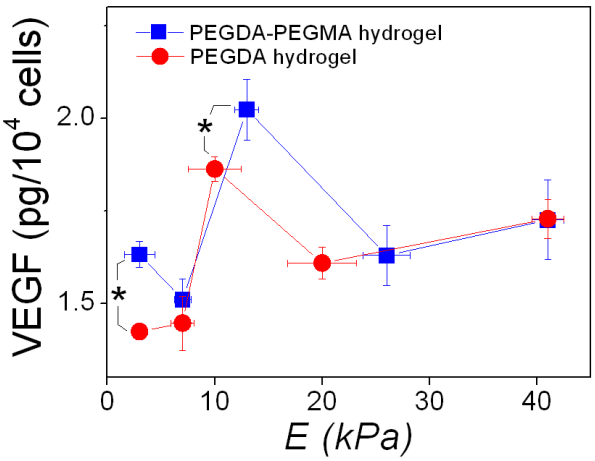

Figure 2.11 VEGF expression level from encapsulated fibroblasts was related to the elastic modulus (E) of PEGDA-PEGMA hydrogels with varying Φ_{PEGMA} (■) and pure PEGDA hydrogel with varying $M_{W,PEGDA}$ (●).(*P<0.05)

Chapter 3 Independent Control of Stiffness from Permeability of Hydrogels with Methacrylic Alginate

3.1 Introduction

Hydrogels are being increasingly used as a cell encapsulation and transplantation device in various preclinical and clinical treatments.[57] The mechanical properties of hydrogels are known to regulate diverse activities of cells adhered to the gel, and potentially the outcome of cell therapies, because cells can probe and sense their mechanical environment.[6,9,10] The successful use of hydrogels in these applications greatly relies on their physical and chemical properties including mechanical rigidity, resistance to fracture, degradation rate, and interaction with bioactive molecules and cells.[6,57,58] Controlling these multiple properties in a desired manner is still a significant challenge in the hydrogel design, because of the interdependency between hydrogel properties. For example, a hydrogel should be rigid enough to maintain its structural integrity for a sufficient period of time to hold drug molecules and cells loaded in the matrix.[57] However, increasing the gel stiffness results in the brittle gel, which is readily fractured at a small deformation. Certain applications require hydrogels to be biodegradable, but the hydrogel degradation rate is dependent on the hydrogel stiffness.[57,58]

It is common to control the hydrogel stiffness with concentrations of gel-forming polymers

---

and the molar ratio of a cross-linking molecule to the gel-forming polymer, so the number of cross-links is increased.[57,58] However, these approaches often result in the decrease of the hydrogel swelling ratio, because the osmotic water entry into the gel matrix is more limited with the larger number of cross-links.[12,59,60] The reduced swelling ratio indicative of the smaller pore diameter further results in the limited diffusivity of bioactive molecules crucial to support the viability of cells encapsulated into the gel matrix.[6,17] Therefore, it is highly critical to decouple the dependency of hydrogel stiffness on the swelling ratio in the design of a cell-encapsulating hydrogel, so the gel mechanics can be controlled over a broad range without altering the hydrogel swelling ratio. However, to date, few efforts have been made to independently control hydrogel stiffness and swelling ratio.

This study therefore demonstrates a new strategy of decoupling the dependency of hydrogel swelling ratio on the stiffness, which is inspired by the role of polysaccharides in an extracellular matrix (ECM). Glycosaminoglycans, polysaccharide components in an extracellular matrix (ECM), are known to play critical roles in both rigidity and water sorption of ECM, because of their rigid sugar units and hydrophilic groups.[61,62] We therefore hypothesized that incorporating a polysaccharide which presents multivalent methacrylic groups and hydrophilic groups into a hydrogel would allow us to control the gel stiffness over a broad range while limiting the change of swelling ratio.[52] This hypothesis was examined with a hydrogel formed from chemical cross-linking between methacrylic alginate and poly(ethylene glycol) dimethacrylate (PEGDA). The number of cross-links of the hydrogel was controlled with the concentration of methacrylic alginate and the degree of substitution of methacrylic groups linked to the alginate.[52,63] For control experiments, the number of cross-links of a hydrogel was controlled solely with

concentration of PEGDA with varied molecular weights. In addition, oxidation of uronic acid residues in alginate results in the formation of hydrolytically labile functional groups. So the degree of oxidation of methacrylic alginate was varied in order to control the rate of hydrogel degradation.

The resulting hydrogel stiffness was evaluated with a measurement of the elastic modulus. The hydrogel swelling ratio was evaluated by measuring the mass of hydrated gel, and also imaging water distribution through the hydrogel using magnetic resonance imaging (MRI).[64,65] The dependency of gel stiffness on the swelling ratio was further tuned by incubating the hydrogel in media of different pH and ionic strength.[59,60,66] Finally, PC12 cells were encapsulated into hydrogels with varying amounts of methacrylic alginate, which presented the varied stiffness but comparable swelling ratio in order to test cell viability in the 3D gel matrix. Overall, this study presents an advanced biomaterial design strategy which enables one to assemble a rigid cell-encapsulating material without deteriorating cellular viability.

3.2 Results

3.2.1 Syntheses of methacrylic alginate and oxidized methacrylic alginate

Methacrylic alginate (MA) was made by linking with 2-aminoethyl methacrylate via amide-forming carbodiimide chemistry (Figure 3.1). Increasing the molar ratio between 2-aminoethyl methacrylate and uronic acid of alginate resulted in the increase of the degree of substitution (*DS*) of methacrylic groups to alginate ('methacrylic *DS*') from 5 to 44 %. The oxidized methacrylic alginate (OMA) was prepared in order to allow degradation of the resulting hydrogels. OMA was made by oxidation reaction of alginate and subsequent chemical reaction to link methacrylic groups to the oxidized alginate. The oxidation reaction opened a sugar ring of alginate to introduce hydrolyzable acetal-like linkages in a polymer chain.[67,68]

The radius of gyration (R_G) of methacrylic alginate was measured to evaluate effects of methacrylic *DS* on R_G. Interestingly, chemical linkages of methacrylic groups to the alginate changed R_G of the polymer, as examined with the static light scattering (SLS). Persistence length (l_P) calculated from the R_G values using Eq. (8) was linearly increased with the methacrylic *DS* (Figure 3.2).

3.2.2 Analysis of hydrogel stiffness incubated in a high ionic strength medium

The elastic modulus of a hydrogel was measured to evaluate the mechanical stiffness of the hydrogel. Prior to the measurements, hydrogels at all conditions were incubated in PBS of high ionic strength (I_{PBS} = 0.22 M).

First, the elastic modulus of a hydrogel consisting of PEGDA 400 and methacrylic alginate was varied by increasing the concentration of methacrylic alginate and the methacrylic *DS* while

keeping the PEGDA 400 concentration constant at 10 wt %. As expected, the elastic modulus of the hydrogel was linearly increased with concentration of methacrylic alginate, and the linear dependency became larger with the methacrylic *DS* (Figure 3.3a). Ultimately, increasing polymer concentration from 10 to 12.5 wt % with methacrylic alginate presenting 220 methacrylic groups (MA-3) per alginate chain resulted in almost ten-fold increase of the elastic modulus.

Incorporation of PEGDA 2000 into the PEGDA 400 hydrogel also resulted in the linear increase of the elastic modulus of a hydrogel with increasing polymer concentration (Figure 3.3b). In contrast, increasing the polymer concentration with PEGDA 14000 made an insignificant increase of the elastic modulus. The overall range of the elastic modulus that was controlled solely with PEGDAs was much smaller than that was controlled with methacrylic alginate.

The elastic modulus of a hydrogel was related to the density of methacrylate groups (Ψ) of a hydrogel, so the effect of the number of methacrylate on the hydrogel stiffness could be evaluated. Interestingly, the linear dependency of the elastic modulus on the density of methacrylic group was specific for the chemical composition of the hydrogel (Figure 3.4a). At any given methacrylate density, the elastic modulus of the hydrogel consisting of PEGDA 400 and methacrylic alginate was higher than that of the hydrogel consisting of PEGDA with varied M_W. The stiffening efficiency of the reinforcing polymer (Φ_E), quantified with a slope of the linear curve of the elastic modulus on Ψ, was larger with the hydrogel consisting of PEGDA 400 and methacrylic alginate as compared with pure PEGDA hydrogels (Figure 3.4b).

Alternatively, the elastic modulus of a hydrogel of the PEGDA 400 and methacrylic alginate

was controlled with mass fraction of methacrylic alginate at a given polymer concentration of 10 wt %. Increasing mass fraction of methacrylic alginate (ϕ_{MA}) with the lowest methacrylic *DS* (MA-1), while decreasing the mass fraction of PEGDA, minimally changed the elastic modulus. In contrast, the use of methacrylic alginate with the higher methacrylic *DS* (MA-2 and MA-3) resulted in the linear increase of the elastic modulus (Figure 3.5).

3.2.3 Analysis of hydrogel swelling ratio in a high ionic strength medium

The swelling ratio of a hydrogel was also measured to evaluate the hydrogel permeability. Again, prior to the measurement, the hydrogel was incubated in PBS (I_{PBS} = 0.22). Interestingly, increasing polymer concentration of the hydrogel with the methacrylic alginate resulted in the minimal decrease of the swelling ratio independent of the methacrylic *DS* (Figure 3.6a). The change of the mass fraction of methacrylic alginate in the hydrogel at a constant polymer concentration also resulted in the minimal decrease of the swelling ratio (Figure 3.6b). In contrast, the swelling ratio of a hydrogel consisting solely of PEGDA with varying M_W was decreased with the polymer concentration, and its dependency was the largest when the hydrogel was formed by cross-linking PEGDA 400 and PEGDA 2000 (Figure 3.7).

Water distribution through a hydrogel was further examined by measuring the local amount of water proton in the hydrogel with the magnetic resonance imaging (MRI). In this study, the mass fraction of methacrylic alginate and the methacrylic *DS* were varied, while keeping the total polymer concentration constant. Incubation of a hydrogel in PBS significantly increased the concentration of water within a hydrogel as confirmed with the increase of the intensity of water proton (Figure 3.8a). The dependency of water concentration on the distance from the

center of the hydrated hydrogel was minimally affected by the changes of the mass fraction of methacrylic alginate and methacrylic *DS* (Figure 3.8b).

3.2.4 Dependency of hydrogel swelling ratio on elastic modulus

The elastic moduli of hydrogels presented in the Figure 2.3 were related to the swelling ratios of the hydrogels presented in Figure 2.6 and Figure 2.7. Interestingly, the swelling ratio of a hydrogel consisting of PEGDA and methacrylic alginate was minimally changed regardless of the increase of elastic modulus by one order of magnitude (Figure 3.9). In contrast, the swelling ratio of the hydrogel consisting of PEGDA with varying M_W was decreased with the elastic modulus of the hydrogel. The overall dependency of pure PEGDA hydrogel was therefore 16 times larger than that of the hydrogel of PEGDA and methacrylic alginate.

3.2.5 Hydrogels properties in media of varying ionic strength and pH

The ionic strength of the hydrogel incubation medium, PBS, was decreased from 2.2 to 0 M to evaluate the role of charged carboxylic groups of the methacrylic alginate on the hydrogel properties. Decreasing the ionic strength from 2.2 to 0.1 M did not alter the independency of the swelling ratio on the elastic modulus of the hydrogel (Figure 3.10a). However, further decrease of the ionic strength to zero resulted in the inversed dependency of the swelling ratio on the elastic modulus of the hydrogel.

The pH of the hydrogel incubation medium was also varied from 3 to 10 while keeping the ionic strength of the PBS at 0.22 M. The pH change of the PBS resulted in the minimal changes of the elastic modulus and swelling ratio (Figure 3.10b). Thus, t

e swelling ratio of the hydrogel was independent of the elastic modulus at any pH of PBS.

3.2.6 Hydrogel degradation controlled with degree of oxidation of OMA

To demonstrate the controlled degradation with degree of oxidation of oxidized methacrylic alginate (OMA), PEGDA 400 and OMA with varying degree of oxidation was The number of oxidized uronic acid groups per chain (oUA) was controlled from 0 (non-oxidized methacrylic alginate) to 50. The hydrogel degradation was monitored with decrease of the elastic modulus over time. The initial elastic modulus of hydrogel was almost independent of the number of oUA (Figure 3.11a), indicating that the oxidation of alginate did not affect the initial mechanical strength of the hydrogels. But the elastic moduli became significantly decreased over time, and the extent of decrease was correlated with the number of oUA (Figure 3.11b).

3.2.7 Analysis of viability of cells encapsulated in hydrogels

PC12 cells were encapsulated into the hydrogel of PEGDA hydrogels incorporated with varying amounts of methacrylic alginate. The resulting hydrogels presented varied elastic moduli but minimal change of the swelling ratio. The mass fraction of the methacrylic alginate in the hydrogel was increased at the constant total polymer concentration of 10 wt %, so the elastic modulus of the hydrogel was varied from 70 to 300 kPa without a significant change of the swelling ratio. Interestingly, the fraction of viable cells positively stained with the MTT reagent was rather increased by a factor of four with the mass fraction of methacrylic alginate (Figure 3.12).

3.2.8 Retention of serum protein in hydrogels

Fetal bovine serum was encapsulated into hydrogels with varying amount of methacrylic alginate, and the amount of serum protein released from the hydrogel was measured to evaluate the effect of methacrylic alginate in retaining bioactive proteins within the hydrogels. The amount of serum protein released was inversely related to the amount of methacrylic alginate in the hydrogel (Figure 3.13).

3.3 Discussion

The results of these studies demonstrated a strategy to decouple the inverse dependency of the stiffness of a cell-encapsulating hydrogel on the swelling ratio, so we could control hydrogel rigidity over a broad range without influencing gel permeability and subsequent cell viability. Specifically, incorporating methacrylic alginate into the poly(ethylene glycol)-based hydrogel allowed the control of elastic modulus while limiting the change of swelling ratio. The MRI-based analysis of water distribution through the hydrogel also confirmed that degree and uniformity of hydration were almost independent of the hydrogel stiffness. In addition, partial oxidation of alginate, which results in hydrolytically labile functional groups, allowed controlled rate of hydrogel degradation.

The incorporation of methacrylic alginate into the PEGDA hydrogel allowed us to significantly increase the elastic modulus of the hydrogel proportional to the methacrylic *DS*. Coupling of methacrylic groups to a flexible polymer commonly leads to molecular collapse because of hydrophobic association between methacrylic groups.[69-72] This molecular collapse may be disadvantageous to derive elastic intermolecular cross-links, because the methacylic groups are shielded from participating in cross-linking. However, it is likely that semi-flexible alginate minimized the molecular collapse as verified with the linear increases of the size and persistent chain length of methacrylic alginate with methacrylic *DS*. Consequently, most of methacrylic groups linked to alginate formed elastic intermolecular networks along with PEGDAs. In contrast, increasing polymer concentration of a hydrogel solely with PEGDA did not significantly increase the elastic modulus, likely because the flexible PEGDA chain allowed intramolecular association between methacrylic groups.

Alginate molecules exist as extended polymer chains in aqueous solutions, as evidenced by a large persistent length and high viscosity. As alginate becomes incorporated into a hydrogel system by co-polymerization, the extended molecular structure of alginate is retained within the hydrogel network. This likely prevented the gel from undergoing swelling by polymeric chain relaxation as the alginate molecules are already well stretched, thus contributing to the consistent swelling ratio values at a wide range of cross-linking density. The effects of chain inflexibility on the hydrogel property will be investigated more systematically in future studies.

The limited changes of swelling ratio and water distribution through the PEGDA-methacrylic alginate hydrogels independent of the gel rigidity were related to the multivalent hydrophilic groups of alginate.[73] In general, increased number of cross-links reduces a molecular weight between cross-links which surrounds nano-sized pores of a hydrogel matrix.[74] Therefore, the osmotic water entry becomes kinetically limited with increase of the number of cross-links as observed with the pure PEGDA hydrogels. However, incorporation of methacrylic alginate with multiple hydrophilic groups into the PEGDA hydrogel likely facilitated the water entry, because of the energetically favorable interaction between hydrophilic groups and water molecules.[73] Overall, we propose that the hydrophilic groups of alginate compensate the effect of cross-linking density on water entry into the hydrogel.

Further studies to examine the hydrogel properties in varied environments suggested that hydroxyl groups of alginate should be more important factor to facilitate water entry than anionic carboxylic groups specifically in a physiological condition. First, the inverse dependency between the swelling ratio and the elastic modulus at zero ionic strength implicates that charged carboxylic groups play an adverse role in decoupling the dependency between stiffness and

permeability. Increasing ionic strength of a medium likely deactivated the role of carboxylic groups in the osmotic water entry, because of limited electrostatic interaction between the carboxylic groups.[59,60,66] Secondly, minimal effect of pH of the incubation medium on the swelling ratio also suggests the minimal role of carboxylic groups because pH of the medium also alters the electrostatic interaction between carboxylic groups.[66] In contrast, the critical role of hydroxyl group in decoupling the dependency between stiffness and permeability of a hydrogel was confirmed with negative controls; PEGDA hydrogels free of hydroxyl groups.

Ultimately, the independency between hydrogel properties allowed multiple bioactive molecules in a cell culture medium to access cells encapsulated in a hydrogel regardless of the gel stiffness. The viability of encapsulated cells showed that the viability was proportional to the amount of methacrylic alginate, even though the swelling ratio values of all hydrogels were similar to one another. This result implicate the role of alginate extends far more than simply facilitating the uptake of biomolecules into the hydrogel systems with multiple hydrophilic functional groups; it may also help retain important biomolecules within the hydrogel system, as evidenced by the ability of methacrylic alginate in retaining the serum protein. The beneficial role of polysaccharide has been discovered in various biological processes including aging and self-healing process.[61,62,75] For example, the decrease in chondroitin sulfate content in cartilage tissue with aging affects transport of water and metabolites and subsequently cellular activities. Also, many growth factors have heparin-binding domains, clusters of basic amino acid residues, which can bind to negatively charged sulfate or carboxylic acid in polysaccharide portion of ECM and help control their transport. We therefore suggest that this beneficial role of polysaccharide in the biological system was successfully harnessed by incorporating

methacrylic alginate into the PEGDA hydrogel system.

3.4 Materials and Methods

3.4.1 Synthesis of oxidized methacrylic alginate

Alginate which presents a large fraction of guluronic acid block (LF20/40, FMC Technologies, weight-average molecule weight (M_W) ~ 250,000 g/mol) was first irradiated with γ-rays from the ^{60}Co source at a dose of 2 Mrad for 4 hours.[76,77] The irradiation process decreased Mw of alginate to 100,000 g/mol as determined by the gel permeation chromatography (GPC). The irradiated alginate was dissolved in deionized (DI) water at 1 wt%. Sodium periodate (Sigma Aldrich) was dissolved in the alginate solution, and stirred for 24 hours. The amount of sodium periodate was varied to control the number of oxidized uronic acid groups in alginate. The mixture was dialyzed against DI water, and lyophilized to obtain dried oxidized alginate. To conjugate methacrylic groups onto oxidized alginate, the oxidized alginate was dissolved in the 0.1M MES ((2-(N-morpholino) ethanesulfonic acid) buffer (pH 6.4, Sigma-Aldrich) at the concentration of 1 % (w/v). Then, 1-hydroxybenzotriazole (HOBt, Fluka), 1-ethyl-3-(3-dimethylaminopropyl) carbodiimide (EDC, Thermo Scientific) and 2-aminoethyl methacrylate (AEMA, Sigma Aldrich) were dissolved in the alginate solution and stirred for 19 hours.[52,63,78] The molar ratio of HOBt, EDC and AEMA was 2:2:1. The mixture was dialyzed against DI water, and lyophilized. The dried OMA was reconstituted to a 3 wt % stock solution. The conjugation of methacrylate groups onto the alginate was confirmed by ^{1}H-NMR (300MHz, QE300, General Electric), as previously done.[52]

The degree of substitution (*DS*) of methacrylic group (methacrylic *DS*) was determined by titration with NaOH to calculate the number of free carboxylate groups. Briefly, 0.01 M NaOH was added into 1 wt% solution of methacrylic alginate, and, after ten minutes, the solution pH

was measured with an electronic pH meter (Mettler Toledo). The NaOH solution was continuously added until the pH reached 10 to obtain the titration curve. The mole of NaOH at the end point of the titration was used as the number of free carboxylate groups. The methacrylic *DS* was calculated as follows,

$$DS\,(\%) = \frac{(N_{total} - N_{free})}{N_{total}} \times 100 \tag{5}$$

where N_{total} was the total number of uronic acid residues determined by dividing the molecular weight of methacrylic alginate by the molecular weight of a uronic acid (~ 198 g/mol), and N_{free} was the number of free carboxylate groups determined by the titration. The methacrylic *DS* of three methacrylic alginate samples (MA-1, MA-2 and MA-3) prepared in this study were 5, 23, and 44%, respectively.

3.4.2 Synthesis of poly(ethylene glycol) dimethacrylate (PEGDA)

First, poly(ethylene glycol) (PEG, Sigma Aldrich) having M_W of 2,000 or 14,000 g/mol were dissolved in dichloromethane at the concentration of 10 wt%. Next, methacryloyl chloride (Sigma Aldrich) and triethylamine (Fisher Chemical) were dissolved in the PEG solution and stirred overnight under dry N_2 gas. The molar ratio of PEG, methacryloyl chloride and triethylamine was 1:4:4. Finally, the insoluble salt (triethylamine-HCl) was filtered, and the product was precipitated by adding ice-cold ether. The product collected by filtration was washed with ether several times. The conjugation of methacrylate groups onto PEG was confirmed by ^{1}H-NMR (300MHz, QE300, General Electric).

3.4.3 Radius of gyration (R_G) of methacrylic alginate

The radius of gyration (R_G) of methacrylic alginate was measured using static light scattering (SLS, BI-200 SM goniometer, Argon Ion 35mW laser, λ=632.8nm, Brookhaven Instruments). The instrument was calibrated with the scattering of toluene at 90° to convert scattering intensity from counts per second to cm^{-1}. The samples were filtered with 0.22 μm syringe filters into glass tubes with a path length of 1 cm. All experiments were made at 25 ℃. To convert the light scattering data into a Zimm plot, dilute polymer solutions were prepared at five different concentrations ranging from 0.1 to 99 mg ml^{-1}.[79] These concentrations were smaller than the semi-dilute concentration regime to prevent multiple scattering.

The radius of gyration (R_G) of a polymer solution was determined from the following Zimm equation.[79-81]

$$\frac{K_C}{R(\theta)} = \frac{1}{M_W}\left(1 + \frac{q^2}{3} R_G{}^2 + \ldots\right) + 2B_C \tag{6}$$

where K_C was an optical constant, $R(\theta)$ was the Rayleigh ratio, q was the scattering vector ($q = (4\pi/\lambda)\sin(\theta/2)$) with the scattering angle, θ, M_W was the molecular weight of a polymer, and B_C was the second viral coefficient (in unit of cm^3 mol/g^2). The K_C in the Zimm equation was defined as follows,

$$K_C = 4\pi^2 n^2 (dn/dc)^2 / N_A \lambda^4 \tag{7}$$

where n was the refractive index of the medium, and dn/dc was the refractive index increment against polymer concentration (ml/g), N_A was the Avogadro's number, and λ was the wavelength of the incident light (633. nm). dn/dc value of alginate determined with a Milton Roy

refractometer was 0.150. The slope of a curve extrapolated to the zero concentration was regarded as R_G in Eq. (6).

The persistence length (l_P) of methacrylic alginate was further calculated from the R_G value, assuming the polymers were freely-jointed linear Gaussian chains.[82]

$$(R_G)^2 = \frac{L \cdot l_P}{3} \tag{8}$$

L was the contour length of a polymer chain (the sum of all skeletal bond lengths).

3.4.4 Hydrogel Preparation

1 mL of pre-gelled solution was prepared by mixing the low M_W PEGDA (PEGDA 400, M_n ~ 400, Polysciences) with methacrylic alginate of varying methacrlyic *DS*. The concentration of PEGDA 400 was kept constant at 10 wt %, while increasing the amount of methacrylic alginate up to 2.5 wt %. For another set of experiments, the total polymer concentration was kept constant at 10 wt %, while increasing the fraction of methacrylic alginate from 0 to 0.2. The mixture of pre-gelled solution was further mixed with 0.01 wt % Irgacure 2959 (Ciba). The pre-gelled solution was subsequently placed between two glass plates with 1 mm spacers, followed by exposure to UV light for 10 minutes to induce radical cross-linking reaction. Gel disks (10 mm in diameter) were punched out, and the disks were further incubated in phosphate buffer saline (PBS, pH 7.4) for 24 hours at 37°C.

For control experiments, 10 wt % PEGDA solution was mixed with PEGDAs with varied Mw (i.e., PEGDA 2000 or PEGDA 14000). The concentration of PEGDA 2000 or PEGDA 14000 was increased up to 3 wt % while keeping PEGDA 400 concentration constant. The pre-

gelled mixture was cross-linked following the same procedure used to prepare the hydrogel of PEGDA 400 and methacrylic alginate.

3.4.5 Characterizations of the hydrogel stiffness and swelling ratio

The hydrogel stiffness was evaluated with measurement of the elastic modulus of a hydrogel. Following the incubation in the neutral PBS for 24 hours, the gel disk was compressed at a rate of 1 mm/min using a mechanical testing system (MTS Insight). The elastic modulus was calculated from the slope of a stress (σ) vs. strain (λ) curve at the first 10% strain.[83,84]

The hydrogel swelling ratio was quantified as the weight ratio of a gel incubated in the PBS for 24 hours to the dried gel. For certain experiments, the gel disks were incubated in PBS of varied pH and ionic strength. The pH of PBS was altered from 3 to 10, and the ionic strength was altered by varying total salt concentration of PBS from 0 (pure DI water) to 1.6 M. The ionic strength (I_{PBS}) of the PBS was calculated as follows,

$$I_{PBS} = \frac{1}{2}\sum_{i=1}^{n} c_i \, z_i^{\,2} \tag{9}$$

where c_i was the molar concentration and z_i was the charge number of each ion.[85]

3.4.6 Magnetic Resonance Imaging (MRI) of a hydrogel

MRI was carried out using 600 MHz Varian Unity/Inova nuclear magnetic resonance (NMR) spectrometer (14.1 T magnet) at room temperature. Each gel disk (10 mm in diameter, 1 mm in thickness) was placed in a glass bottle (20 mm in diameter, 40 mm in height), then inserted into a RF (Radio Frequency) coil. Spin echo multi-slice (SEMS) pulse sequence was used to acquire

resonance data, which were then converted into water density map using VNMR 6.1C software.[65] For SEMS pulse sequence, the repetition time (T_R) of 2.5 s and the echo time (T_E) of 5 ms were used. The field of view (FOV) was 1.6 x 1.6 cm, and the image matrix was 128 x 64 pixels. The resulting water density images were processed to present the density spectrum for comparison using MATLAB (The Mathworks™). For visualization, pseudo-color was added to the images using the ImageJ software (free image analysis software from National Institutes of Health). For counting water intensity peaks, the rectangular gel picture from the image was selected, and the histogram of the image (count vs. color intensity) was taken using the ImageJ software (free software from National Institutes of Health). The amount of water in a hydrogel was calculated by integrating the histogram for the color intensity higher than 150.

3.4.7 Cell encapsulation into a hydrogel and analysis of the cell viability

PC12 cells, from a rat pheochromocytoma (ATCC), were expanded and passaged at 37 ºC with 5% CO_2 in F-12K medium supplemented by 15% horse serum, 2.5% fetal bovine serum and 1% penicillin/streptomycin (all from ATCC). All the cells before the passage number of 7 were used in this study. The PC12 cells were resuspended in 1 mL of the pre-gelled solution which contained 10 wt % of a gel-forming polymer and 0.01 wt % of Irgacure 2959. The cell density was kept constant at 3×10^6 cells mL^{-1}. The cell-encapsulating gel disks (5 mm diameter, 1 mm thickness) were made, as described in the section 2.4, and incubated in the cell growth medium for one day.

The viability of encapsulated cell was evaluated by adding 0.1 mL of a growth medium and 0.01 mL of MTT (3-(4,5-dimethylthiazol-2-yl)-2,5-diphenyltetrazolium bromide) reagent (ATCC)

into a well of a 96-well plate which contains each gel disk. Following the addition of MTT reagent, the medium was incubated for four hours at 37 ℃ with 5% CO_2 while being gently shaken. Live cells (stained as dark purple) in the hydrogels were imaged using a CCD camera (Leica D-LUX 3) mounted on an inverted microscope (Leica DMIL). The live cell fraction was further quantified by adding 0.1 mL of a MTT detergent solution (ATCC) to each well and further incubating at 37 ℃ overnight to dissolve the dark purple product. The gel disk was removed from each well, and the absorbance of the surrounding medium at 570 nm was measured using a spectrophotometer (Synergy HT, Biotek).

3.4.8 Release of serum protein from hydrogels

0.1 mL of fetal bovine serum (Invitrogen) was included in 1 mL of gel-forming polymer solution. The gel-forming polymer consisted of PEGDA and varying concentration of methacrylate alginate (0 to 2.4 wt %), while keeping the total concentration at 10 wt %. Hydrogel was fabricated as described in Section 2.4.4. Each hydrogel disk (10 mm in diameter, 1 mm in thickness) was placed in 0.5 mL of PBS, and incubated at 37 ℃ for 3 days. The PBS was collected and the protein content was analyzed with BCA Protein Assay Kit (Thermo Scientific) following the manufacturer's instructions.

3.5 Figures

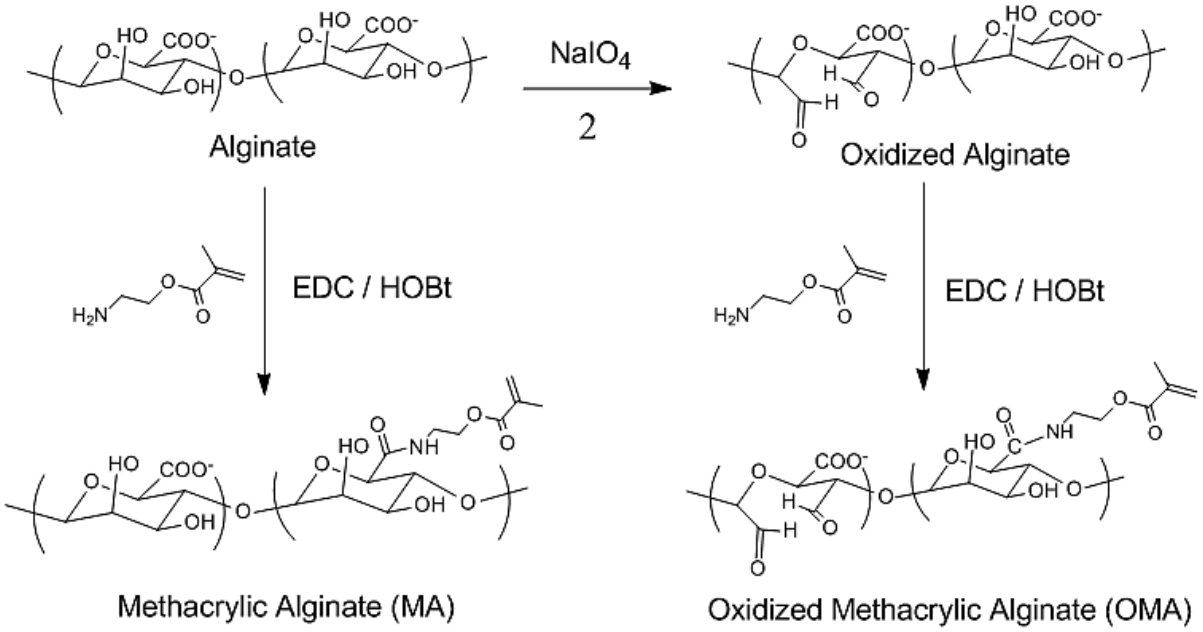

Figure 3.1 2-aminoethyl methacrylate was conjugated to alginate by amide-forming EDC chemistry to make methacrylic alginate (MA). To induce hydrogel degradation, alginate was oxidized to present hydrolytically labile functional groups prior to conjugation of methacrylate to prepare oxidized methacrylic alginate.

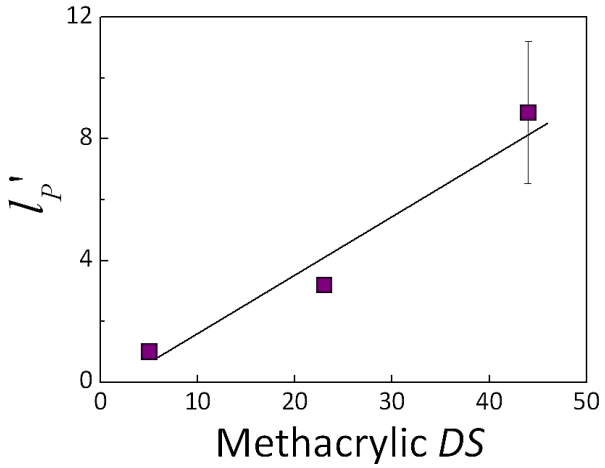

Figure 3.2 Persistence length (l_P) of various methacrylic alginate molecules, calculated from their radius of gyration (R_G) values measured using static light scattering. The l_P values were normalized with the l_P value of MA-1 to demonstrate the relative difference among different methacrylic alginate molecules (denoted as l_P').

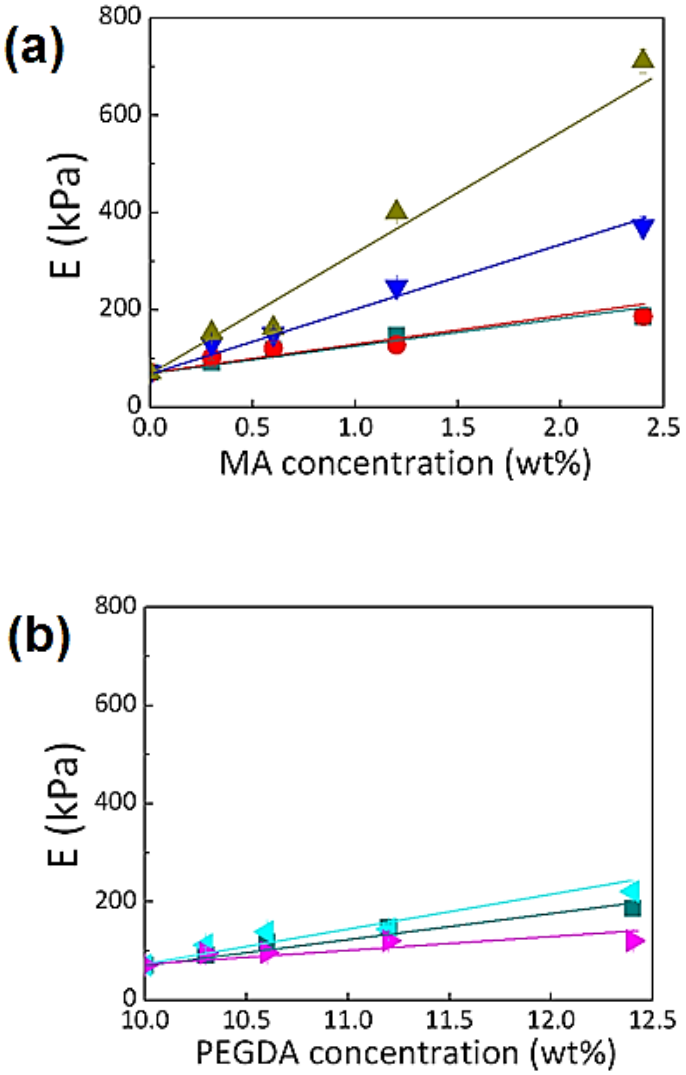

Figure 3.3 Elastic moduli (*E*) of PEGDA hydrogels copolymerized with (a) methacrylic alginate or (b) PEGDA with varying M_W. The concentration of PEGDA 400 was kept constant at 10 wt % while increasing the concentration of MA with varying methacrylic *DS* (MA-1(●), MA-2 (▼), and MA-3(▲)) or high M_W PEGDA (PEGDA 2000 (◀) and PEGDA 14000 (▶)) up to 2.5 wt %. For pure PEGDA 400 hydrogel, the same amount of PEGDA 400 was increased up to 2.5 wt % for comparison (■).

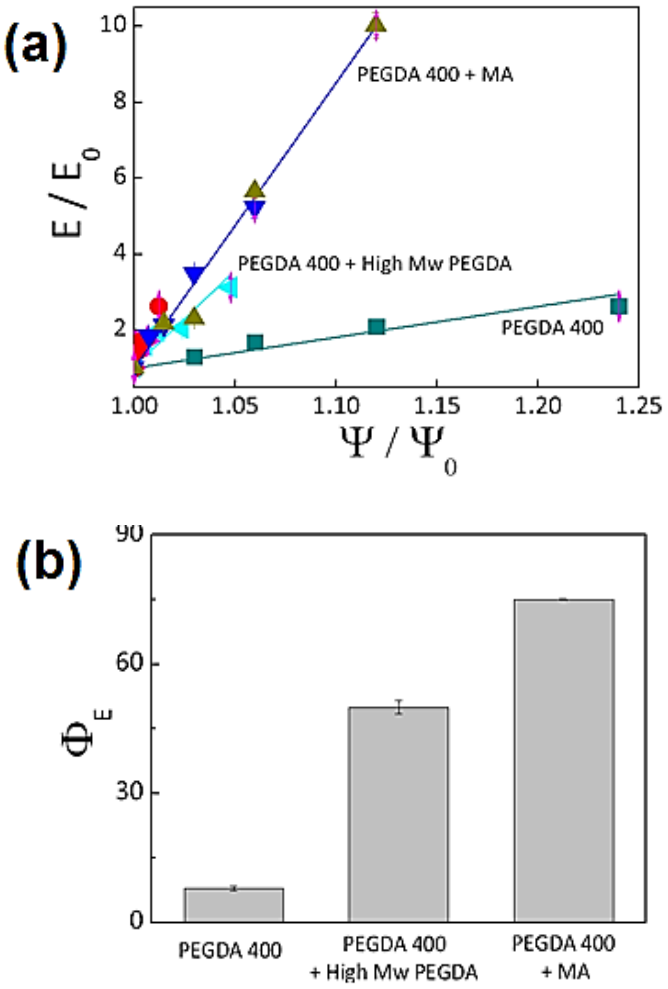

Figure 3.4 (a) Normalized elastic modulus (E/E_0) values of hydrogels were related to the normalized density of methacrylic groups (Ψ/Ψ_0). E and Ψ were normalized to those of pure PEGDA 400 hydrogel at 10 wt % (E_0, Ψ_0). (b) The stiffening efficiency (Φ_E), defined as the slope of E/E_0 and Ψ/Ψ_0 in (a), increased with incorporation of MA into PEGDA 400 hydrogel.

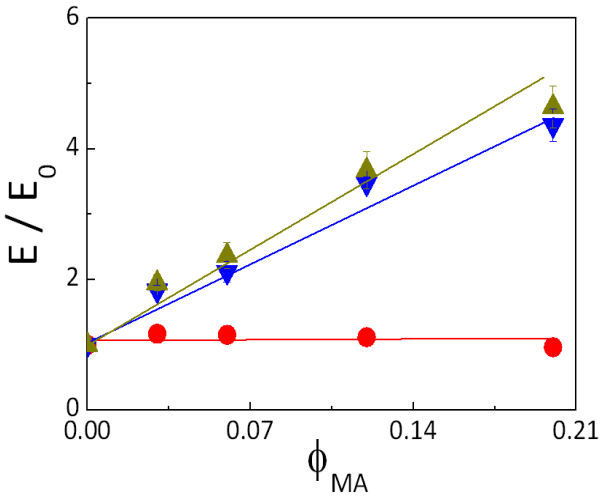

Figure 3.5 Normalized elastic modulus (E/E_0) values of PEGDA 400-MA hydrogels were also increased with mass fraction of MA (ϕ_{MA}) at a constant total concentration of 10 wt %. E was normalized to that of pure PEGDA 400 hydrogel at 10 wt % (E_0). ●, ▼, and ▲ represent PEGDA 400 hydrogel reinforced by MA-1, MA-2, and MA-3, respectively.

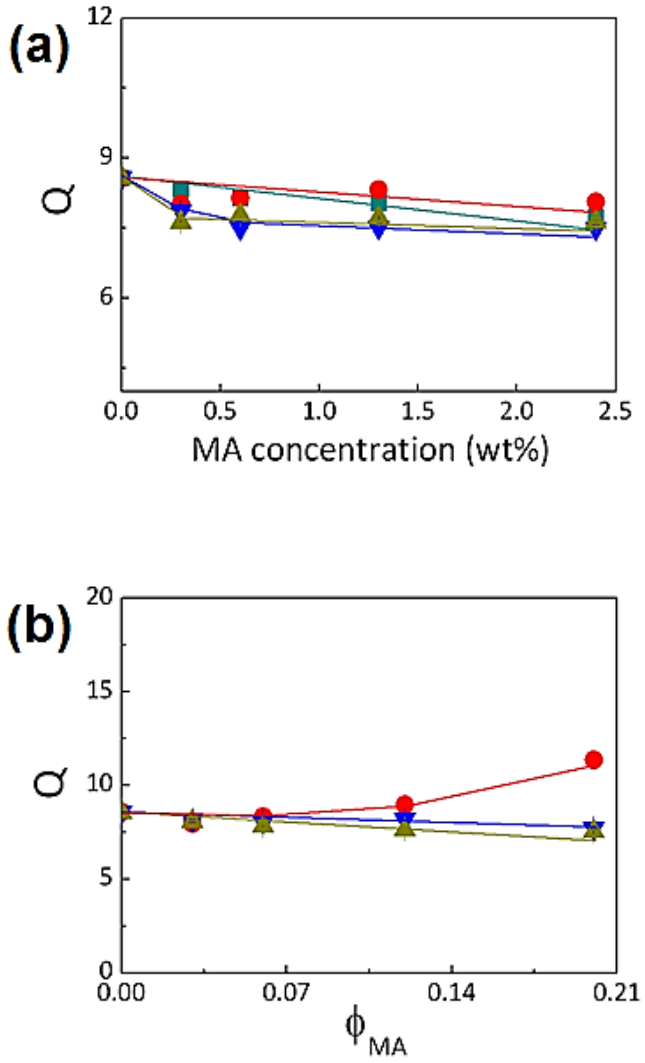

Figure 3.6 (a) Incorporation of MA into PEGDA 400 hydrogel made minimal change of the swelling ratio (*Q*) of a hydrogel, independent of the concentration and methacrylic *DS*. The concentration of PEGDA 400 was kept constant at 10 wt % while increasing the concentration of MA with varying methacrylic *DS* (MA-1(●), MA-2 (▼), and MA-3(▲)) up to 2.5 wt %. For pure PEGDA 400 hydrogel (■), the same amount of PEGDA 400 was increased up to 2.5 wt %. (b) Increasing the mass fraction of methacrylic alginate (ϕ_{MA}) while keeping the total concentration at 10 wt % also made minimal change of the swelling ratio (Q) of the hydrogel. In (b), ●, ▼, and ▲ represent PEGDA 400 hydrogels reinforced by MA-1, MA-2 and MA-3, respectively.

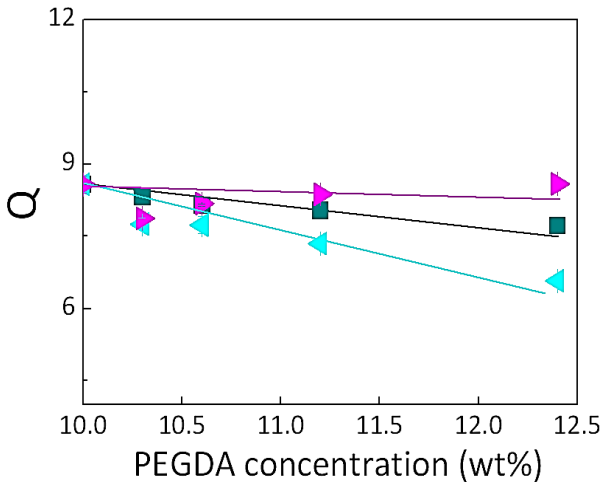

Figure 3.7 Swelling ratio (Q) of PEGDA hydrogels with varying M_W. The concentration of PEGDA 400 was kept constant at 10 wt% while increasing the concentrations of high Mw PEGDA (PEGDA 2000 or PEGDA 14,000) up to 2.5 wt%. For pure PEGDA 400 hydrogel, the same amount of PEGDA 400 was increased up to 2.5 wt% for comparison. PEGDA 400 (■), PEGDA 400 with PEGDA 2000 (◀), PEGDA 400 with PEGDA 14000 (▶).

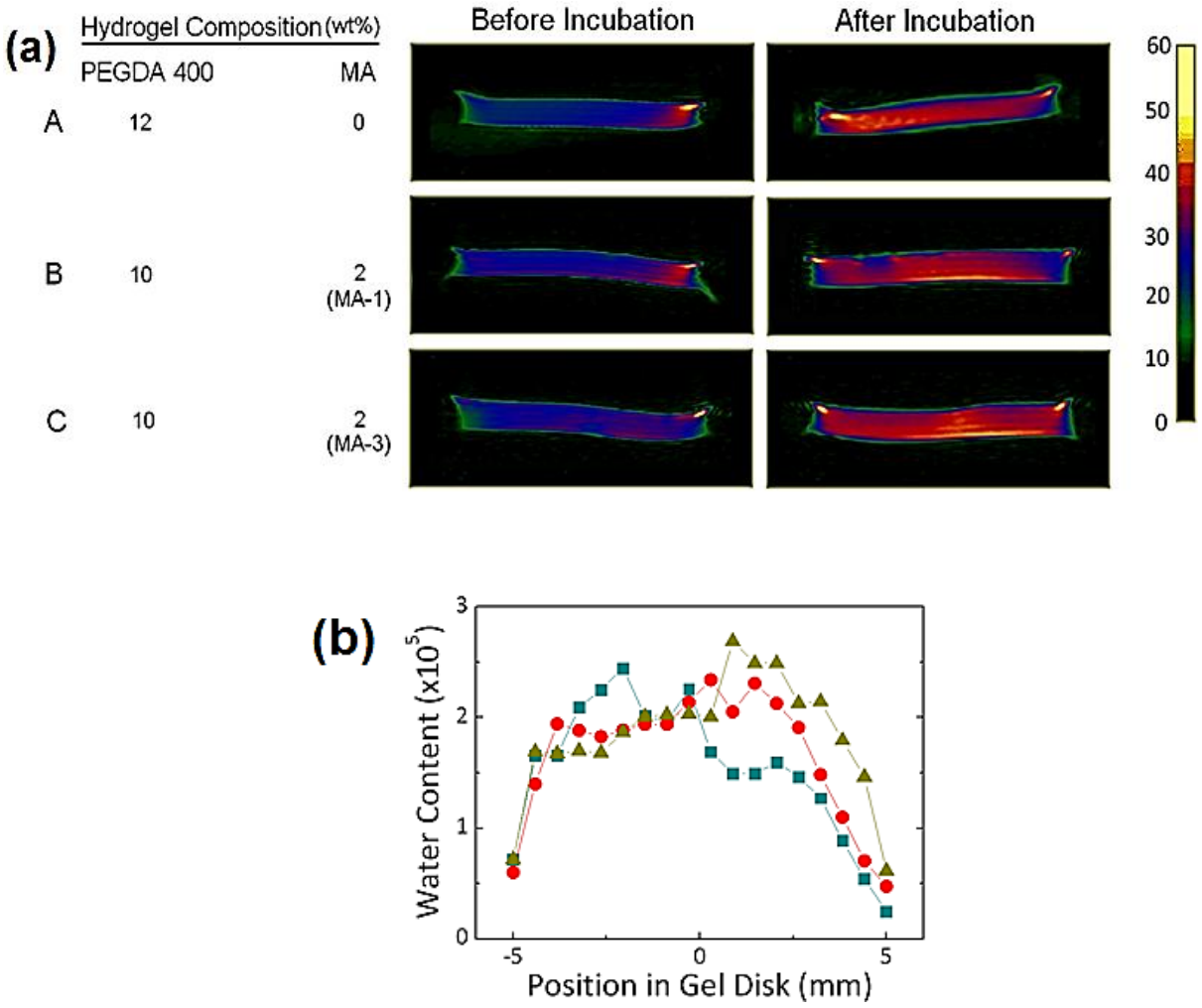

Figure 3.8 (a) The water distribution through the hydrogel before and after the incubation in PBS (I_{PBS} = 0.22 M) was visualized with magnetic resonance imaging (MRI). Total polymer concentration of a hydrogel was kept constant at 12 % (w/w), and the mass fraction of MA with varying methacrylic *DS* was changed from 0 to 0.02. Pseudo-color was added to show the water proton peak intensity (see the scale bar on the right). (b) The distribution of water in a hydrogel was quantified by dissecting the images along the horizontal axis, and calculating the amount of water in each segment. In (b), ■ represents pure PEGDA 400 hydrogel. ● and ▲ represent PEGDA 400 hydrogels reinforced by MA-1 and MA-3, respectively.

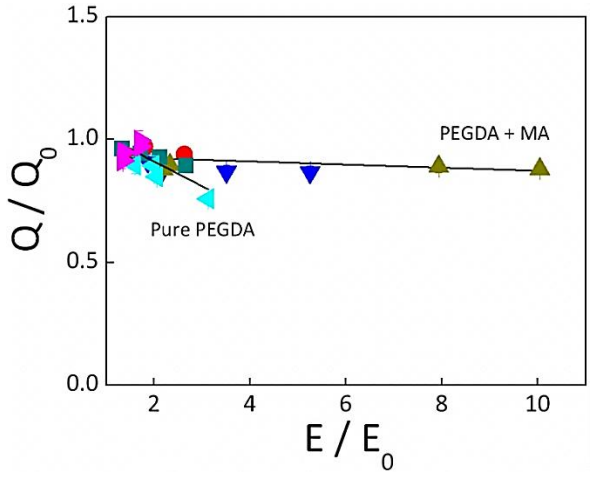

Figure 3.9 Normalized elastic modulus (E/E_0) and swelling ratio (Q/Q_0) were related to each other. E and Q were normalized to those of pure PEGDA 400 hydrogel at 10 wt% (E_0, Q_0). The elastic modulus was inversely related to the swelling ratio for the pure PEGDA hydrogel, whereas incorporation of methacrylic alginate (MA) into the PEGDA 400 hydrogel made minimal change in the swelling ratio independent of elastic modulus. ■ represents pure PEG400 hydrogel. ●, ▼, and ▲ represent PEGDA 400 hydrogel reinforced by MA-1, MA-2, and MA-3, respectively. ◀ and ▶ represent PEGDA 400 hydrogels reinforced by PEGDA 2000 and PEGDA 14000, respectively.

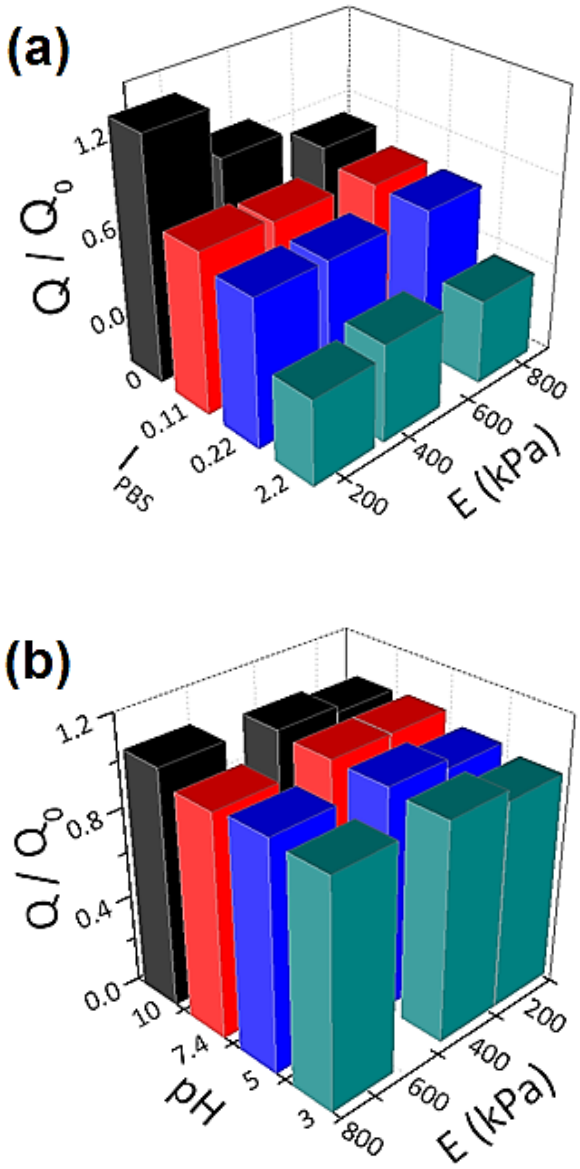

Figure 3.10 Normalized swelling ratio (Q/Q_0) and elastic modulus (E) of PEGDA-methacrylic alginate hydrogels were related to (a) ionic strength (I_{PBS}) and (b) pH of the incubating medium (PBS). The swelling ratio values (Q) of a hydrogel were normalized to the swelling ratio at I_{PBS} of 0.22 M and pH of 7.4 (Q_0).

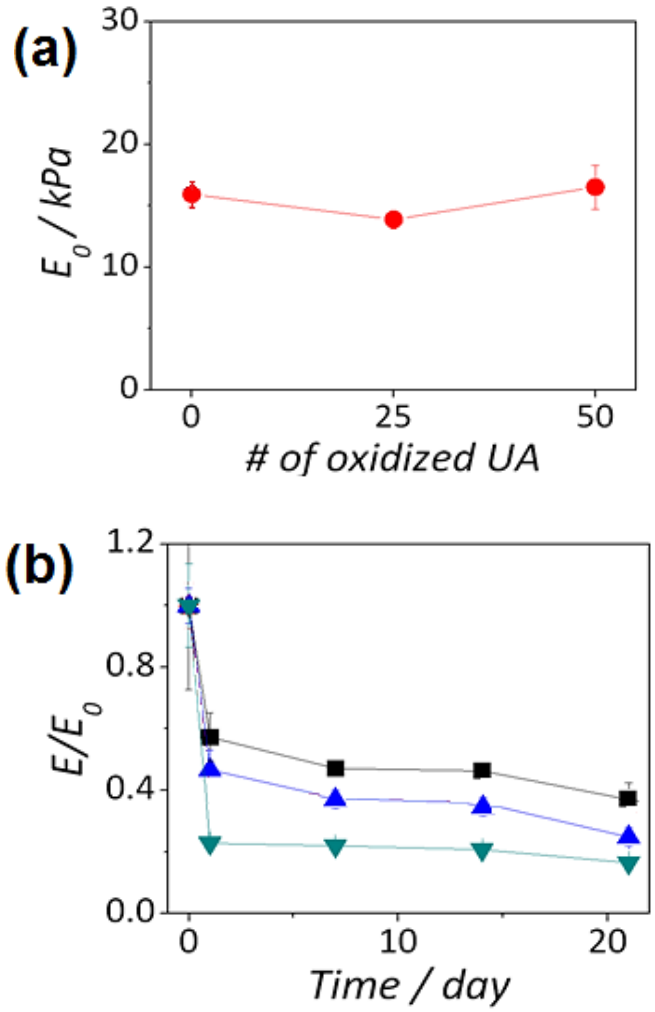

Figure 3.11 (a) The initial elastic moduli (E_0) of PEGDA-OMA hydrogels were independent of the number of oxidized uronic acid (oUA) residues per OMA molecule. (b) The hydrogels were incubated in PBS at 37 ℃, and the changes in their elastic moduli (E/E_0) were measured over time. E values at various time points were normalized with those measured before incubation (E_0). ■ hydrogel cross-linked with MA (0 oUA), ▲ hydrogel cross-linked with OMA (25 oUA), and ▼hydrogel cross-linked with OMA (50 oUA).

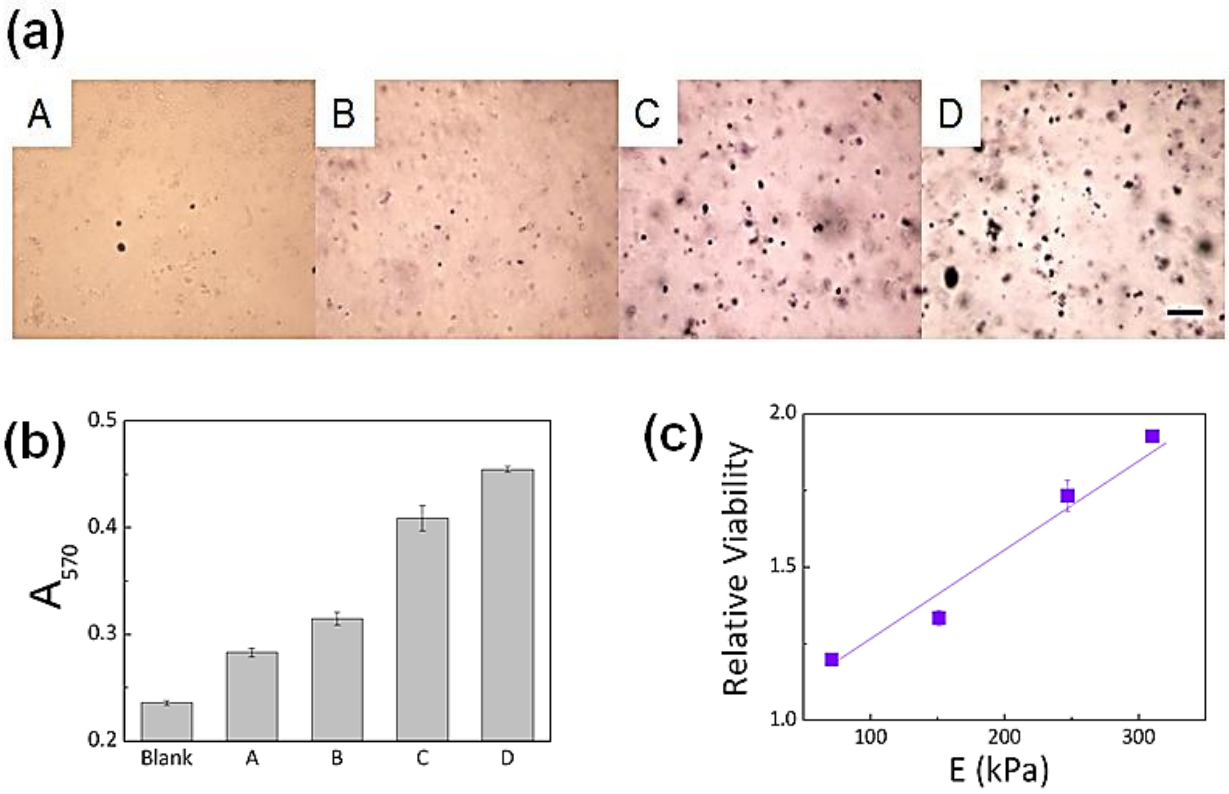

Figure 3.12 (a) PC12 cells encapsulated in PEGDA 400 hydrogels (A) and PEGDA 400 hydrogels with varying amounts of methacrylic alginate (B,C,D) were stained with MTT (dark purple in live cells). The total polymer concentration was kept constant at 10 wt%, while increasing the mass fraction of methacrylic alginate. A: pure PEGDA 400 (10 wt %), B: PEGDA 400 (9.4 wt %) + MA-2 (0.6 wt %), C: PEGDA 400 (8.8 wt %) + MA-2 (1.2 wt %), D: PEGDA (7.6 wt %) + MA-2 (2.4 wt %). (Scale bar: 100 μm) (b) The amounts of live cells in the hydrogels were quantified by dissolving the MTT product and measuring the absorbance at 570 nm (A_{570}). In (b), blank condition represents the negative control (assay performed on cell growth media). (c) The relative cell viability, calculated as the absorbance value of each condition normalized with that of negative control (blank) shown in (b), was related to the elastic modulus (E) of the hydrogel.

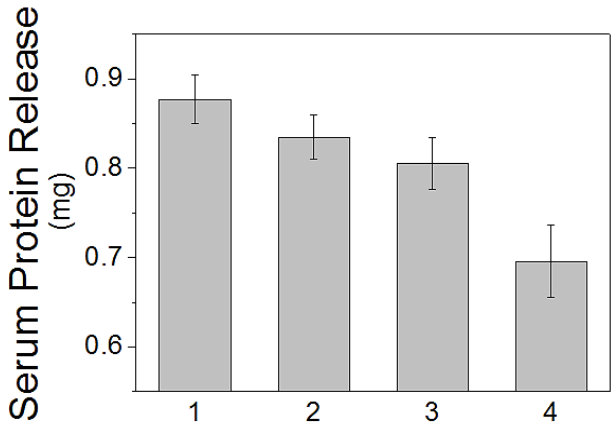

Figure 3.13 Amount of serum protein released from hydrogels was measured. Hydrogels consisted of PEGDA and methacrylate. The total polymer concentration was kept constant at 10 wt%, while increasing the mass fraction of methacrylic alginate. **1**: pure PEGDA 400 (10 wt %), **2**: PEGDA 400 (9.4 wt %) + MA-2 (0.6 wt %), **3**: PEGDA 400 (8.8 wt %) + MA-2 (1.2 wt %), **4**: PEGDA (7.6 wt %) + MA-2 (2.4 wt %)

Chapter 4 Polyaspartamide-Based Linkers Allow Single-Step Conjugation of Protein to Materials

4.1 Introduction

A variety of organic and inorganic materials are widely used in the assembly of in vitro cell culture platforms, biomedical implants, and bio-microelectromechanical systems (bio-MEMS) devices.[6,19,86-89] These materials are usually chemically linked with a series of proteins, such as fibronectin, collagen, and antibodies, in order to control cellular adhesion to the materials.[90,91] The number and spacing of these proteins act as insoluble signals to regulate cellular phenotypes.[7,10,25] Various forms of bi-functional linkers are increasingly used for stable protein conjugation.[92-95] These linkers largely contain two monovalent functional groups: one reactive to a protein and the other reactive to a material. These linkers require multiple modification and purification steps during molecular synthesis and protein conjugation to target substrates, thus necessitating extensive labor. In addition, the number of monovalent linkers should increase in tandem with the amount of protein conjugated to the materials due to their monovalency, which raises concerns over increased cytotoxicity and inadvertent changes in material properties.

To resolve these challenges encountered with the use of monovalent linkers, this study presents a simple top-down synthetic strategy to prepare a polyaspartamide linker with controlled multivalencies of reactive groups to both proteins and materials. In addition, this study also

demonstrates that the polymeric linkers allow us to conjugate cell adhesion proteins with a single step. Polysuccinimde (PSI) consists of a series of succinimidyl units which allow ring-opening nucleophilic addition.[96,97] In this study, we partially opened the succinimidyl rings of PSI with a controlled amount of amine-based nucleophiles that are reactive to a target material, in order to create a polyaspartamide linker in a top-down manner. The protein of interest, which also contains amine groups, would be conjugated to the intact succinimidyl groups of polyaspartamide in the same fashion as the amine-based nucleophilic substituents. This synthetic strategy allows the linker to present a variety of functional groups needed for conjugation to specific materials simply by using nucleophiles containing different functional groups. Here, we demonstrate the function and versatility of this polyaspartaminde linker with two applications: (1) protein conjugation to a hydrogel using a polyaspartamide linker containing methacrylic groups; and (2) protein conjugation to a gold coated bio-MEMS device using a polyaspartamide linker containing thiol groups.

4.2 Results

4.2.1 Synthesis of polysuccinimide

Polysuccinimide (PSI) with the average molecular weight of 22,000 g mol^{-1} was polymerized by acid-catalyzed polycondensation of aspartic acid and used as a starting molecule (Figure 4.1, **I**).[98] The chemical structure was determined from ^{1}H-NMR, and the molecular weight of PSI determined by gel permeation chromatrography was 22,000 g mol^{-1}. Ths PSI consists of a series of succinimidyl ring moieties that allow ring-opening nucleophilic reaction of amine-functionalized molecules.

4.2.2 Synthesis of poly(2-hydroxyethyl-co-2-methacryloxyethyl aspartamide)

First, a polyaspartamide linker that can conjugate cell adhesion proteins to a hydrogel was prepared. For this purpose, designated amounts of ethanolamine and 2-aminoethyl methacrylate were added sequentially to PSI to prepare poly(2-hydroxyethyl-co-2-methacryloxyethyl aspartamide) (PHMAA) (Figure 4.1, **II**). The addition of 2-aminoethyl methacrylate to PSI presented the linker with methacrylic groups needed for radical polymerization. The ethanolamine allowed us to control the number of unreacted succinimidyl groups independent of the number of methacrylic groups, and also to render the linker water-soluble by presenting hydroxyl groups.

The ability of PHMAA to co-polymerize with gel-forming monomers was evaluated by examining whether the PHMAA can cross-link acrylamide monomers to form a hydrogel, and to further control hydrogel properties. PHMAA was able to cross-link acrylamide to form a hydrogel via in situ free radical polymerization (Figure 4.2). Furthermore, the PHMAA could

increase the elastic modulus and resistance to fracture of the hydrogel with the number of methacrylate (Figure 4.3a). PHMAA was then reacted with fibronectin (Fn), a cell adhesion protein, to prepare Fn reactive to a hydrogel (Fn-PHMAA) (Figure 4.1, **III**). The reaction between PHMAA and Fn was confirmed by monitoring the decrease of free amine groups quantified with TNBS (trinitrobenzenesulfonic acid) assay (Figure 4.3b).[99] Increasing the amount of Fn while keeping PHMAA constant led to a more rapid decrease of amine groups in the TNBS assay, indicating that the multivalency of unreacted succinimidyl groups in PHMAA could tune the number of Fn molecules linked with PHMAA.

4.2.3 Cell adhesion on Fn-PHMMA modified hydrogel surface

Fn-PHMAA was used to control the size and spacing of cell adhesion domains on a polyacrylamide hydrogel, combined with a micro-contact printing technique (Figure 4.4)[100] Briefly, a circular array of Fn-PHMAA was placed on a glass surface using a micro-contact stamp onto which the Fn-PHMAA was physically adsorbed. Both the diameter and spacing of the circles were kept constant at 500 μm. The subsequent in situ polymerization and cross-linking reaction of acrylamide on top of the micropatterened Fn-PHMAA resulted in a polyacrylamide hydrogel which presented circular arrays of fibronectin with regular size and spacing on its surface, as confirmed with immunofluorescent labeling (Figure 4.5). The fibronectin density per circular pattern was kept constant at 5 μg cm^{-2}. In contrast, the in situ polymerization and cross-linking reaction of acrylamide on top of pure Fn without PHMAA, a negative control, resulted in limited conjugation of Fn to the surface.

The circular patterns of Fn on the hydrogel were recognized by cells plated on the gel. Fibroblasts seeded on the hydrogel surface with circularly patterned Fn-PHMAA adhered exclusively on the patterned area (Figure 4.5). Furthermore, the cells adhered to the circular pattern proliferated over time, while remaining confined to the patterned area (Figure 4.6). In contrast, the hydrogel patterned with pure Fn displayed limited cell adhesion.

The same results were also observed when type I collagen and human airway smooth muscle cells (haSMCs) were used instead of Fn and fibroblasts (Figure 4.7). For this study, collagen linked with PHMAA was used to prepare the hydrogel with a circular array of collagen at a density of 10 μg cm^{-2}, following the same procedure as described in Figure 4.4. haSMCs exclusively adhered and proliferated within this circularly patterned hydrogel area. This result verifies that PHMAA can chemically link a variety of cell adhesion proteins to the hydrogel and control spatial organization of a wide array of anchorage-dependent cells.

4.2.4 Synthesis of poly(2-hydroxyethyl-co-2-mercaptoethyl aspartamide)

Poly(2-hydroxyethyl-2-mercaptoethyl aspartamide) (PHMCA) with the controlled number of thiol groups was synthesized for its use in protein conjugation to gold-coated inorganic substrates. Gold has been extensively used in biosensors such as bio-MEMS and surface plasmon resonance (SPR), due to its inertness, robust structural integrity, and excellent conductivity.[101,102] The same synthetic procedure to create PHMAA was used, except that cysteamine was used as a nucleophile to present thiol groups (Figure 4.8). The number of thiol groups in PHMCA, which are available to react with gold, was determined to be 10 per

molecules, according to a colorimetric assay using Ellman's reagent.[103] PHMCA was then mixed with Fn to prepare the Fn-PHMCA.

4.2.5 Fn-PHMCA on Bio-MEMS device for cell traction force measurement

Fn-PHMCA was used to chemically modify the surface of the gold-coated probe of a bio-MEMS device which is designed to measure cell traction force.[104,105] The bio-MEMS device is made from a single crystal silicon wafer, and the surface of its probe was coated with gold to prevent non-specific interaction with cells (Figure 4.9). Then, the probe was immersed in a solution of Fn-PHMCA to chemically link Fn to the probe (Figure 4.8). Separately, another device was also immersed in a solution of pure Fn as a negative control.

The probe modified with Fn-PHMCA or pure Fn was allowed to contact a fibroblast to form specific bonds between Fn and cellular integrins. The device was then pulled from the cell at a rate of 1 μm s^{-1}, and the force that the cell exerts to pull the probe from the device was calculated by the equation $F = k\delta$, where k is the spring constant of the sensor beams to which the probe is attached, and δ is the displacement of the probe from its original position (Figure 4.10a). The probe coated by the pure Fn was readily detached from the cell with only a small displacement (average $\delta \sim 6$ μm), indicating poor linkage between Fn and the probe. In contrast, the cell contacted by a Fn-PHMCA modified probe exerted a significant traction force resulting in an average δ of 55 μm. The maximum force generated with the Fn-PHMCA modified probe reached 185 nN, whereas the force generated with the Fn-modified probe was limited to only 20 nN (Figure 4.10b).

4.3 Discussion

This study presents a novel strategy of synthesizing versatile polyaspartamide linkers that allow convenient conjugation of proteins to a variety of materials. The synthetic strategy of introducing functional groups by nucleophilic addition to PSI in a top-down manner allowed us to independently control the number of units reactive to proteins and those to materials in a highly efficient manner. In addition, these linkers allow a convenient one-step conjugation of various proteins to organic and inorganic materials.

The polyaspartamide linker developed in this study fully utilizes the unique and favorable properties of PSI: (1) PSI can be easily synthesized by one-step polycondensation reaction of aspartic acid. This bypasses the necessity of multiple synthesis and purification steps required for many conventional systems. (2) A series of succinimidyl ring moieties in PSI allows nucleophilic addition reaction, thus allowing desirable functional groups to be conjugated simply by using nucleophiles which contain the functional groups. Amine-based nucleophiles are generally used to create polyaspartamide products, as primary amine groups undergo facile nucleophilic reaction with succinimidyl groups with high yield and result in stable amide bonds. (3) The PSI which undergoes the ring-opening nucleophilic reaction becomes a beta peptide structure which is stable, water soluble and biocompatible, and thus highly suitable for biological applications.

An important feature of the polyaspartamide linker that sets apart from other linkers and should be recognized is the controlled multivalency of reactive groups. Small molecule linkers generally have a limited number of reactive groups, so the amount of linkers should increase with the amount of protein, which may lead to unwanted change in material properties. On the

other hand, polyaspatamide linker has multiple reactive groups to both material and protein, thus the amount of linker can be kept constant and minimal. This multivalency of polyaspartamide linker could be easily controlled by the amount of nucleophiles used to conjugate functional groups to PSI. Furthermore, it does not require any additional chemicals to link functional groups (i.e. coupling agents, secondary linkers), as the amine-based nucleophiles are directly and efficiently conjugated to the PSI via ring-opening nucleophilic addition.

Another important feature of polyaspartamide linker is the versatility. As PSI allows ring-opening addition of amine-based nucleophiles to form polyaspartamide, a variety of molecules that contain an amine group and another functional group which is reactive towards a material could be presented to the polyaspartamide linker. In this study, we have explored the versatility of the linker by creating a polyaspartamide linker presenting thiol groups, as well as the linker presenting methacrylate for its use in hydrogels. The thiol-presenting polyaspartamide linker was successfully applied to conjugating a protein to a gold-coated bio-MEMs device. Thus, it is expected that it could be possible to further utilize a wide array of conjugation chemistries necessary for tailor-made materials.

4.4 Materials and Methods

4.4.1 Synthesis of poly(2-hydroxyethyl-co-2-methacryloxyethyl aspartamide) (PHMAA) and poly(2-hydroxyethyl-co-2-mercaptoethyl aspartamide) (PHMCA)

[Synthesis of polysuccimide]

Polysuccinimide (PSI) was synthesized by acid-catalyzed polycondensation of aspartic acid.[98] Briefly, L-aspartic acid (50 g, 376 mol, Sigma Aldrich) and o-phophoric acid (18 mmol, Fisher Scientific) were mixed in sulfolane (100 mL, Sigma Aldrich), and refluxed at 180 ℃ for 10 hours under dry N_2. Water formed during the reaction was continuously removed with a Dean-Stark trap. After the reaction, the product was precipitated in methanol. The product was filtered and washed several times with deionized (DI) water to remove excess acid catalyst, and the removal was confirmed with an electronic pH meter (Mettler Toledo). The molecular structure of the product was analyzed with ^{1}H-NMR (DMSO-d_6, Figure 4.11). The molecular weight of PSI was determined by gel permeation chromatography (Breeze 2 GPC, Waters), with Styragel® HT column (Waters). Dimethylformamide (DMF) containing 20 mM LiBr was used as the eluent, with the elution rate of 1 mL min-1. Polystyrene standards were used for calibration. Mn = 17,200 g mol^{-1}, Mw = 22,000 g mol^{-1}, PDI = Mw/Mn = 1.28.

[Syntheses of poly(2-hydroxyethyl-co-2-methacryloxyethyl aspartamide) (PHMAA) and poly(2-hydroxyethyl-co-2-mercaptoethyl aspartamide) (PHMCA)]

PSI (0.2 g, 0.009 mmol) was first dissolved in DMF (20 mL). Ethanolamine (Fisher Scientific) was added and stirred for 6 hours at 60 ℃ under dry N_2. Then, 2-aminoethyl methacrylate hydrochloride (AEMA, Sigma Aldrich) and triethylamine (TEA, Fisher Chemicals)

were added to the mixture and further stirred at room temperature overnight. The molar ratio of AEMA to TEA was 1:3. The insoluble salt formed (TEA-HCl) was removed by filtration. The product was precipitated in dry ether and filtered. The product was then washed with methanol 3 times, and dried under vacuum. The chemical structure of PHMAA was analyzed with ^{1}H-NMR (DMSO-d_6, Figure 4.12). The amount of AEMA was varied from 0.041 to 0.515 mmol to control the degree of methacrylate substitution, defined as the percentage of succinmidyl groups reacted with AEMA, from 2 to 25 %. The amount of ethanolamine was adjusted accordingly, from 0.825 to 1.299 mmol, so as to keep the percentage of unopened succimidyl groups constant at 35 %.

For the synthesis of poly(2-hydroxyethyl-co-2-mercaptoethyl aspartamide) (PHMCA), ethanolamine (1.44 mmol), cysteamine hydrochloride (0.21 mmol, Sigma Aldrich) and triethylamine (5 mmol) were dissolved separately in 1 mL of DMF and stirred for 10 minutes. Then, the mixture was added to PSI (0.2 g, 0.009 mmol) dissolved in 20 mL of DMF, and stirred at 60 ℃ overnight under dry N_2 gas. The product was acquired by precipitation in methanol, and analyzed with ^{1}H-NMR (DMSO-d_6, Figure 4.13). The degree of thiol substitution, defined as the percentage of succinimidyl groups reacted with cysteamine was 5 %, as determined by Ellman's test, indicating 50 % of cysteamine reacted to present thiol groups in PHMCA.

To account for the possible side reaction, in which cysteamine reacts with succinimidyl groups to form thioester linkage, elemental analysis was performed to determine the total number of sulfur in PHMCA (Microanalysis Laboratory, School of Chemical Sciences, University of Illinois). The percentage of thioester formation was calculated by, $(\Gamma_S - \Gamma_{SH})/\Gamma_S \times 100$, where

Γ_S is the total number of sulfur from the elemental analysis, and Γ_{SH} is the number of thiol from Ellman's test.

[Quantification of thiol groups in PHMCA with Ellman's test]

The number of thiol groups in PHMCA was determined with a colorimetric assay using Ellman's reagent.[103] Briefly, PHMCA dissolved in 10 μL of water was mixed with 990 μL of Ellman's reagent (0.1 mM 5,5'-dithio-bis(2-nitrobenzoid acid) and 2.5 mM sodium acetate dissolved in 0.1 M Tris buffer (pH 8.0)). After 5 minutes of incubation at room temperature, the absorbance at 415 nm was obtained with a spectrophotometer (Synergy HT, BioTek). The assay was also performed on varying amounts of cysteamine standards to obtain a standard curve.

4.4.2 Preparation and characterization of PHMAA-crosslinked hydrogel

[PHMAA cross-linked polyacrylamide hydrogel formation]

1 mL of pre-gel solution consisting of 8 wt % of acrylamide (Fluka), 3 wt % of PHMAA, and 0.1 wt % of Irgacure 2959 (Ciba), was prepared. The solution was placed between two glass plates with a 1 mm spacer, and irradiated with ultraviolet (UV) light (Jelight Co.) for 10 minutes to form a hydrogel.

[Evaluation of mechanical properties of the hydrogel]

Hydrogel disks (10 mm diameter) were incubated in phosphate buffered saline (PBS) for 24 hours at 37 ℃. Then, each gel disk was subjected to uniaxial compression at the rate of 1 mm min^{-1} (Insight, MTS Systems).[52] The elastic modulus was calculated from the slope of a stress

vs. strain curve at the first 10 % strain. The hydrogel toughness was evaluated by measuring the tensile energy. The rectangular hydrogel strip (3 × 5 cm) was subjected to uniaxial stretching at the rate of 1 mm min^{-1}, until the gel strip was fractured into two pieces. The tensile energy (in J kg^{-1}) was quantified by first calculating the area under the force vs. displacement curve to acquire the tensile work, then dividing it by the mass of the hydrogel.

4.4.3 Conjugation of fibronectin (Fn) (or type I collagen) to PHMAA

Fibronectin (Fn) (BD Biosciences) was dissolved in phosphate buffered saline (PBS, pH 7.4) at the concentrations of 0.02 or 0.1 mg mL^{-1}. 1 mg of PHMAA (or PHMCA) was added to 1 mL of each Fn solution, and stirred at room temperature for 4 hours. The conjugation was confirmed with TNBS (trinitrobenzenesulfonic acid) assay which measures the amount of primary amine groups.[99] Briefly, a sample of 0.05 mL was taken from the reaction mixture at each time point. Then, 0.05 mL of TNBS working solution (0.1 % TNBS, 4 % $NaHCO_3$, pH 8.5) was added to the sample and allowed to react for 2 hours at 37 ℃. After the reaction, 0.05 mL of 10 % sodium dodecyl sulfate was added, followed by addition of 0.05 mL of 1 M HCl. The absorbance at 335 nm was read using a spectrophotometer (Synergy HT, BioTek). To conjugate type I collagen to PHMAA, 1 mg of PHMAA was added to 1 mL of type I collagen solution (1 mg mL^{-1}), and stirred for 4 hours at room temperature. The collagen solution was prepared by diluting a 3 mg mL^{-1} stock solution (Advanced BioMatrix) with 1 M HEPES buffer (pH 7.5), and kept on ice before the addition of PHMAA. The percentage of free amine groups in Fn reacted with succinimidyl groups of PHMAA was assessed by the decrease of absorbance in the TNBS assay (Table 4.1).

4.4.4 Covalent attachment of Fn-PHMAA on hydrogel surface

[Micropatterning of Fn-PHMAA (or collagen-PHMAA) on a glass surface by micro-contact printing]

Fn-PHMA (or collagen-PHMAA) was placed on top of a PDMS stamp which consists of an array of circular posts with a diameter of 500 um (Figure S3), and incubated at 37 ℃ for 2 hours.5 The Fn-PHMAA solution on top of the PDMS was removed, and the PDMS stamp was dried by blowing dry N_2 gas. The PDMS stamp was placed on top of a glass slide and gently pressed, followed by incubation at 37 ℃ for 1 hour. The PDMS stamp was removed, and the glass slide was kept under vacuum until further use. Pure Fn (or collagen) was used as a negative control.

[Hydrogel formation on Fn-PHMAA (or collagen-PHMAA) patterned glass]

Glass coverslips (1.8 × 1.8 cm) were treated with 0.4 % 3-(trimethoxysilyl propyl) methacrylate (pH 3.5, adjusted with glacial acetic acid) for 1 hour, in order to allow covalent bonding of hydrogel to the coverslip via co-polymerization.[106] A pre-gel solution, which consists of 8 wt % acrylamide and 0.2 wt % N,N,N',N'-methylenebisacrylamide, was added wit 0.1 wt % of ammonium persulfate and 0.1 wt % of tetramethylethylenediamine to initiate the polymerization. The solution was placed on a Fn-PHMAA (or collagen-PHMAA) micropatterned glass slide, and immediately covered with a pre-treated coverslip. After 30 minutes to allow the hydrogel to form, the coverslip was gently detached from the glass slide. The hydrogel is attached on the coverslip, not on the glass slide. The hydrogel was washed

with PBST (PBS supplemented with 0.05 % Tween 20) 3 times to remove unreacted Fn-PHMAA (or collagen-PHMAA), followed by washing with PBS.

[Immunofluorescent labeling of Fn-PHMAA (or collagen-PHMAA) patterned hydrogel]

To confirm the covalent attachment of micropatterned Fn-PHMAA (or collagen-PHMAA) on the hydrogel surface, immunofluorescent labeling with an antibody was used.[107] Briefly, the Fn-PHMAA (or collagen-PHMAA) conjugated hydrogel was incubated in a blocking solution (1 % BSA and 0.05 % sodium azide in PBS) for 30 minutes. After removing the blocking solution, the hydrogel was incubated with a primary antibody (mouse anti-fibronectin antibody, mouse anti-type I collagen antibody (Sigma Aldrich)) for 2 hours at room temperature. After washing with PBST 3 times, the hydrogel was incubated with fluorescent-labeled secondary antibody (anti-mouse IgG-FITC, Sigma Aldrich) for 2 hours at room temperature. After removing secondary antibody and washing with PBST 3 times, the fluorescent image of the hydrogel surface was captured with a fluorescence microscope (DM6000 B, Leica). The dilution ratios of primary and secondary antibodies were 1:500 and 1:200, respectively.

4.4.5 Cell culture on Fn-PHMAA (or collagen-PHMAA) patterned hydrogel

[Fibroblast culture on Fn-PHMAA patterned hydrogel]

To test the functionality of Fn-PHMAA, fibroblasts (NIH 3T3, from American Type Cell Culture) were placed on the hydrogel surface patterned with Fn-PHMAA. 1×10^4 cells suspended in 0.1 mL of culture medium (Dulbecco's Modified Eagle Medium (DMEM) supplemented with 10 % fetal bovine serum and penicillin/streptomycin, all purchased from

Invitrogen) were placed on top of each hydrogel. The cells were incubated at 37 ℃ with 5 % CO_2 for 1 hour to allow the cells to adhere to the hydrogel surface. Then, the hydrogel was washed with PBS to remove unbound cells, and further incubated in fresh culture medium. The cells growing on the hydrogel were imaged with a CCD camera mounted on an inverted microscope (Leica DMIL).

To visualize the actin organization and nuclei of the cells adhered on the hydrogel, the cells were stained with fluorescently labeled phalloidin (Alexa Fluor® 488 phalloidin) and 4',6-diamidino-2-phenylindole (DAPI). The fluorescent image of the cells was captured with a fluorescence microscope (DM6000 B, Leica).

[Human airway smooth muscle cell culture on collagen-PHMAA patterned hydrogel]

Primary human airway smooth muscle cells (haSMCs) were isolated using a previously described method.[108] Briefly, human bronchi from lung specimens incidental to patient surgery (Mayo Clinic, Rochester, MN) were used to obtain haSMCs (de-identified specimens not considered human subjects research; approved by Mayo Clinic Institutional Review Board). Specimens were derived from lobectomy or pneumenectomy samples where surgeries were performed for removing localized tumors or for transplant. Specimens removed for metastatic tumors or infections were not used. Bronchial samples were immersed in ice-cold Hanks' Balanced Salt Solution (HBSS, with 2.5 mM Ca^{2+}), the epithelial layer was removed by blunt dissection, and then the haSMC layer was excised and finely minced in ice-cold Ca^{2+}-free HBSS. The cells were isolated using collagenase digestion, followed by ovomucoid/albumin separation. The collected cells were resuspended in culture medium (DMEM/F-12K (50:50) supplemented

with 10 % fetal bovine serum and penicillin/streptomycin, all purchased from Invitrogen), and plated on a tissue-culture flask. The cells were expanded and passaged twice before use.

1×10^4 cells suspended in culture medium were placed on top of collagen-PHMAA patterned hydrogel, and incubated at 37 ℃ with 5 % CO_2 for 1 hour to allow the cells to adhere to the patterns. Then, the hydrogel was washed with PBS to remove unbound cells, and further incubated in fresh culture medium. The cells growing on the hydrogel were imaged with a CCD camera mounted on an inverted microscope (Leica DMIL).

4.4.6 Fn-PHMCA treatment of gold-coated bio-MEMS force sensor

The bio-MEMS device used to measure a cell-exerted traction force is depicted in Figure 4.9. The device was made by fabricating single-crystal silicon wafer using a modified SCREAM (Single-Crystal Reactive Etching and Metallization) process. The detailed fabrication procedure is described elsewhere.[104,105] The probe of the bio-MEMS device was coated with 10 nm chrome followed by 40 nm gold by evaporative deposition. The device was immersed in Fn-PHMCA (0.020 mg mL^{-1} of Fn) solution for 6 hours, followed by washing in PBS and deionized water for 1 hour each.

4.4.7 Imaging and force calculation.

The experimental setup for the force measurement using the bio-MEMS device is depicted in Figure 4.9. The device is mounted on a holder which is connected to a piezo actuator that can move in x-, y-, and z-direction by 1 nm resolution. Fibroblasts were plated on a tissue-cultured petri dish (35 mm), and incubated in the culture medium at 37 ℃ with 5 % CO_2 for one hour,

and then the dish was placed on the microscope stage. The position of the dish and the focus of the microscope were adjusted to visualize the cell to be measured. Then, the device was moved so that the probe contacted the cell, as evidenced by a small indentation of the cell. After 30 minutes, the device was slowly moved away from the cell in a lateral direction (+x direction), controlled with the piezo actuator at a rate of 1 μm min^{-1}. The entire process of the cell force measurement was monitored and recorded with a CCD camera (Olympus MagnaFire) mounted on an inverted microscope (Olympus CK40).

The traction force (F) exerted by the cell was calculated using the following equation,

$$F = k\,\delta \tag{10}$$

where k was the spring constant of sensor beams to which the probe was attached (3.4 nN μm^{-1}),[105] and δ was the maximum displacement of the sensor beams, measured by the distance between the reference point and the measure point of the device.

4.5 Figures & Tables

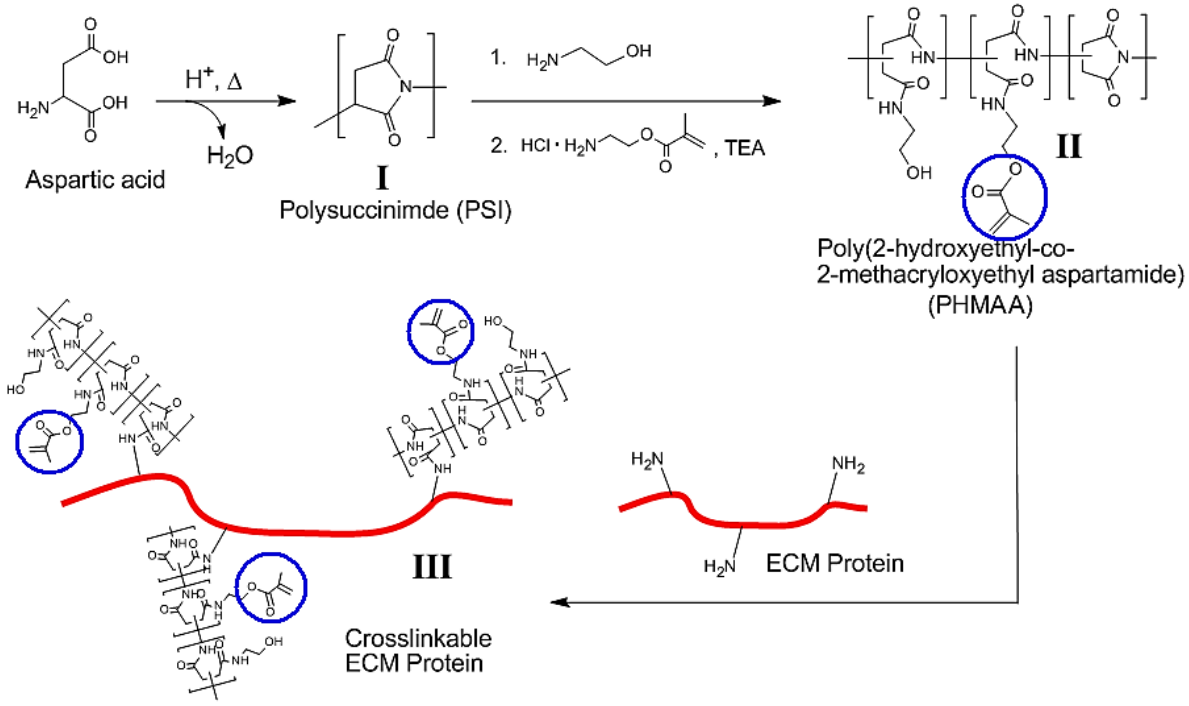

Figure 4.1 Synthesis of poly(2-hydroxyethyl-co-2-methacryloxyethyl aspartamide) (PHMAA) linker, and its linkage to ECM protein. Polysuccinimide (PSI) was first synthesized by acid-catalyzed polycondensation reaction of aspartic acid (**I**). PSI was then treated with ethanolamine and 2-aminoethyl methacrylate to form PHMAA via ring-opening nucleophilic addition (**II**). Finally, PHMAA was linked to ECM by the same mechanism (**III**).

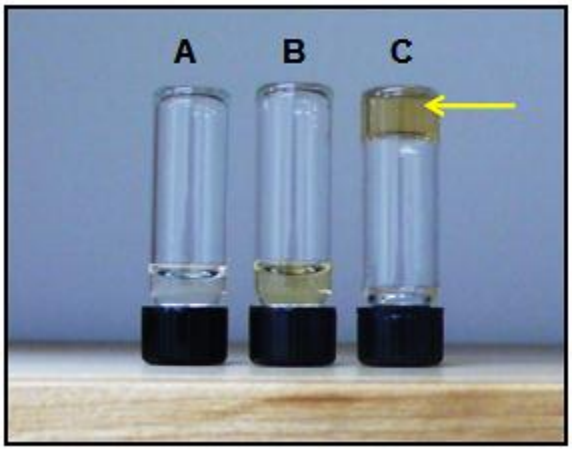

Figure 4.2 The ability of PHMAA to co-polymerize with gel-forming polymers was confirmed by using it to cross-link acrylamide to form hydrogel. PHMAA could cross-link acrylamide to form a hydrogel (**C**), whereas acrylamide (**A**) or PHMAA (**B**) alone at the same concentration could not form hydrogel.

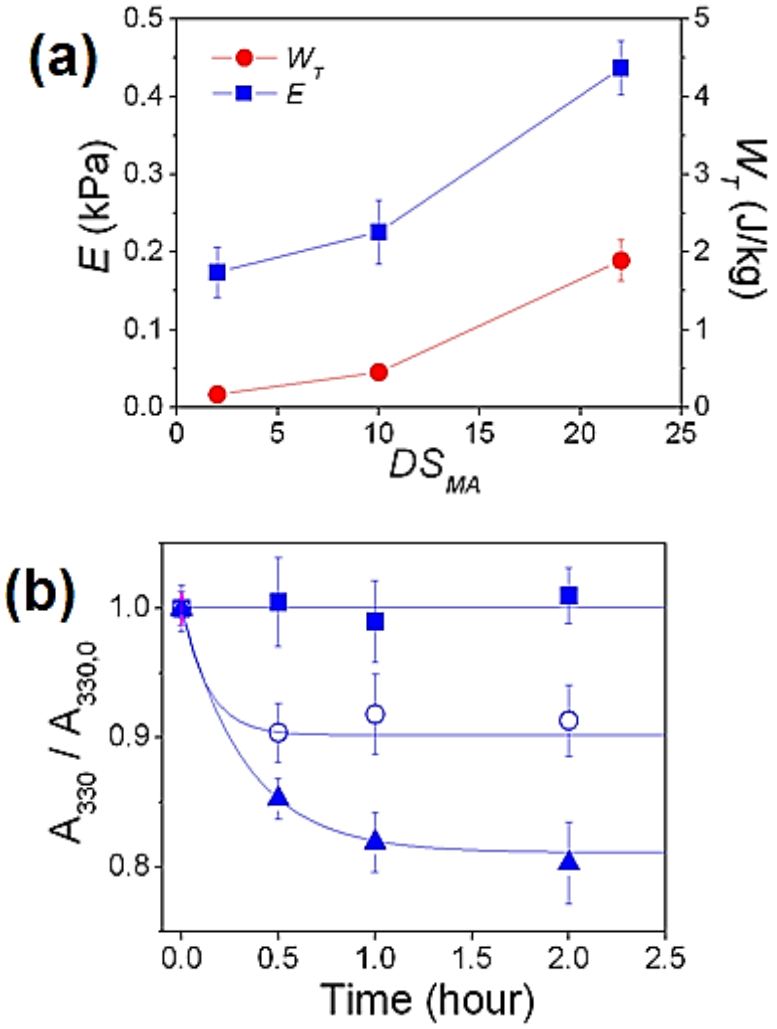

Figure 4.3 (a) Elastic modulus (E) and tensile energy (W_T) of polyacrylamide hydrogel cross-linked with PHMAA with varying degree of methacrlyate substitution (DSMA). Conjugation of Fn to PHMAA was monitored with TNBS assay. (b) The absorbance at 330 nm (A_{330}) was measured over time, which indicates the reduction in free amine groups of Fn. The absorbance values were normalized with the initial value ($A_{330,0}$) to represent the relative change. The reaction between Fn (0.02 mg mL^{-1}(○), 0.1 mg mL^{-1}(▲) and PHMAA resulted in decreased normalized absorbance values, whereas that of pure Fn remained constant (■).

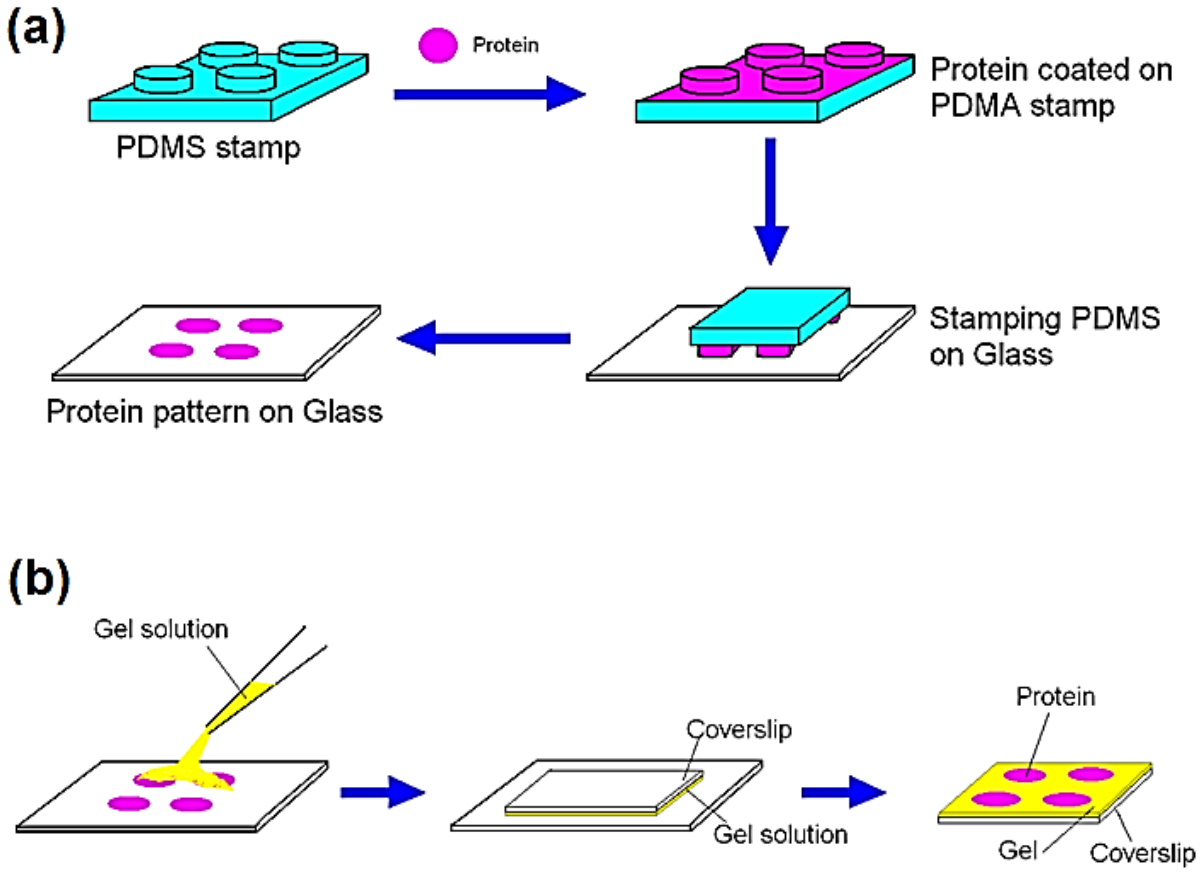

Figure 4.4 Schematic descriptions of (a) preparing a micro-pattern of protein on a glass surface using micro-contact printing technique, and (b) fabricating a hydrogel on top of micro-patterned protein on the glass surface.

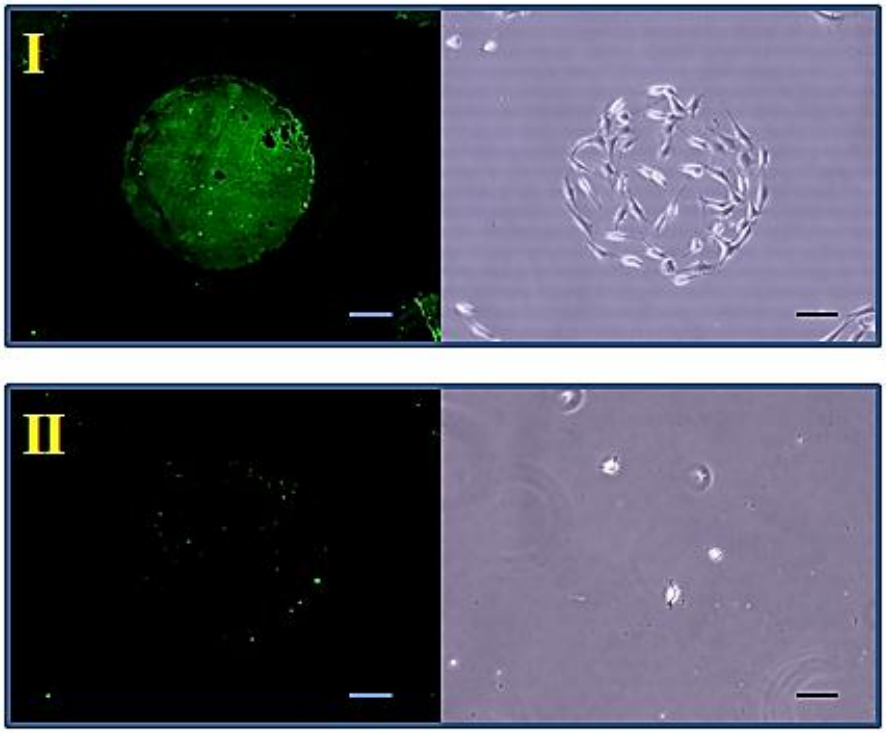

Figure 4.5 Circular pattern of Fn-PHMAA (**I**, left) or pure Fn (**II**, left) on polyacrylamide hydrogel visualized with immunoflurescent labelling. Fibroblast adhesion was more active on the Fn-PHMAA pattern (**I**, right), compared with pure Fn pattern (**II**, right) (Scale bar: 100 μm.)

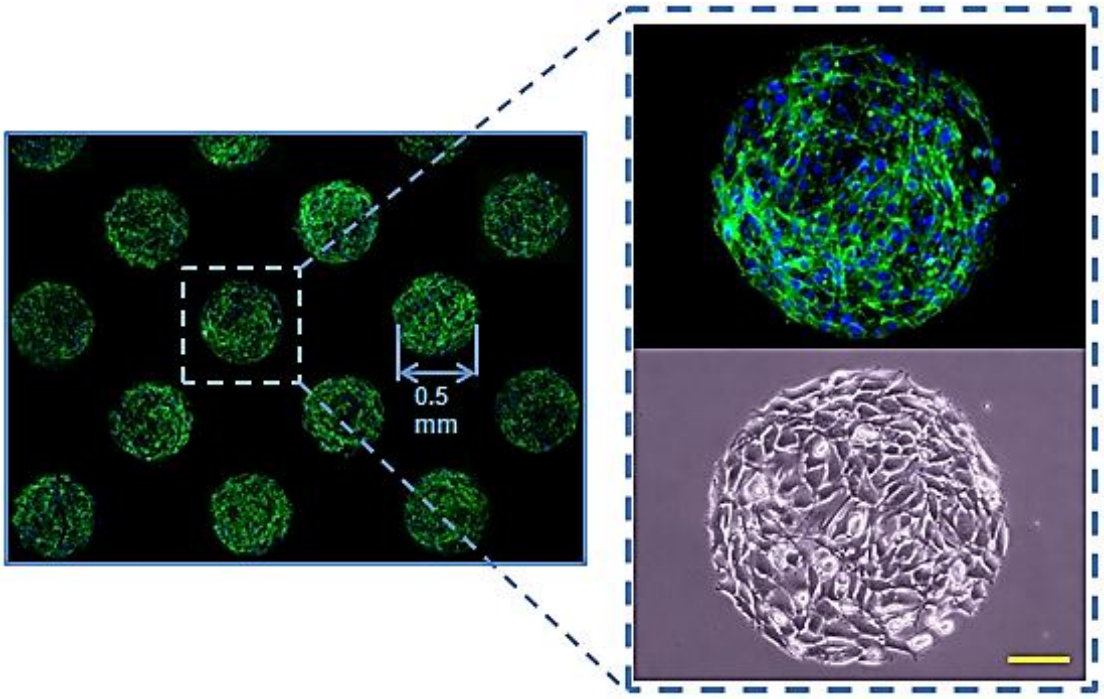

Figure 4.6 Proliferation of fibroblasts within the circular pattern of Fn-PHMAA visualized with fluorescein-phalloidin (green) and DAPI (blue), respectively (a magnified image of a circular pattern shown on right). (scale bar: 100 μm)

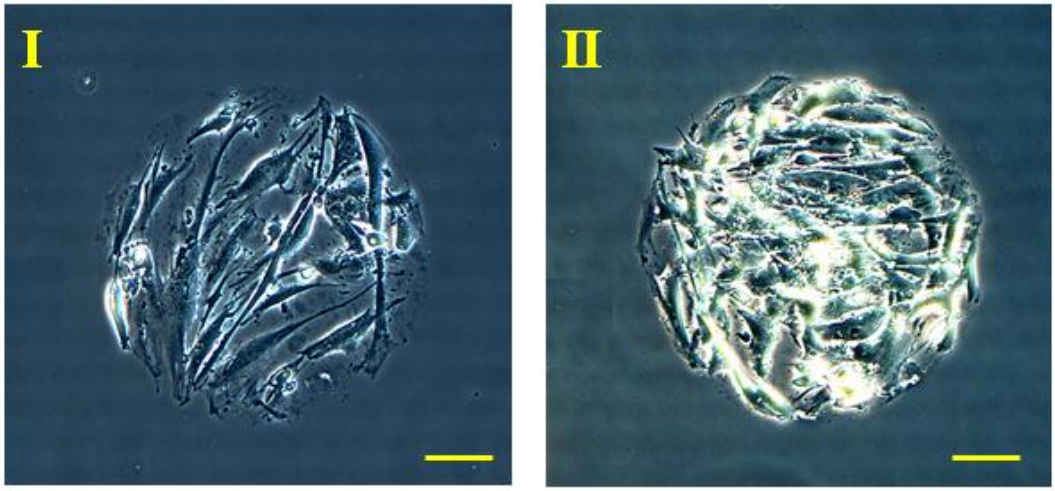

Figure 4.7 Microscopic images of human airway smooth muscle cells adhered on a circular pattern of collagen-PHMAA on a hydrogel. The cells were imaged 1 day (**I**) and 3 days (**II**) after incubation. The cells adhered and proliferated only on the circular pattern of collagen-PHMAA. (Scale bar: 100 μm)

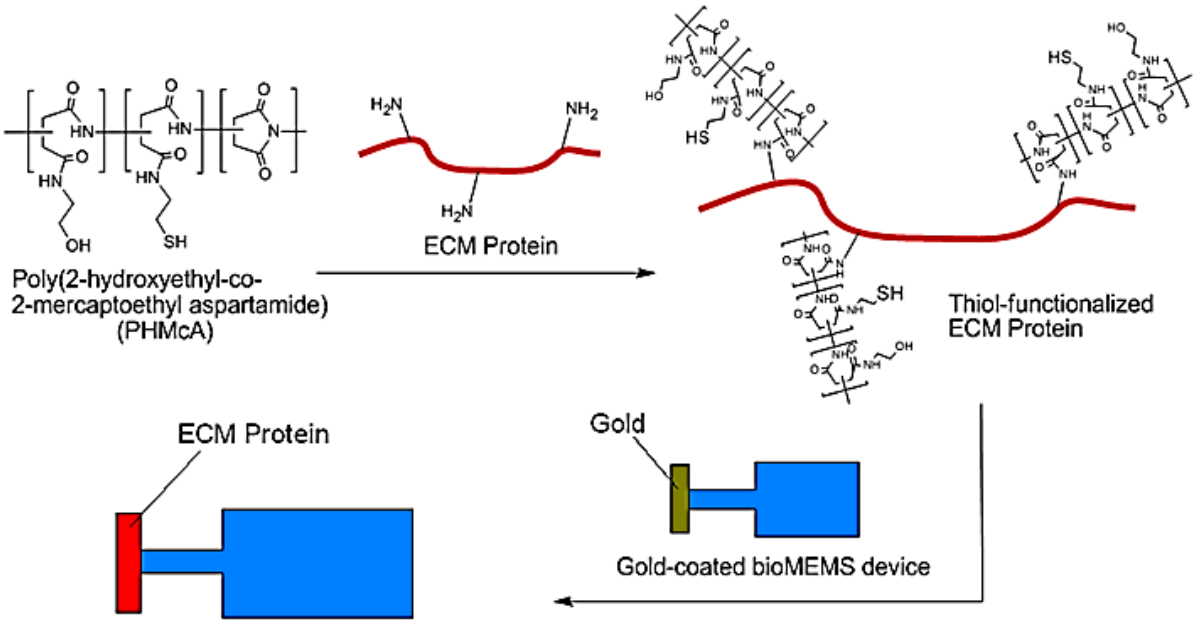

Figure 4.8 Synthesis of PHMCA and its reaction with fibronetin (Fn) to form Fn-PHMCA. Chemically reactive thiol groups are marked with green circles. Fn-PHMCA was used to conjugate Fn to gold-coated bio-MEMS device.

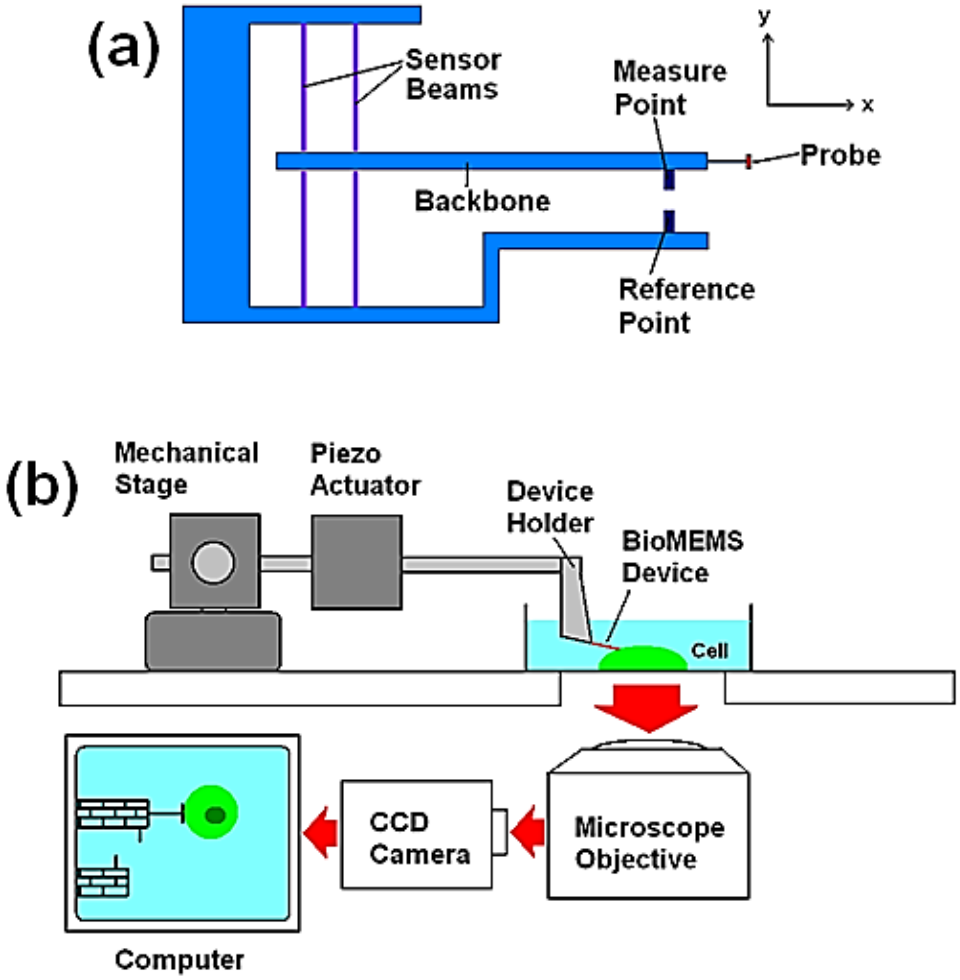

Figure 4.9 (a) Schematic description of the bio-MEMS device to measure the traction force exerted by a cell. The probe, which is coated with a cell-adhesion protein, is placed to contact the cell surface. The device is moved away from the cell, and the traction force exerted by the cell deflects the sensor beams to which the probe is connected. The force (F) is calculated from the equation, $F = k\delta$, where k is the spring constant of the sensor beams and δ is their displacement. (b) The experimental setup for the cell force measurement. The bio-MEMS device attached to a device holder is connected to a piezo actuator and a mechanical stage which can control the movement of the device in a nanometer and micrometer scale, respectively. The experiment is contiuously monitored and recorded with a CCD camera mounted on an inverted microscope.

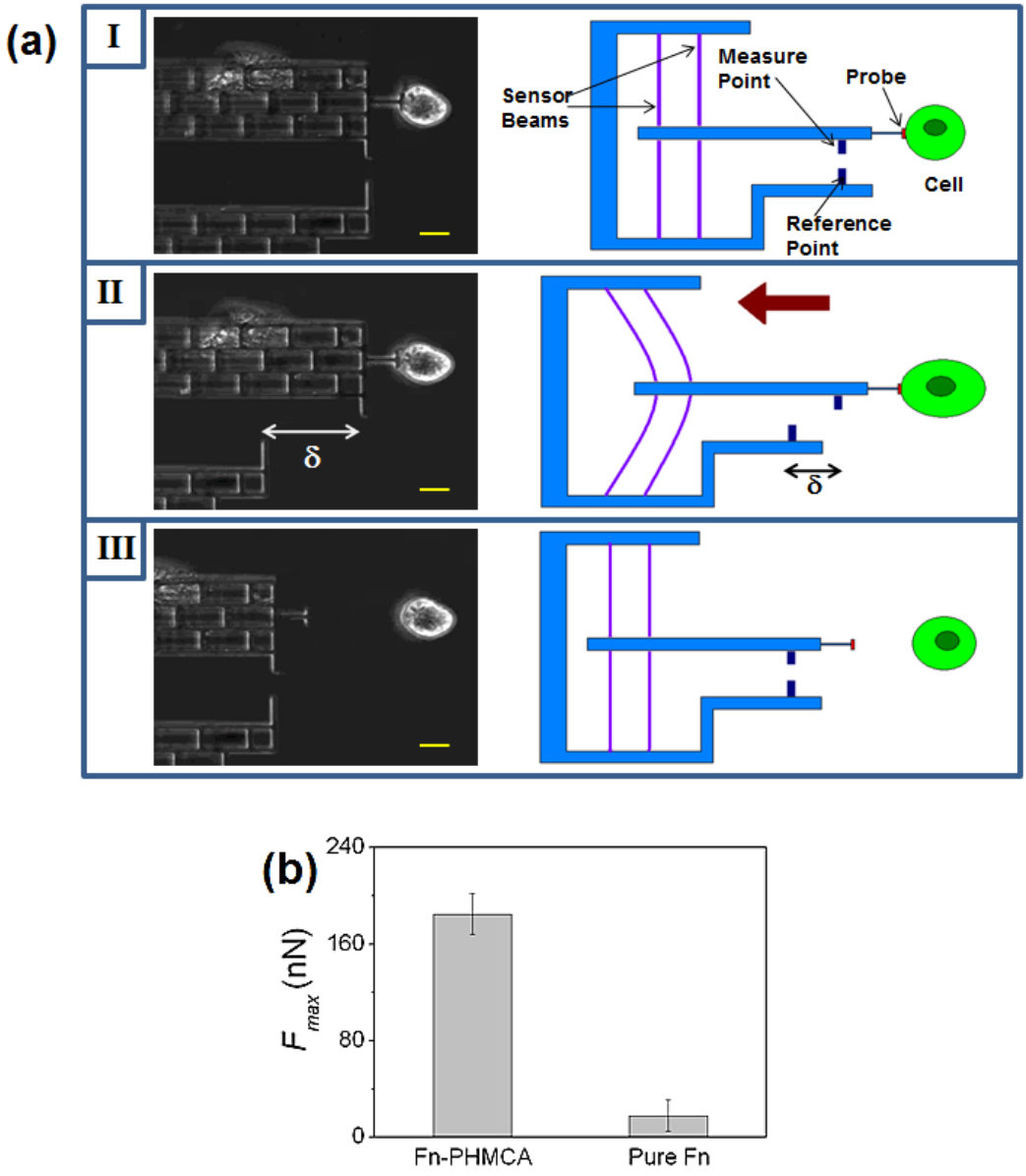

Figure 4.10 (a) Schematic description of cell force measurement using the bio-MEMS device. First, the probe which is coated with Fn is placed to contact the cell (**I**). After incubation, the device is moved away from the cell laterally (red arrow) at a constant rate (**II**). The probe is connected to sensor beams. Due to the cell's adhesion to the probe, it is displaced from the original position, as indicated by the difference between the measure point and reference point. The probe is continuously pulled until it is finally detached from the cell (**III**). (Scale bar: 15 μm.) (b) The maximum force (F_{max}) exerted by the cell was significantly larger when the probe was conjugated with Fn-PHMCA than with pure Fn.

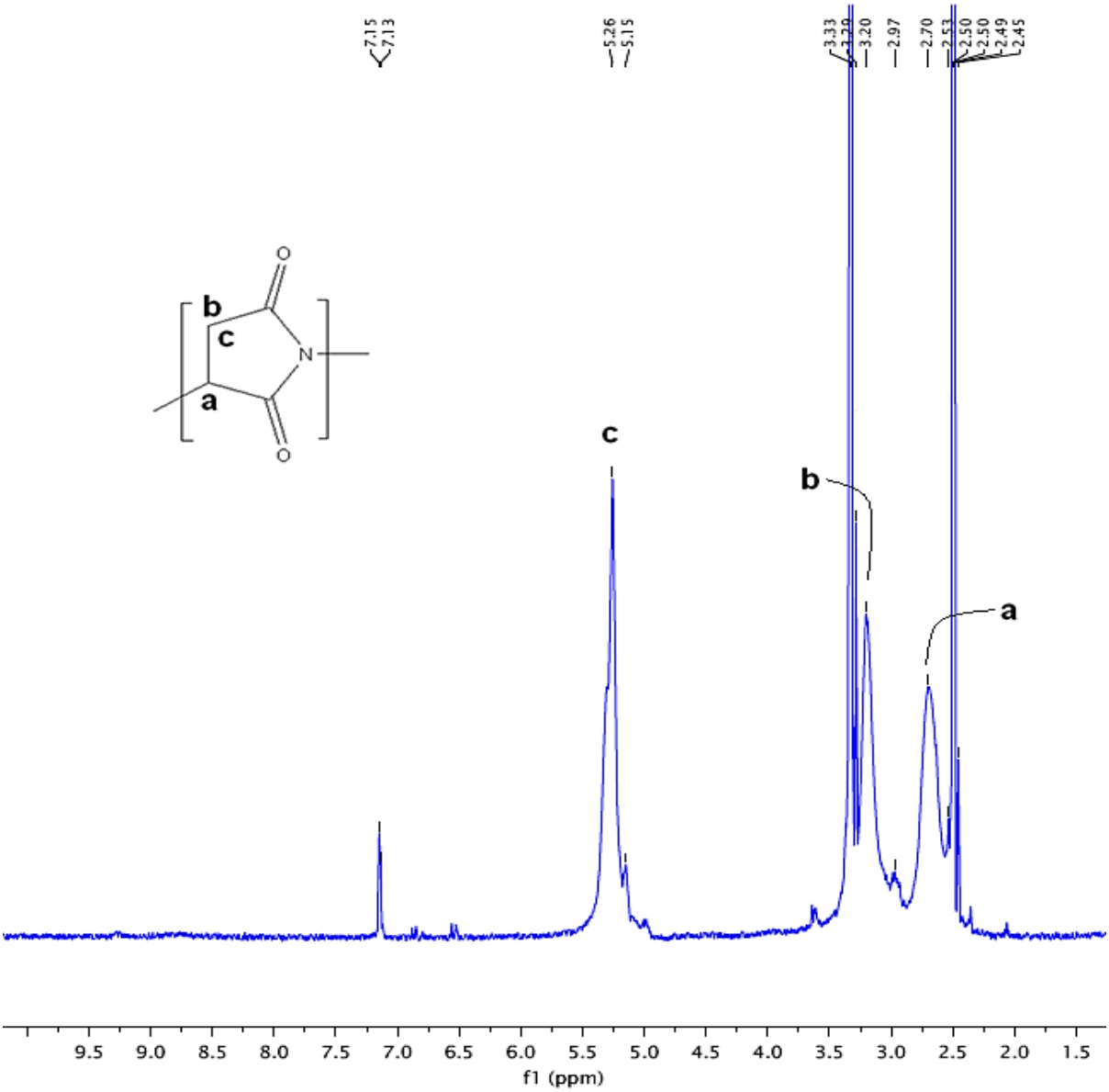

Figure 4.11 ^{1}H-NMR spectrum of polysuccinimide (PSI).

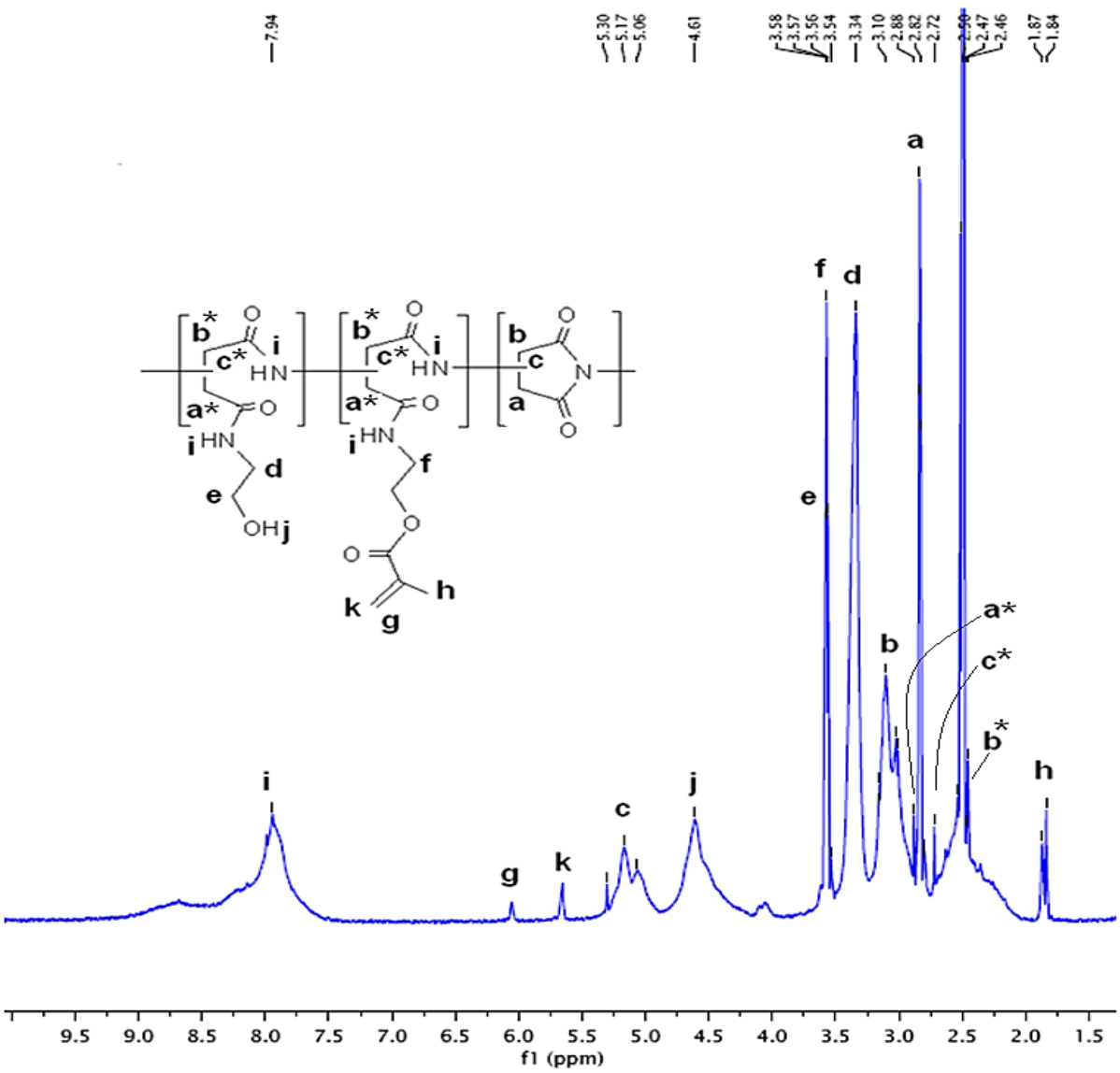

Figure 4.12 ^{1}H-NMR spectrum of poly(2-hydroxyethyl-co-2-methacryloxyethyl aspartamide) (PHMAA).

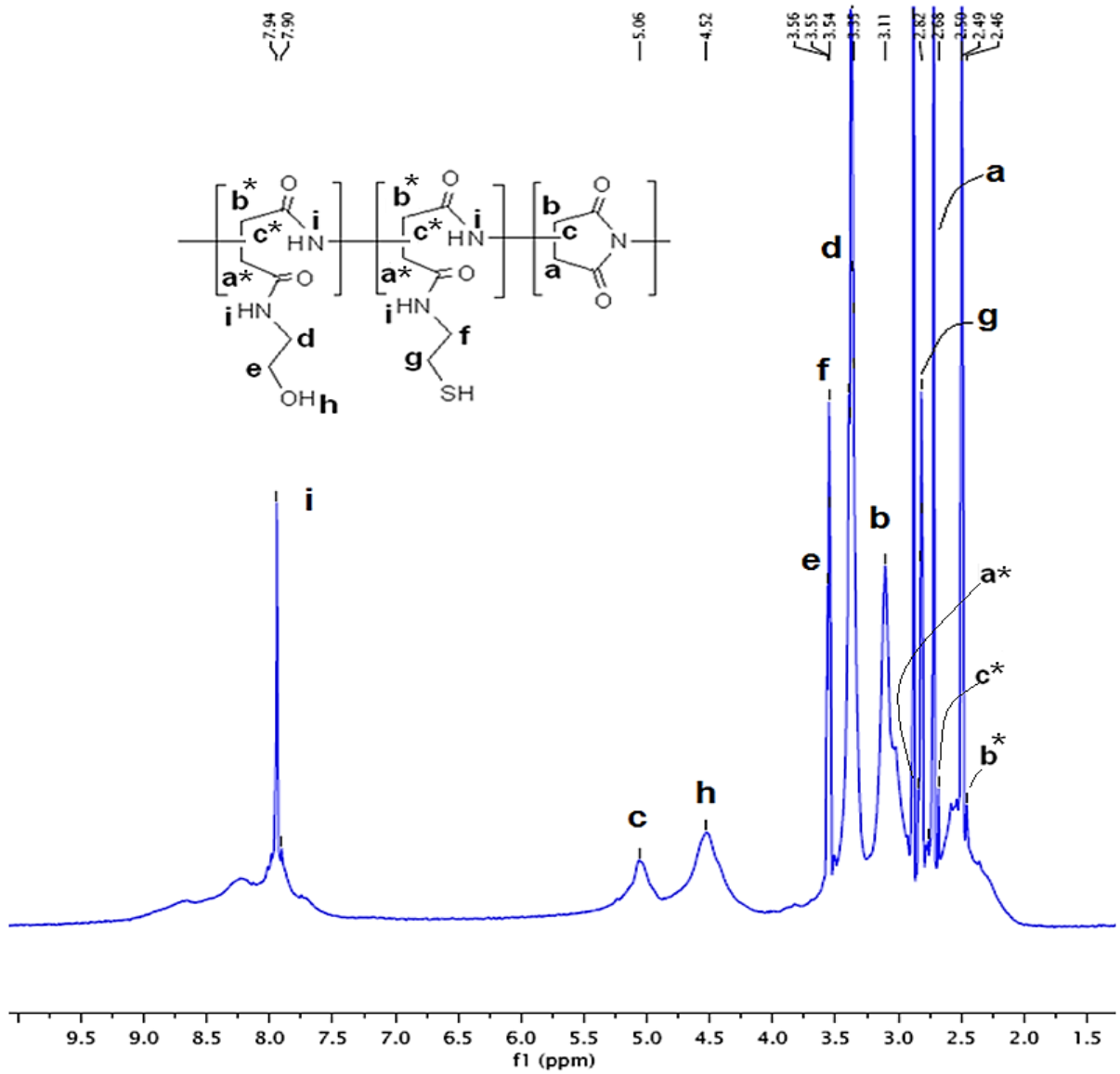

Figure 4.13 ^{1}H-NMR spectrum of poly(2-hydroxyethyl-co-2-mercaptoethyl aspartamide) (PHMCA).

Table 4.1 The percentage of free amine groups in protein reacted with the polyaspartamide linker was evaluated by the decrease of absorbance in TNBS assay.

Protein linker	Protein	Mass ratio (protein: linker)	Percentage of amine reacted (%)
PHMAA	Fibronectin	1 : 0.02	9.8
PHMAA	Collagen	1 : 1	4.8
PHMCA	Fibronectin	1 : 0.02	7.4

Chapter 5 Assembly of Multi-Functional Hydrogel and Encapsulation of Therapeutic Cells

5.1 Introduction

In this chapter, functional modules developed and described in Chapters 2, 3 and 4 are assembled to fabricate multi-functional hydrogel. These modules serve different roles in controlling the hydrogel properties: (1) Introduction of hydrophilic pendant chains, described in Chapter 3, allows control of hydrogel stiffness by varying the number of pendant chains at the same polymer concentration, while limiting the change in permeability.[109] (2) Methacrylic alginate, described in Chapter 2, allows facilitation of transport of bioactive molecules to improve the viability of encapsulated cells, while controlling the range of hydrogel stiffness with its concentration and degree of methacrylic substitution.[52,53] (3) Polyaspartamide-based linker, described in Chapter 4, was used to conjugate a cell recognition protein into the hydrogel system in order to allow the cells to adhere to the hydrogel matrix. The mechanical properties of the hydrogel, stiffness and permeability, are evaluated by measuring elastic modulus and swelling ratio. Various structural factors, such as hydrophilic pendant chains, polymer concentration and degree of methacrylic substitution of alginate, were varied to evaluate their effects on controlling the mechanical properties. Finally, mesenchymal stem cells are encapsulated into the hydrogels, and the effects of mechanical properties of hydrogel on their viability, proliferation and expression of vascular endothelial growth factor (VEGF) are explored.

5.2 Results

5.2.1 Hydrogel fabrication

Hydrogel was made by photo-initiated radical co-polymerization of three gel-forming polymers: poly(ethylene glycol) diacylate (PEGDA), poly(ethylene glycol) monoacrylate (PEGMA) and methacrylic alginate (MA) (Table 5.1). The degree of methacrlyic substitution, defined as the percentage of uronic acid residues in alginate conjugated with methacrylate, was fixed at 20 %. The concentration of MA was also kept constant at 2 wt%. To control hydrogel stiffness, the mass ratio of PEGDA to poly(ethylene glycol) monoacrylate (PEGMA) was varied, while keeping the total PEG concentration constant.

5.2.2 Mechanical properties of hydrogels with varying Φ_{PEGMA}

The stiffness of hydrogel was evaluated by measuring elastic modulus. First, the concentration of MA (ϕ_{MA}) was kept constant 2 wt%, and the fraction of PEGMA (Φ_{PEGMA}) from total PEG concentration (PEGDA and PEGMA combined) was varied (Table 5.1). Increasing Φ_{PEGMA} at the same total PEG concentration (ϕ_{PEG}) at 10 wt% led to the 10-fold decrease in elastic modulus of the hydrogel from 32 kPa to 3 kPa (Figure 5.1a). Swelling ratio on the other hand increased only by a factor of 1.6. These results were similar to those obtained with PEGDA-PEGMA hydrogels described in Chapter 3. However, the total polymer concentration of 20 wt% was used to acquire those results, whereas only 10 wt% of total PEG concentration was needed to achieve the similar results when a small amount of MA was incorporated.

5.2.3 Effects of polymer components on hydrogel mechanical properties

5.2.3a Concentration of PEG

Total PEG concentration (ϕ_{PEG}) was varied from 6 wt% to 12 wt% to evaluate its effect on mechanical properties of hydrogels (Table 5.2). The MA concentration (ϕ_{MA}) was kept constant at 2 wt%. The range of elastic modulus controlled by Φ_{PEGMA} became wider with ϕ_{PEG}, as the range increased from 20 kPa to 40 kPa when ϕ_{PEG} increased from 6 wt% to 12 wt% (Figure 5.2a). There was a small decrease in swelling ratio with increasing ϕ_{PEG}. However, the range of swelling ratio controlled by Φ_{PEGMA}, on the other hand, was not greatly affected by ϕ_{PEG} (Figure 5.2b).

5.2.3b Concentration of MA

Next, the concentration of MA (ϕ_{MA}) was varied from 0.6 wt% to 2 wt% to evaluate its effect on mechanical properties (Table 5.3). ϕ_{PEG} was kept constant at 10 wt%. Increasing ϕ_{MA} at constant ϕ_{PEG} had a greater impact on the overall mechanical properties of the hydrogels than increasing ϕ_{PEG} at constant ϕ_{MA}, as both elastic modulus and swelling ratio changed more with smaller change in ϕ_{MA} than with larger change in ϕ_{PEG}. Elastic moduli were significantly increased with increasing ϕ_{MA} at all Φ_{PEGMA}, even though the increment was less than 1 wt% (Figure 5.3a). Conversely, swelling ratio values decreased significantly with increasing ϕ_{MA} at all Φ_{PEGMA} (Figure 5.3b). This result shows that presence of MA within a hydrogel system contributes greatly to the overall hydrogel structure.

5.2.3c Degree of methacrylic substitution of MA

Degree of methacrylic substitution (DS_{MA}), defined as the percentage of uronic acid residues in alginate conjugated with methacrylate, was varied from 10 % to 45 % (Table 5.4) to evaluate its effect on mechanical properties. ϕ_{PEG} and ϕ_{MA} were kept constant at 10 wt% and 1.6 wt%, respectively. Elastic modulus increased in proportion to DS_{MA} at all Φ_{PEGMA} (Figure 5.4a). Also, the range of elastic modulus controlled with Φ_{PEGMA} became wider with DS_{MA}, from 20 kPa to 75 kPa. Swelling ratio decreased at all Φ_{PEGMA} with increasing DS_{MA}, although the extent of decrease was not as significant as increase in elastic modulus (Figure 5.4b). The range of swelling ratio controlled by Φ_{PEGMA} was not significantly affected by DS_{MA}.

5.2.4 Dependency between elastic modulus and swelling ratio

Elastic modulus (E) and swelling ratio (Q) of hydrogels were correlated to evaluate the effect of modulating (1) concentration of PEG (ϕ_{PEG}), (2) concentration of MA (ϕ_{MA}) or (3) DS_{MA} of MA, described in the previous section, on their dependency while varying Φ_{PEGMA}. The dependency was quantified by $\Psi_{E\text{-}Q}$, defined as the slope of E vs. Q curves.

Increasing ϕ_{PEG} resulted in a small increase in the range of elastic modulus, while the range of swelling ratio was not significantly affected (Figure 5.5a). Increasing ϕ_{MA} increased the range of E and decreased the range of Q. It also shifted the range of E to higher values and the range of Q to lower values (Figure 5.5b). Increasing ϕ_{PEG} did not have significant effect on the $\Psi_{E\text{-}Q}$ values, whereas increasing ϕ_{MA} resulted in increased $\Psi_{E\text{-}Q}$, indicating greater change in E at a given range of Q (Figure 5.6a-b).

Increasing DS_{MA} increased the range of E more significantly than increasing ϕ_{PEG} or ϕ_{MA},

while the range of *Q* was not greatly changed (Figure 5.5c). Consequently, the increase in $\Psi_{E\text{-}Q}$ values was much greater than those controlled with ϕ_{PEG} or ϕ_{MA}.

5.2.5 Effect of hydrogel properties on viability and growth factor expression of encapsulated cells

Mesenchymal stem cells were encapsulated into hydrogels with varying elastic modulus, and their viability and vascular endothelial growth factor expression (VEGF) were evaluated. The stiffness of hydrogel was controlled by Φ_{PEGMA}, while keeping ϕ_{PEG} and ϕ_{PEG} constant at 10 wt% and 1.2 wt%, respectively. To promote cell adhesion, fibronectin conjugated with poly(2-hyroxyethyl-co-2-methacryloxyethyl aspartamide) (PHMAA) linker was incorporated into the hydrogel. First, the viability of cells encapsulated in the hydrogel was determined by staining the cells with MTT after 24 hours. The viability showed biphasic dependence on the hydrogel stiffness, with the maximal viability value at 10 kPa (Figure 5.6a-b). VEGF expression per viable cell on the other hand was not significantly affected by the hydrogel stiffess, as the expression level remained constant at all conditions (Figure 5.6c).

5.3 Discussion

In this study, hydrogel system was developed by combining the three modules described in previous chapters: hydrophilic pendant chains, methacrylic alginate (MA) and protein linked with polyaspartamide linker. Mechanical properties of hydrogels were controlled with the fraction of hydrophilic chains, which allowed control of hydrogel stiffness while limiting the change in permeability. They were further modulated with the concentration of poly(ethylene glycol) (PEG), the concentration of MA, and the degree of methacrylic substitution of MA. Finally, mesenchymal stem cells were encapsulated within the hydrogels conjugated with cell adhesion protein linked by a polyaspartamide linker to evaluate the effect of mechanical properties on cell functions.

Presenting hydrophilic pendant chains, by incorporating poly(ethylene glycol) monoacrylate (PEGMA), limited the increase in permeability while controlling the stiffness, as demonstrated in Chapter 3. Incorporation of methacrylic alginate (MA) into the PEGDA-PEGMA hydrogels allowed the same range of stiffness and permeability to be achieved while using much lower polymer concentration. For example, due to the presence of 1.6 wt% of MA, only 10 wt% of total PEG concentration was needed to get the same range of hydrogel stiffness, which was acquired with 20 wt% of total PEG concentration without MA. This result demonstrates the dominating influence of MA within a hydrogel system in modulating mechanical properties, due to its robust molecular structure and hydrophilicity, as previously discussed. Furthermore, MA also allows further control of mechanical properties by changing either concentration or degree of methacrylic substitution.

The dependency between hydrogel stiffness and permeability was modulated by the

concentration and degree of methacrylic substitution (DS_{MA}) of MA, but not with the concentration of PEG. Increasing the PEG concentration from 6 wt% to 12 wt% did increase the range of elastic modulus, but the range of swelling ratio conversely decreased at a similar extent. So the overall dependency was not affected by the concentration of PEG. On the other hand, increasing the concentration or degree of methacrylic substitution of MA resulted in a significant increase in the range of elastic modulus, but the range of swelling ratio was not greatly affected. This is due to the unique properties of alginate that was extensively investigated and presented in Chapter 2; methacrylic alginate imparts mechanical strength to the hydrogel structure through its stiff molecular structure and multivalency of methacrylic groups, while facilitates diffusion by its hydrophilicity that compensates for increased cross-linking density. Thus, incorporation of methacrylic alginate into PEGDA-PEGMA hydrogel system allows control of hydrogel stiffness in a wider range, either with concentration or DS_{MA}, and still limits the change in permeability.

The hydrogel system was used to evaluate the effect of hydrogel stiffness on the viability and growth factor expression of mesenchymal stem cells (MSC). The viability of MSCs displayed a biphasic dependence on the hydrogel stiffness. This result is similar to that presented in Chapter 3, in which NIH 3T3 fibroblasts were encapsulated in hydrogels with varying stiffness. But the maximal viability was shown at different hydrogel stiffness; the maximal viability of MSCs was at ~10 kPa, and that of fibroblasts was at ~25 kPa. This hydrogel system therefore demonstrated the various responses from different types of cells towards hydrogel stiffness in 3D, and thus successfully provided the 3D platform for exploring cellular behavior under various mechanical environments.

Interestingly, VEGF expression from MSCs was not influenced by the hydrogel stiffness, which is in contrast to that from fibroblasts, which displayed biphasic dependence on the stiffness. It may be possible that stimulation of VEGF expression from the fibroblasts using a chemical modulator may have enhanced the effect of hydrogel stiffness, since the chemical modulator stimulated protein kinase C which is also well known to be influence by external mechanical stimuli.[110] VEGF expression from MSCs was measured without any soluble factors, since they constitutively express VEGF. It is therefore expected that the similar chemical stimulation of MSCs may further reveal the effect of hydrogel stiffness on the VEGF expression.

5.4 Materials and Methods

5.4.1 Hydrogel fabrication

1 mL of pre-gel solution containing 0.01 wt% Irgacure 2959 (Ciba) was placed in between two glass plates with 1 mm spacer. The solution was then irradiated with UV (Jelight Co.) for 10 minutes to allow gel to form. Hydrogel disks were punched out (10 mm in diameter) and incubated in PBS (pH 7.4) at 37 ℃ for 24 hours before characterization of elastic modulus and swelling ratio

5.4.2 Evaluation of elastic modulus and swelling ratio

The hydrogel stiffness was evaluated with measurement of the elastic modulus of a hydrogel subjected to uniaxial compression. Following the incubation in the neutral PBS for 24 hours, the gel disk was compressed at a rate of 1 mm min^{-1} using a mechanical testing system (MTS Insight). The elastic modulus was calculated from the slope of a stress (σ) vs. strain (λ) curve at the first 10% strain.[83,84] The hydrogel swelling ratio was quantified as the weight ratio of a gel incubated in the PBS for 24 hours at 37 ℃ to the dried gel.

5.4.3 Encapsulation of mesenchymal stem cells into hydrogels

Mesenchymal stem cells, derived from human embryonic cell line, H9, were obtained from Aruna Biomedical Inc. The cells were adherently grown and expanded in culture medium (alpha-MEM supplemented with 10% fetal bovine serum and penicillin/streptomycin, all purchased from Invitrogen), and passaged twice before using. The cells were suspended in pre-gel solution at a density of 5×10^5 cells mL^{-1}, and gel was fabricated as described previously.

To promote cell adhesion, fibronectin conjugated with PHMAA linker (0.1 mg mL-1, detailed synthesis is described in Chapter 4) was incorporated into each pre-gel solution. The gel disks (5 mm in diameter) were incubated in the culture medium at 37 ℃ with 5% CO_2.

5.4.4 Analysis of cell viability in hydrogels

Cell-encapsulated hydrogels were exposed to MTT (3-(4,5-dimethylthiazol-2-yl)-2,5-diphenyltetrazolium bromide) to assess the number of viable cells.[53] MTT is taken up and enzymatically reduced by viable cells to become MTT formazan which has a maximum absorbance at 570 nm. Briefly, each hydrogel disk was placed in one well of a 96-well plate with 0.1 mL of growth medium. 10 μL of MTT Reagent (ATCC) was added to each well and incubated for 4 hours at 37 ℃. Then, 0.1 mL of stop solution (20 % sodium dodecyl sulfate in water/dimethylformamide (50:50)) was added to the well and incubated overnight to let the product diffuse out of the hydrogel and completely dissolve. The absorbance of the surrounding medium at 570 nm, which represents the number of viable cells positively stained with MTT, was measured using a spectrophotometer (Synergy HT, BioTek). The absorbance was normalized by that of a pure medium, due to color variations of growth medium over time. The normalized absorbance was divided by that measured right after cell encapsulation, in order to quantify the cell viability as percentage of cells that remained viable.

5.4.5 Analysis of vascular endothelial growth factor expression in hydrogels

After incubating cell-encapsulated hydrogels in cell culture medium, the medium was collected and the amount of VEGF released was quantified with an enzyme-linked

immunosorbent assay (Human VEGF Quantikine ELISA kit, R&D systems). The medium incubated with cell-free hydrogel disks was assayed as a negative control. The amount of VEGF released from each hydrogel disk was normalized with the number of viable cells measured at the same time point to represent VEGF expression level by each viable cell.

5.5 Tables and Figures

Table 5.1 Formulations of hydrogels consisting of PEGDA, PEGMA and methacrylic alginate (MA). Mechanical properties were controlled by varying the mass fraction of PEGMA (Φ_{PEGMA}).

ϕ_{PEG} (wt%)*	ϕ_{MA} (wt%)*	Φ_{PEGMA} (%)*	DS_{MA} (%)*
10	2	0	20
10	2	12.5	20
10	2	25	20
10	2	75	20
10	2	100	20

*ϕ_{PEG}: total PEG concentration, ϕ_{MA}: MA concentration, Φ_{PEGMA}: mass fraction of PEGMA from total PEG, DSMA: degree of methacrylic substitution

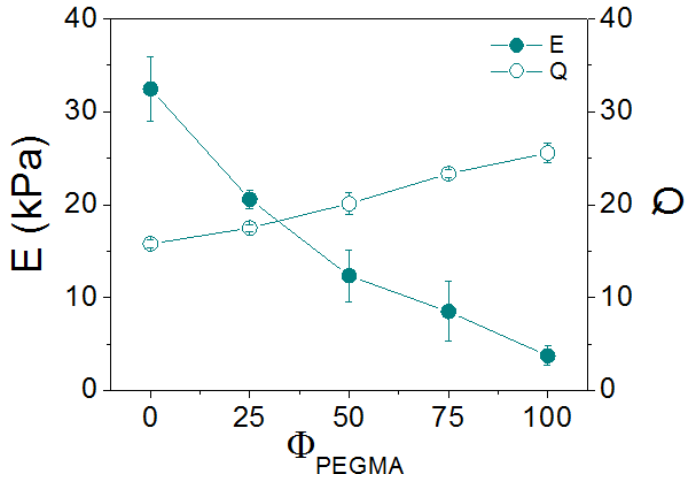

Figure 5.1 Elastic moduli (E,●) and swelling ratios (Q,○) of hydrogels consisting of PEGDA, PEGMA and methacrylic alginate (MA). The mass fraction of PEGMA from total PEG concentration (Φ_{PEGMA}) was varied while keeping the total PEG and MA concentrations constant.

Table 5.2 Formulations of hydrogels consisting of PEGDA, PEGMA and methacrylic alginate (MA). Mechanical properties controlled by varying the mass fraction of PEGMA (Φ_{PEGMA}) were examined at various total PEG concentrations (ϕ_{PEG}).

(a)

ϕ_{PEG} (wt%)*	ϕ_{MA} (wt%)*	Φ_{PEGMA} (%)*	DS_{MA} (%)*
6	2	0	20
6	2	12.5	20
6	2	25	20
6	2	75	20
6	2	100	20

(b)

ϕ_{PEG} (wt%)*	ϕ_{MA} (wt%)*	Φ_{PEGMA} (%)*	DS_{MA} (%)*
10	2	0	20
10	2	12.5	20
10	2	25	20
10	2	75	20
10	2	100	20

(c)

ϕ_{PEG} (wt%)*	ϕ_{MA} (wt%)*	Φ_{PEGMA} (%)*	DS_{MA} (%)*
12	2	0	20
12	2	12.5	20
12	2	25	20
12	2	75	20
12	2	100	20

*ϕ_{PEG}: total PEG concentration, ϕ_{MA}: MA concentration, Φ_{PEGMA}: mass fraction of PEGMA from total PEG, DS_{MA}: degree of methacrylic substitution of MA

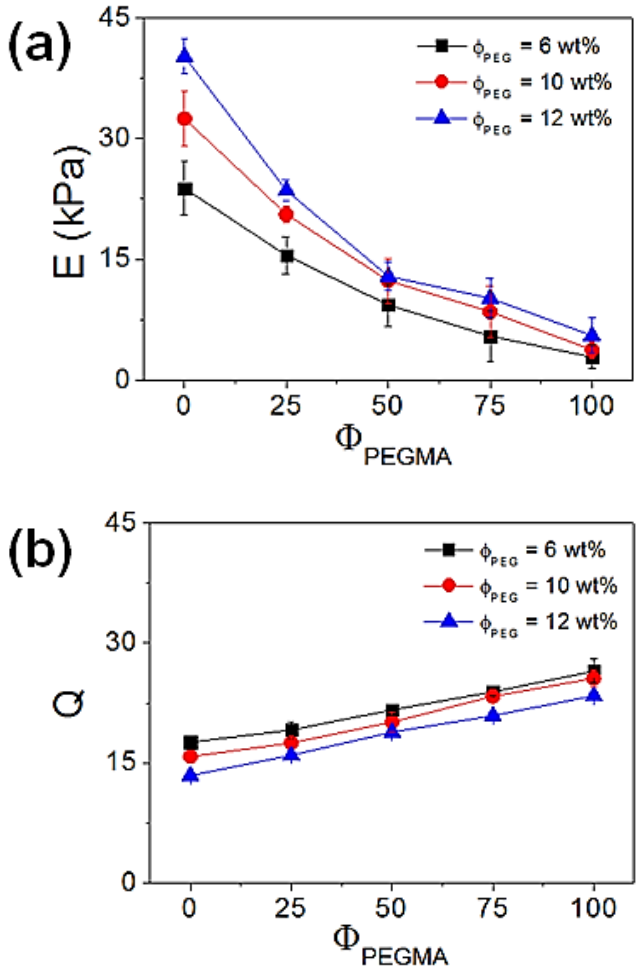

Figure 5.2 Effect of total PEG concentration (ϕ_{PEG}) on modulating (a) elastic modulus (*E*) and (b) swelling ratio (*Q*) of hydrogels with Φ_{PEGMA}. The concentrations of ϕ_{PEG} were 6 wt% (■), 10 wt% (●) and 12 wt% (▲).

Table 5.3 Formulations of hydrogels consisting of PEGDA, PEGMA and methacrylic alginate (MA). Mechanical properties controlled by varying the mass fraction of PEGMA (Φ_{PEGMA}) were examined at various total MA concentrations (ϕ_{MA}).

(a)

ϕ_{PEG} (wt%)*	ϕ_{MA} (wt%)*	Φ_{PEGMA} (%)*	DS_{MA} (%)*
10	0.6	0	20
10	0.6	12.5	20
10	0.6	25	20
10	0.6	75	20
10	0.6	100	20

(b)

ϕ_{PEG} (wt%)*	ϕ_{MA} (wt%)*	Φ_{PEGMA} (%)*	DS_{MA} (%)*
10	1.2	0	20
10	1.2	12.5	20
10	1.2	25	20
10	1.2	75	20
10	1.2	100	20

(c)

ϕ_{PEG} (wt%)*	ϕ_{MA} (wt%)*	Φ_{PEGMA} (%)*	DS_{MA} (%)*
10	2	0	20
10	2	12.5	20
10	2	25	20
10	2	75	20
10	2	100	20

*ϕ_{PEG}: total PEG concentration, ϕ_{MA}: MA concentration, Φ_{PEGMA}: mass fraction of PEGMA from total PEG, DS_{MA}: degree of methacrylic substitution of MA

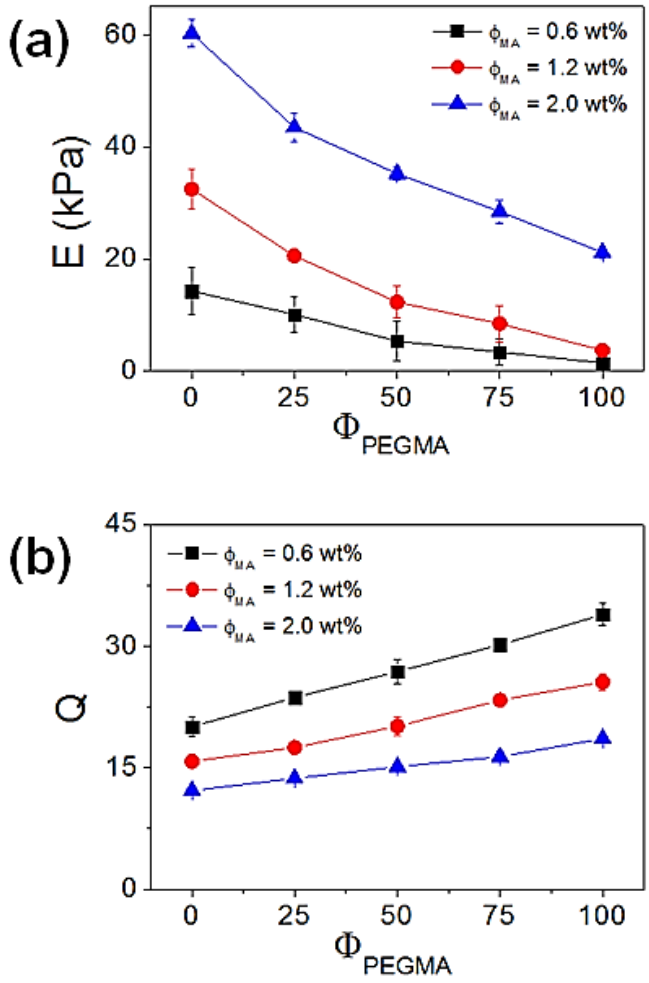

Figure 5.3 Effect of total MA concentration (ϕ_{MA}) on modulating (a) elastic modulus (*E*) and (b) swelling ratio (*Q*) of hydrogels with Φ_{PEGMA}. The concentrations of ϕ_{MA} were 0.6 wt% (■), 1.2 wt% (●) and 2 wt% (▲).

Table 5.4 Formulations of hydrogels consisting of PEGDA, PEGMA and methacrylic alginate (MA). Mechanical properties controlled by varying the mass fraction of PEGMA (Φ_{PEGMA}) were examined at various degree of methacrylic substitution of MA (DS_{MA}).

(a)

ϕ_{PEG} (wt%)*	ϕ_{MA} (wt%)*	Φ_{PEGMA} (%)*	DS_{MA} (%)*
10	1.6	0	10
10	1.6	12.5	10
10	1.6	25	10
10	1.6	75	10
10	1.6	100	10

(b)

ϕ_{PEG} (wt%)*	ϕ_{MA} (wt%)*	Φ_{PEGMA} (%)*	DS_{MA} (%)*
10	1.6	0	20
10	1.6	12.5	20
10	1.6	25	20
10	1.6	75	20
10	1.6	100	20

(c)

ϕ_{PEG} (wt%)*	ϕ_{MA} (wt%)*	Φ_{PEGMA} (%)*	DS_{MA} (%)*
10	1.6	0	45
10	1.6	12.5	45
10	1.6	25	45
10	1.6	75	45
10	1.6	100	45

*ϕ_{PEG}: total PEG concentration, ϕ_{MA}: MA concentration, Φ_{PEGMA}: mass fraction of PEGMA from total PEG, DS_{MA}: degree of methacrylic substitution of MA

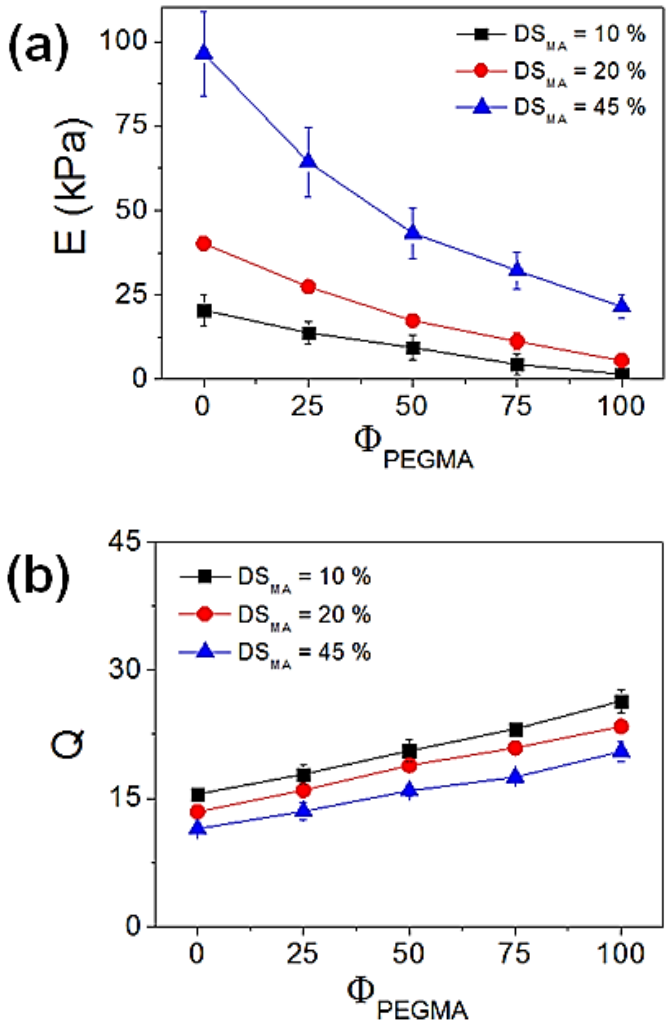

Figure 5.4 Effect of degree of methacrylic substitution of MA (DS_{MA}) on modulating (a) elastic modulus (*E*) and (b) swelling ratio (*Q*) of hydrogels with Φ_{PEGMA}. The DS_{MA} were 10 % (■), 20 % (●) and 45 % (▲).

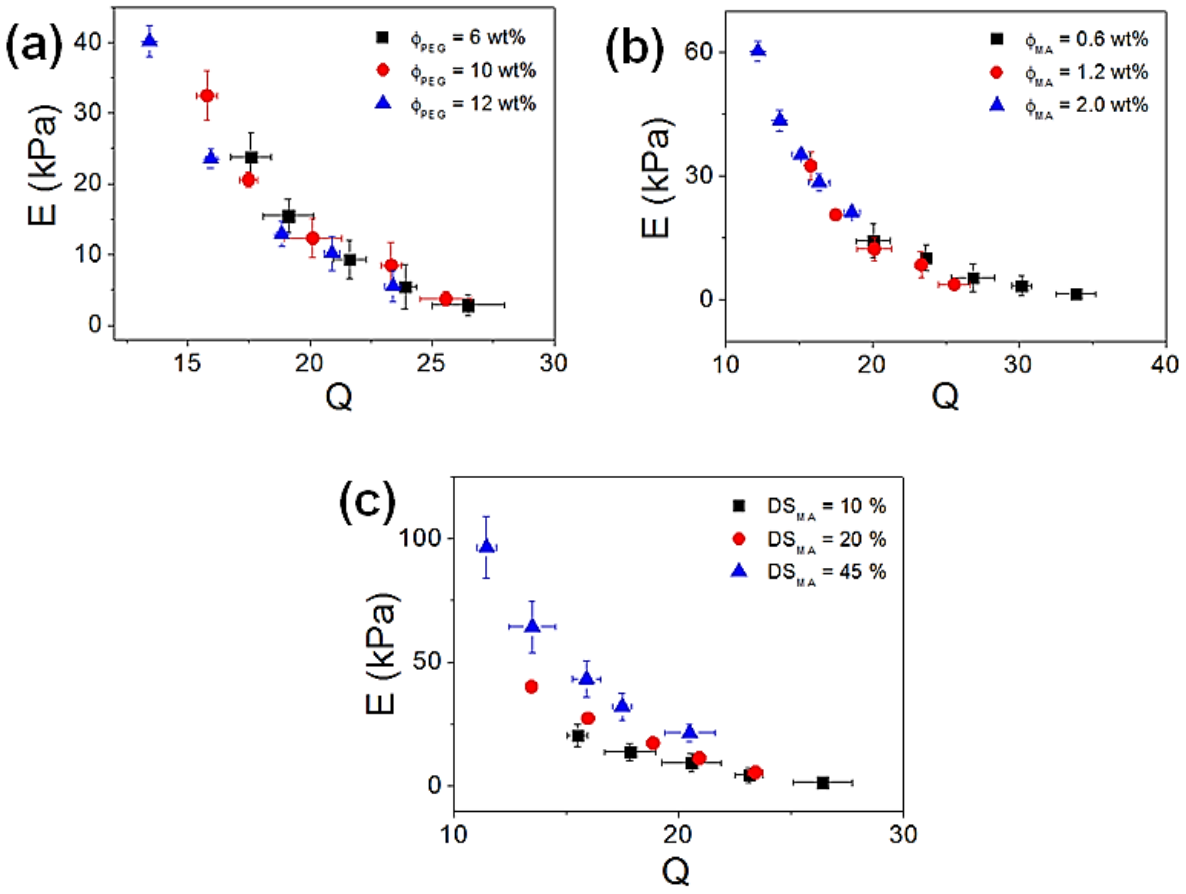

Figure 5.5 Elastic modulus (*E*) and swelling ratio (*Q*) of hydrogels controlled with Φ_{PEGMA} were correlated while changing (a) total PEG concentration (ϕ_{PEG}), (b) MA concentration (ϕ_{MA}), and (c) degree of methacrylic substitution of MA (DS_{MA}).

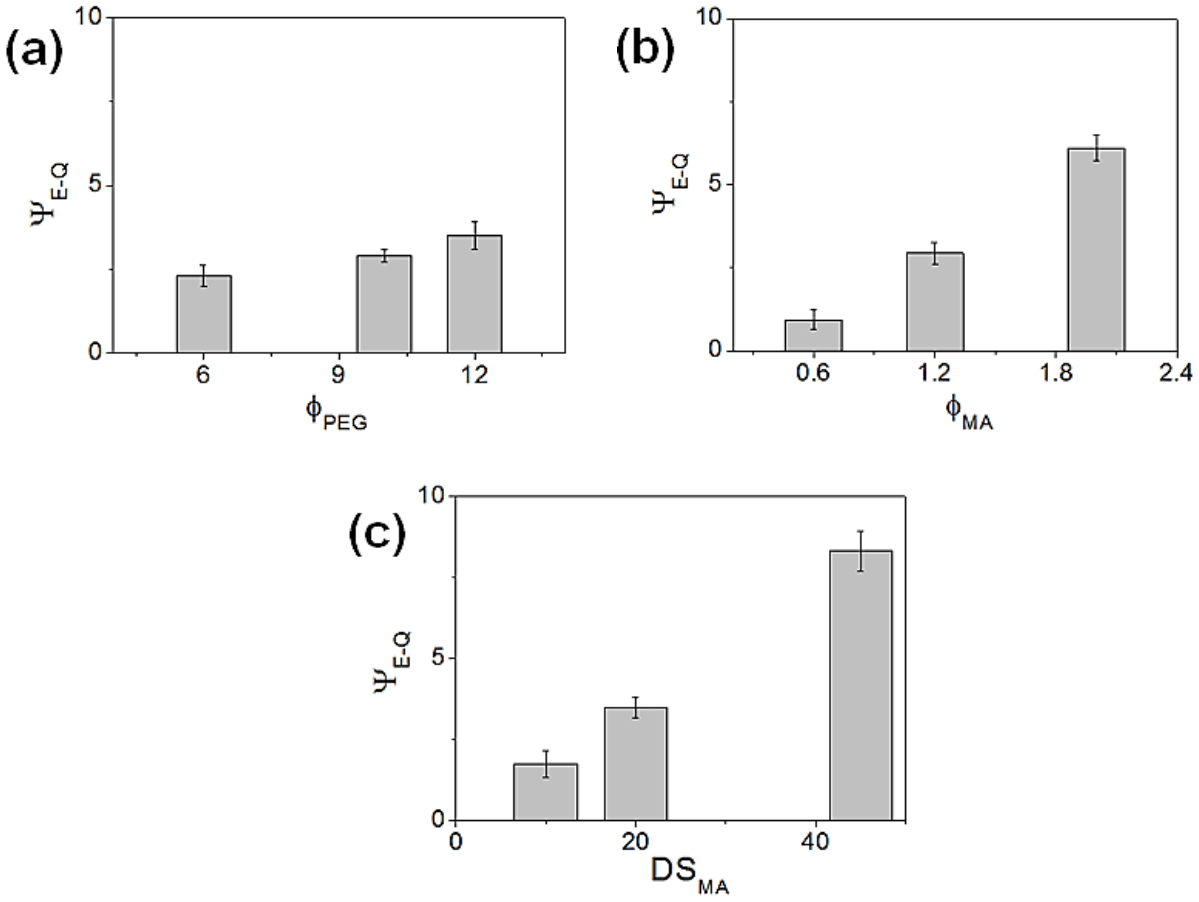

Figure 5.6 The dependency between elastic modulus (*E*) and swelling ratio (*Q*) was quantified by Ψ_{E-Q}, the slope of *E* vs. *Q* curves shown in Figure 5.5. Ψ_{E-Q} values were obtained for hydrogels controlled with (a) total PEG concentration (ϕ_{PEG}), (b) MA concentration (ϕ_{MA}) and (c) degree of methacrylic substitution (DS_{MA}).

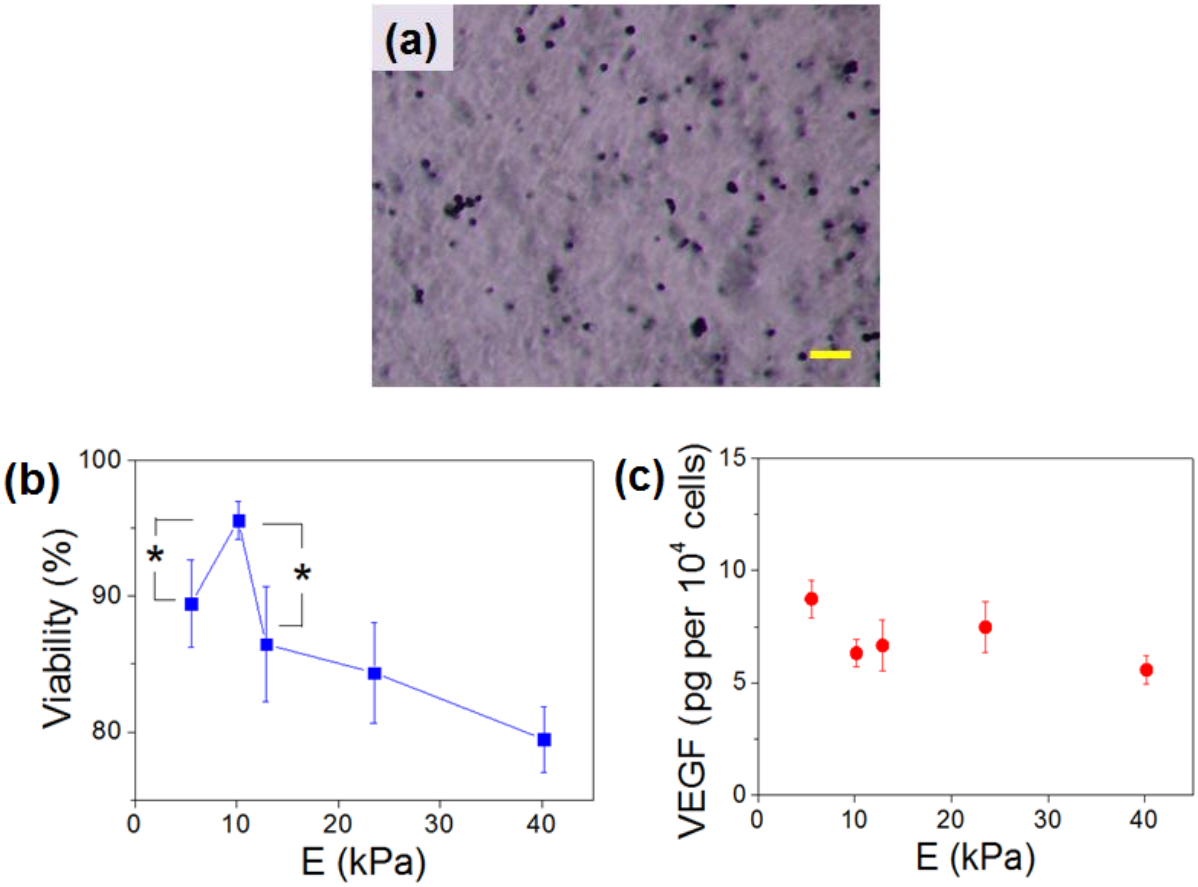

Figure 5.7 (a) Phase-contrast microscopic images of mesenchymal stem cells (MSC) taken 24 hours after encapsulation in hydrogels with with varying stiffness. Stiffness was controlled by Φ_{PEGMA}, while keeping ϕ_{PEG} and ϕ_{MA} constant at 12 wt% and 1.2 wt%, respectively. The viable cells were positively stained with MTT (dark purple). (Scale bar: 100 μm) (b) The viability was related to elastic modulus (*E*) of hydrogels. (*$p<0.05$) (c) VEGF expression from MSCs normalized by the number of viable cells was related to *E*.

Chapter 6 Biomineralization of Hydrogel Controlled by Hydrophobicity, Charge Density and Porosity

6.1 Introduction

Mineralized polymeric matrices have emerged as promising tools to uncover the complex roles of the cellular microenvironment in regulating the diverse phenotypic activities of stem and progenitor cells related to the development, repair, regeneration, and remodeling of bone tissue.[111-113] The success in using the mineralized matrix for these studies greatly relies on the ability to assemble a mineralized matrix chemically and morphologically similar to a natural bone matrix. During the last two decades, extensive efforts have been made to understand the complex roles of soluble and insoluble factors in controlling the chemical composition and structure of minerals deposited onto polymer matrices.[114-116] It is now common to incorporate charged polymers[115-119] or oligopeptides[114,120,121] in the polymer matrix in order to facilitate deposition of mineral ions throughout the matrix.

Furthermore, it has often been suggested that the role of chemical motifs should be mediated by other matrix variables, such as pore size and the density of hydrophobic motifs, specifically for the mineralization of a three dimensional (3D) matrix.[16,122-126] However, the potential interplay among matrix variables in mineralization has not yet been systematically examined because of a lack of tools enabling the independent control of the density of chemical motifs, the density of hydrophobic motifs, and pore size.

In this study, we uncover the combined effects of charge density, hydrophobicity, and pore size of a matrix on the 3D mineralization process using a hydrogel formulated to tune the matrix variables in an independent manner. The resulting mineralized hydrogel matrices were then used to examine the role of minerals in enhancing the viability of stem cells cultured within the 3D matrix. There have been previous studies on the mineralization of hydrogels and their subsequent use to enhance the viability of cells cultured on the matrices; however, these studies largely focused on controlling mineralization solely by modifying the density of charged groups in the hydrogel.[127] In this study, we systematically examined the interplay between several matrix variables in mineralization using a hydrogel system consisting of hydrophilic poly(ethylene glycol) monomethacrylate (PEGmM), hydrophobic poly(propylene glycol) monomethacrylate (PPGmM), and negatively charged methacrylic alginate (MA). Specifically, the charge density and hydrophobicity of the hydrogel were separately controlled with the mass fraction of MA and the mass ratio between PPGmM and PEGmM. Furthermore, pore size was independently controlled to investigate both hydrogels containing only nano-sized pores and those processed to create micro-sized pores.[128-130] Hydrogels with varying mass fractions of PEGmM, PPGmM, and MA (Table 6.1) were incubated in the modified simulating body fluid (mSBF) for one week to induce mineralization. The chemical properties and morphology of the minerals, analyzed with several imaging and spectroscopic tools, were related to the hydrogel variables. Adipose derived stem cells (ADSCs) were then incorporated into the mineralized pores to examine the effects of minerals on cellular viability during cell culture.

6.2 Results

6.2.1 Hydrogel design and characterization

Hydrogels consisting of poly(propylene glycol) monomethacrylate (PPGmM), poly(ethylene glycol) monomethacrylate (PEGmM), and methacrylic alginate (MA) were prepared by chemically cross-linking the three polymers (Figure 6.1). The hydrogels could not be formed without MA, indicating that MA acts as a cross-linker of PPGmM and PEGmM. The hydrogel formed via radical polymerization, termed a nanoporous hydrogel, presented pores with diameters on the order of tens of nanometers, according to the calculation from the swelling ratio at equilibrium using Eq. (11) (Table 6.1a). The nanoporous hydrogel was further lyophilized to prepare a hydrogel which presents micro-sized pores with diameters on the order of tens of micrometers, termed a microporous hydrogel. Incorporation of the micro-sized pores significantly increased the water diffusivity by one order of magnitude as compared with the nanoporous hydrogel (Table 6.1b). In addition, introducing micro-sized pores into the hydrogel did not significantly alter initial elastic modulus of the hydrogel (data not shown).

For both nanoporous and microporous hydrogels, the charge density of the hydrogel was tuned with the mass fractions of MA (Φ_{MA}) at the same mass fractions of PPGmM (Φ_{PPGmM}) and PEGmM (Φ_{PEGmM}). As expected, an increase of Φ_{MA} from 0.007 to 0.04 doubled both the charge density (C_{gel}) and the diameter of nanopores (ξ_{nano}) in the hydrogel (Table 6.1a). However, the diameter of the micro-sized pores (ξ_{micro}) was independent of Φ_{MA}. The initial elastic modulus of the hydrogel (E_0) was slightly increased with Φ_{MA}, due to the increase of cross-linking density. The hydrophobicity of the hydrogel was tuned separately varying Φ_{PPGmM} from 0 to 0.72 at a given Φ_{MA} of 0.04, thereby decreasing Φ_{PEGmM} from 0.96 to 0.24

(Table 6.1b). Increasing Φ_{PPGmM} decreased the water diffusivity of microporous hydrogels (D_{micro}) more significantly than that of the nanoporous hydrogels (D_{nano}). Increasing Φ_{PPGmM} slightly decreased ξ_{nano} from 23 to 17 nm, but made minimal change in ξ_{micro}. There was no significant difference of initial elastic modulus with changes in Φ_{PPGmM}.

6.2.2 Mineralization of a hydrogel controlled by mass fractions of methacrylic alginate (Φ_{MA}) and poly(propylene glycol) monomethacrylate (Φ_{PPGmM})

The hydrogels prepared and characterized above were incubated in modified simulated body fluid (mSBF) to induce mineralization of the gel matrices, marked by changes in the transparency and stiffness of the hydrogel. As expected, the concentrations of calcium and phosphate accumulated within the hydrogel were significantly increased with increasing Φ_{MA} for both nanoporous and microporous hydrogels (Figure 6.2). The calcium and phosphate concentrations were therefore dependent on the charge density of the gel matrix (C_{gel}) altered with Φ_{MA} (Table 6.1a).

At a given Φ_{MA}, Φ_{PPGmM} of the hydrogel also tuned the extent of mineralization, indicated by varying degrees of changes in the transparency, volume, and mechanical stiffness of the hydrogels incubated in mSBF. The increase in opaqueness was more significant with increasing Φ_{PPGmM} (Figure 6.3a), and the rigidity increase was roughly proportional to Φ_{PPGmM} (Figure 6.3b). In addition, the increase of the elastic modulus was greater for microporous hydrogels than for nanoporous hydrogels, regardless of Φ_{PPGmM}. Such effects of Φ_{PPGmM} on the increases in opaqueness and stiffness of the hydrogel throughout the incubation in mSBF were related to the concentrations of calcium and phosphate within the hydrogel.

The calcium and phosphate concentrations of the nanoporous hydrogel were lower than those of the microporous hydrogel by approximately 30 %. The calcium concentration was much higher than that of phosphate for both nanoporous and microporous hydrogels, and it was almost independent of Φ_{PPGmM}. In contrast, the phosphate concentration increased with Φ_{PPGmM} for both nanoporous and microporous hydrogel (Figure 6.4a-b). The dependency of the phosphate concentration on Φ_{PPGmM} was inversely related to the change of water diffusivity within the microporous hydrogel (Figure 6.4c).

To quantify the overall effects of the Φ_{MA}, Φ_{PPGmM} and micro-sized pores on the extent of mineralization, the relative supersaturation of calcium and phosphate with respect to apatite, σ_{Ca-P}^{rel}, was calculated.[131-134] According to the calculation, increasing Φ_{MA} at a constant ratio of Φ_{PPGmM} and Φ_{PEGmM} or increasing Φ_{PPGmM} at a constant Φ_{MA} of 0.04 led to the increase in σ_{Ca-P}^{rel} (Figure 6.5). In both cases, the σ_{Ca-P}^{rel} values of microporous hydrogels were larger than those of nanoporous hydrogels.

6.2.3 Microscopic and spectroscopic analyses of mineralized hydrogels

The minerals formed within a hydrogel matrix were further analyzed using microscopic and spectroscopic methods. First, the morphology of minerals deposited within the hydrogel was imaged with scanning electron microscopy (SEM). Spherulitic calcium phosphate particles were extensively deposited within the microporous hydrogels at the highest Φ_{PPGmM} (at 0.72, Figure 6.6a). In contrast, many fewer spherulitic minerals were formed within the microporous hydrogel at the lowest Φ_{PPGmM} (at 0, Figure 6.6b). Next, the chemical composition of the minerals was analyzed with energy-dispersive X-ray spectroscopy (EDX). This analysis

confirmed that the spherulitic minerals mostly consisted of calcium and phosphate, and the average Ca/P ratio of the particles was 1.7, a typical value for apatite (Figure 6.7a).[135] Finally, the organization of calcium and phosphate was examined with X-ray diffraction (XRD) spectroscopy, and the peak at 32° in the XRD spectrum suggested that the calcium and phosphate were organized in a crystalline form, a characteristic of apatite minerals (Figure 6.7c).[136]

Fourier-transform infrared (FT-IR) spectroscopic analysis was performed to further characterize the minerals formed within the microporous hydrogels (Figure 6.8). Interestingly, both the peaks associated with carbonate substitutions of apatite (1502, 1378, 1221 cm^{-1}) and apatite peaks (1110, 1031, 943 cm^{-1}) were seen.[15,136] This indicates that the spherulitic mineral particles were carbonated hydroxyapatite minerals. In addition to the apatite, a certain fraction of calcite was found in the microporous hydrogels, as confirmed on FT-IR by characteristic peaks of calcite (851, 746 cm^{-1}).[137]

In contrast, nanoporous hydrogels incubated in mSBF presented mostly rhombohedral crystals when imaged with SEM (Figure 6.6c-d). The number of rhombohedral crystals was qualitatively dependent on Φ_{PPGmM}. EDX analysis of the rhombohedral crystal indicated the presence of calcium and oxygen, but not the presence of phosphorous (Figure 6.7b). The XRD analysis showed a peak at 29° in the spectrum, which is characteristic of calcite minerals (Figure 6.7d).[138] Also, a certain fraction of apatite was found in the nanoporous hydrogel as indicated by the peak at 32°, which is consistent with the small amount of phosphate detected by the quantitative analysis in Fig. 3.

6.2.4 Analysis of cell viability in mineralized hydrogels

Mesenchymal stem cells were incorporated into micropores of both non-mineralized and mineralized hydrogel of PEGmM, PPGmM and MA with varied Φ_{PPGmM}. Incorporation of the cells into mineralized pores of the hydrogel significantly increased the number of viable cells which stained positively with MTT reagents (Figure 6.9). In addition, the enhancement of the cell viability level was more significant with the use of the hydrogel which contained the higher Φ_{PPGmM} which also presented the larger number of spherulitic apatite particles within the hydrogel.

6.3 Discussion

The results of this study demonstrate that the charge density, hydrophobicity, and pore size of a hydrogel matrix should be controlled in an integrated manner to regulate mineralization within the 3D matrix and further enhance the viability of cells cultured in it. In this study, the charge density of a PEGmM-PPGmM-MA hydrogel was controlled with the mass fraction of charged MA, and the hydrophobicity was controlled with the mass fraction of hydrophobic PPGmM. In addition, micro-sized pores were incorporated into the nanoporous hydrogel via lyophilization. Interestingly, an increase in the mass fractions of MA and PPGmM coupled with the presence of micro-sized pores in the hydrogel promotes the formation of apatite layers within the hydrogel. The critical roles of hydrogel variables in regulating mineralization were related to the relative supersaturation of calcium and phosphate with respect to apatite (σ_{Ca-P}^{rel}).[131-134,139] The higher supersaturation was associated with extensive apatite formation, while the lower or zero supersaturation was related to the formation of calcium carbonate instead of apatite. The resulting apatite layers within the microporous hydrogel significantly increased the viability of stem cells laden into the micropores.

The chemical composition and morphology of minerals grown within a 3D hydrogel matrix were predominantly determined by the presence of micro-sized pores in the hydrogel matrix, likely because of the change in permeability of mineral ions. It is well known that ion transport through a 3D matrix and interactions between the ions and the matrix significantly regulate the mineralization process.[123-125] Therefore, it is likely that the entry of bigger and more negatively charged phosphate ions into the nanoporous hydrogel is limited compared to that of carbonate, leading to the predominant formation of calcium carbonate minerals within the nanoporous

hydrogel. In addition, the limited pore space in nanoporous hydrogels favored the formation of single crystals of rhombohedral morphology, typical of calcium carbonate.[140] The small fraction of apatite found in the nanoporous hydrogel may have resulted from the minerals formed within a matrix closer to the gel surface. In contrast, mineral ions, including calcium, carbonate, and phosphate, diffused into the microporous hydrogel more readily than into the nanoporous hydrogel, leading to the significant increase of supersaturation within the gel matrix. Coupled with the larger pore space for crystallization, spherulitic apatite minerals grew into a laminated structure more favorably in the microporous hydrogel. It is possible that carbonate also diffused into the microporous hydrogel, and likely associated with calcium. However, it is suggested that the apatite formation should be more predominant, because the supersaturation with respect to apatite is higher than that for the more soluble calcium carbonate.

This study also demonstrated that the mass fraction of MA of the hydrogel regulated the growth of minerals because of the changes in charge density. Specifically, carboxylic groups in alginate induced the deposition of calcium ions in both nanoporous hydrogel and microporous hydrogel, leading to the accumulation of mineral ions. The calcium ions associating with carboxylic groups facilitated the phosphate deposition onto the micropore surface. For nanoporous hydrogels, however, the limited entry of phosphate into the gel matrix likely led to the association of calcium with carbonate. The higher Ca/P ratio measured from the quantitative assay than from a spectroscopic assay should be attributed to calcium ions binding with carboxylic groups of alginate. It is well known that divalent calcium ions ionically cross-link alginate by binding with carboxylic groups, but they do not contribute to increasing the elastic modulus of the hydrogel below a critical concentration.[141] The concentration of MA

used to prepare the hydrogel with PEGmM and PPGmM was much lower than the critical concentration.

In addition, the phosphate deposition to the gel matrix was further enhanced by an increase in Φ_{PPGmM}, specifically in the microporous hydrogel. It was interpreted that an increase in Φ_{PPGmM} (hence a decrease in Φ_{PEGmM}) increased hydrophobicity of the hydrogels, as evidenced by the gradual decrease in water diffusivity. The limited water diffusion through the micro-sized pores of the hydrogel increased the extent of supersaturation with respect to apatite, thus making the association between phosphate and calcium kinetically favorable. Furthermore, the increased hydrophobicity of the hydrogel matrix likely enhanced the enthalpic interaction between the matrix and minerals, leading to increased mineral deposition.[122] These interpretations suggest that hydrophobicity of the gel matrix imparts the phosphate deposition both kinetically and thermodynamically.

Overall, we found that pore size, density of charged units, and hydrophobic units should be orchestrated together to control the composition of minerals and the degree of mineralization. This is distinctive from previous studies that largely focused on controlling mineralization solely with the density of charged units of the hydrogel.[127,142] In addition, the mineralization in those studies mostly occurred on the surface, and was limited within the hydrogel. Furthermore, regardless of the presence of charged groups, the hydrogel systems previously used to derive 3D mineralization had to be subjected to an external stimulus, such as electrophoresis.[143,144] These results imply that it is difficult to reach supersaturation within hydrogels because the small size and hydrophilic environment of the pores in conventional hydrogels limits the influx and subsequent deposition of mineral ions to the matrix. We suggest that incorporation of PPGmM

and micro-sized pores into the charged hydrogel should readily lead to supersaturation and subsequent formation of minerals within the hydrogel in physiological conditions.

Furthermore, the mineralized matrix generated by modulating both charge density and hydrophobicity of the hydrogel was beneficial to supporting the viability of cells incorporated into its micropores. It was initially predicted that the increase in mass fraction of PPGmM would result in limited cell viability because of the decrease of water diffusivity through the gel matrix. However, the enhanced apatite formation with PPGmM promoted the viability of encapsulated cells. This result clearly demonstrated the relationship between the degree of mineralization of a 3D matrix and cellular viability.

We envisage the result of this study reflects the mineralization of osteoid, the unmineralized organic portion of the bone matrix.[145] Apatite formed in bone is known to contain a certain portion of carbonate. This complex mineral structure of bone implies that the osteoid has sophisticated control over the supersaturation of biomaterials and transport of calcium, phosphate, and carbonate through the matrix. A hydrogel developed to independently control charge density, hydrophobicity, and pore size may allow one to identify osteoid variables critical for both bone development and repair. However, this should be preceded by a study to relate hydrogel variables to the incorporated amounts of carbonate in apatite. Ultimately, further studies would enable one to create a hydrogel to regulate apatite formation and the carbonation of apatite in a controlled manner.

6.4 Materials and Methods

6.4.1 Synthesis of methacrylic alginate (MA)

Alginate with a high guluronic acid content (LF 20/40, M_W 250,000 g mol^{-1}, FMC BioPolymer) was dissolved in 0.1 M MES (2-(N-morpholino) ethanesulfonic acid) buffer (pH 6.4) at 1 wt %. 1-hydroxybenzotriazole (Fluka), 1-ethyl-3-(3-dimethylaminopropyl) carbodiimide (Thermo Scientific), and 2-aminoethyl methacrylate (Sigma Aldrich) were subsequently dissolved in the molar ratio of 1.6: 1.6: 1, and the mixture was stirred for 19 hours.[52,63] The molar ratio between uronic acid residues in an alginate chain and 2-aminoethyl methacrylate was 4:1. After the reaction, the mixture was dialyzed against deioninzed (DI) water for two days, exchanging for fresh DI water every twelve hours. The dialyzed mixture was lyophilized, and the dried sample was reconstituted with DI water to 1 wt % solution.

6.4.2 PPGmM-PEGmM-MA hydrogel formation

Pre-gel solutions were prepared by mixing 10 wt % poly(propylene glycol) monomethacrylate (PPGmM, M_n ~ 375 g/mol, Sigma Aldrich), 10 wt % poly(ethylene glycol) monomethacrylate (PEGmM, M_n ~ 526 g/mol, Sigma Aldrich), and 1 wt % MA in various mass ratios (Table 1). 30 μL of 1 M ammonium persulfate (Sigma Aldrich) and 5 μL of N,N,N',N'-tetramethylethylenediamine (Fluka) were added to 1.0 ml of each pre-gel solution and mixed thoroughly. Then, 200 μL of a pre-gel solution was quickly added to a well in 24-well plate. The plate was placed on a rotating shaker (50 rpm) for 10 minutes to form the hydrogel. The pore diameters (ξ) of the resulting nanoporous hydrogels were determined from the following equation.[55,74]

$$\xi = \upsilon_{2s}^{-\frac{1}{3}} l (2 \frac{\overline{M_c}}{M_r} C_n)^{\frac{1}{2}} \quad (11)$$

where υ_{2s} is the polymer volume fraction of a swollen hydrogel which is equivalent to the inverse of swelling ratio. The swelling ratio was measured after incubating the gel in phosphate buffered saline (pH 7.4) at 37 ℃ for 24 hours. l is the average bond length of a polymer backbone (1.46 Å for PEGmM[146], 1.48 Å for PPGmM, 5.15 Å for alginate[147]), M_r is the molecular mass of the repeating unit (44 g mol^{-1} for PEGmM, 58 g mol^{-1} for PPGmM, 175 g mol^{-1} for alginate), $\overline{M}_C$ is the number average molecular weight between cross-links (263 g mol^{-1} for PEGmM, 187.5 g mol^{-1} for PPGmM, 125,000 g mol^{-1} for alginate).[74] C_n is the characteristic ratio of a polymer (4 for PEGmM[146], 5.05 for PPGmM[148], 19.4 for alginate[149]).

To introduce micro-sized pores into the hydrogel, the hydrogel was frozen at -20 ℃ and subsequently lyophilized until the solvent was completely sublimated.[128-130] The volume of the hydrogel expanded during lyophilization was not changed after rehydration, indicating the expanded pores remain unchanged. The diameter of these pores was quantified with microscopic images captured with a scanning electron microscope (SEM, JEOL-6060LV). The diameters of ten randomly chosen pores from each hydrogel were measured. Three hydrogels were examined for each condition.

6.4.3 Measurement of charge density

The charge density of a hydrogel was calculated from the amount of free carboxylic groups in MA, which was measured using titration.[53] Briefly, 300 μL of 1 wt % MA was diluted with DI water to 5 mL. The solution was titrated by adding 10 mM NaOH and measuring the

change in pH. pH was recorded 20 minutes after each addition of NaOH to ensure complete reaction between carboxylate and NaOH (marked by no change in pH). The titration curve was obtained from this experiment, and the amount of charge in MA, with a unit of C mol^{-1}, was calculated from the amount of NaOH required to reach the equivalence point. The amount of charge per mole of MA was further multiplied with the density of MA (in mol m^{-3}) in a hydrogel to calculate the charge density with a unit of C m^{-3}.

6.4.4 Characterization of water diffusivity of a hydrogel

Hydrogels with different compositions were incubated in DI water, and the amount of water diffused into each hydrogel was measured. Briefly, for each gel, the amount of absorbed water (W_t) at various time points, and the amount of water at equilibrium (W_∞) (marked by no change in weight) were measured. W_t / W_∞ was plotted as a function of time (t), and the diffusivity (D) was calculated using the following equation for $W_t / W_\infty \leq 0.8$,[150,151]

$$\frac{W_t}{W_\infty} = \frac{4}{\sqrt{\pi}} \times \left(\frac{D \times t}{L^2} \right)^{\frac{1}{2}} \tag{12}$$

where L is the thickness of the hydrogel. For each condition, the experiment was done in triplicate and averaged.

6.4.5 Mineralization

The nanoporous hydrogels and microporous hydrogels were incubated in modified simulating body fluid (mSBF) at 37 ℃ for one week. The buffer was changed on a daily basis

to supply a sufficient amount of ions. The mSBF contained 141 mM NaCl, 4.0 mM KCl, 0.5 mM $MgSO_4$, 1.0 mM $MgCl_2$, 4.2 mM $NaHCO_3$, 5 mM $CaCl_2$, and 2.0 mM KH_2PO_4. The pH of mSBF was adjusted to pH 7.4 by adding Tris-HCl buffer (pH 8).[15] After mineralization, the hydrogels were washed for one hour with DI water three times to remove mSBF inside the hydrogels.

6.4.6 Characterization of mineralized hydrogels

The amounts of Ca^{2+} and PO_4^{3-} in the hydrogel were quantified with QuantiChrom™ Calcium Assay Kit and Malachite Green Phosphate Assay Kit (BioAssay Systems), respectively.[152] Briefly, a mineralized hydrogel was lyophilized, followed by incubation in 5 M sulfuric acid solution for twelve hours to dissolve minerals.[15] The amount of each ion was determined using the appropriate assay kit following the manufacturer's instructions. The hydrogels were subjected to compression with a mechanical testing system (MTS Insight) before and after mineralization to measure mechanical stiffness. Each hydrogel was compressed at a rate of 2 mm min^{-1} and the elastic modulus was calculated from the slope of stress vs. strain curve at the first 10 % strain.[83,84] The experiment for each condition was done in triplicate and averaged.

The tendency to form apatite in a hydrogel was quantified by calculating the supersaturation with respect to the apatite from the quantitative analysis of Ca^{2+} and PO_4^{3-} described above. σ_{Ca-P}^{rel}, the relative supersaturation with respect to apatite, was calculated using the following equation,

$$\sigma_{Ca-P}^{rel} = [(Ca^{2+})^{10} (PO_4^{3-})^6]^{\frac{1}{16}} \quad (13)$$

where (Ca^{2+}) and (PO_4^{3-}) are the concentrations of calcium and phosphate ions, respectively. The equation was modified to represent only calcium and phosphate, since the concentration of OH^- and the solubility product constant for apatite were not determined in this study.[139] The normalized σ_{Ca-P}^{rel} was obtained by dividing the values by the highest σ_{Ca-P}^{rel} value, which was obtained in the microporous hydrogel with Φ_{PPGmM} of 0.72 and Φ_{MA} of 0.04.

6.4.7 Morphological analysis of mineralized hydrogels

Following the mineralization, the hydrogels of all conditions were washed with DI water, and subsequently lyophilized. The morphology and elemental composition of minerals formed within the hydrogels were analyzed with SEM and an energy-dispersive X-ray spectroscopy (EDX) module attached to the SEM (LinkISIS, Oxford), respectively. Then, each sample was fractured and its cross-section was analyzed with the SEM under high vacuum.

6.4.8 X-ray diffraction (XRD) and Fourier-transform infrared (FT-IR) spectroscopic analyses of mineralized hydrogels

The minerals formed within the hydrogels were further characterized with XRD and FT-IR spectroscopic methods. For XRD analysis, each lyophilized hydrogel was mounted flat on a glass sample holder. The XRD spectrum was obtained using Rigaku D/Max-b (Rigaku Americas) with 2θ angles from 20° to 40° at a scan rate of 1.5 ° min^{-1}. For FT-IR analysis, each lyophilized hydrogel was mechanically ground and made into a pellet with potassium bromide

powder. The FT-IR transmittance spectrum in a wavelength region from 600 to 2000 cm^{-1} was acquired using a FT-IR spectrometer (Spectrum BX, Perkin Elmer).

6.4.9 Analysis of cell viability in mineralized hydrogels

Mesenchymal stem cells derived from porcine adipose tissue (ADSCs) were a kind gift from Prof. Lawrence Schook (Department of Animal Sciences, University of Illinois). The isolation, characterization, and expansion procedures are provided elsewhere.[153] ADSCs before passage 4 were used in this experiment. The mineralized hydrogel disks (5 mm diameter, 1 mm thickness) were washed in ethanol for one hour for sterilization. Next, the hydrogels were rehydrated in deionized water and then lyophilized. 5×10^3 ADSCs suspended in 30 μL of culture medium (Dulbecco's Modified Eagle Medium supplemented with 10 % fetal bovine serum and 1% penicillin/streptomycin, all purchased from Gibco) were placed on top of a lyophilized hydrogel, allowing the mixture to be soaked into the dried gel mesh. Then, the hydrogel was immersed in culture medium and incubated at 37 ℃ with 5 % CO_2. The viability of cells in the hydrogel was measured using MTT Cell Proliferation Assay kit (ATCC) after 3 days. Briefly, the cell laden hydrogel was incubated in culture media containing MTT, 3-(4,5-dimethylthiazol-2-yl)-2,5-diphenyltetrazolium bromide, which is enzymatically metabolized by living cells into dark purple MTT formazan. After 4 hours of incubation, MTT detergent was added to stop the process and dissolve the product. The hydrogel was removed and the absorbance of the medium at 570 nm was measured using a spectrophotometer (Synergy HT, BioTek). The experiment for each condition was done in triplicate and averaged. As a negative control for each condition, a hydrogel without encapsulated cells was assayed.

6.5 Figures & Tables

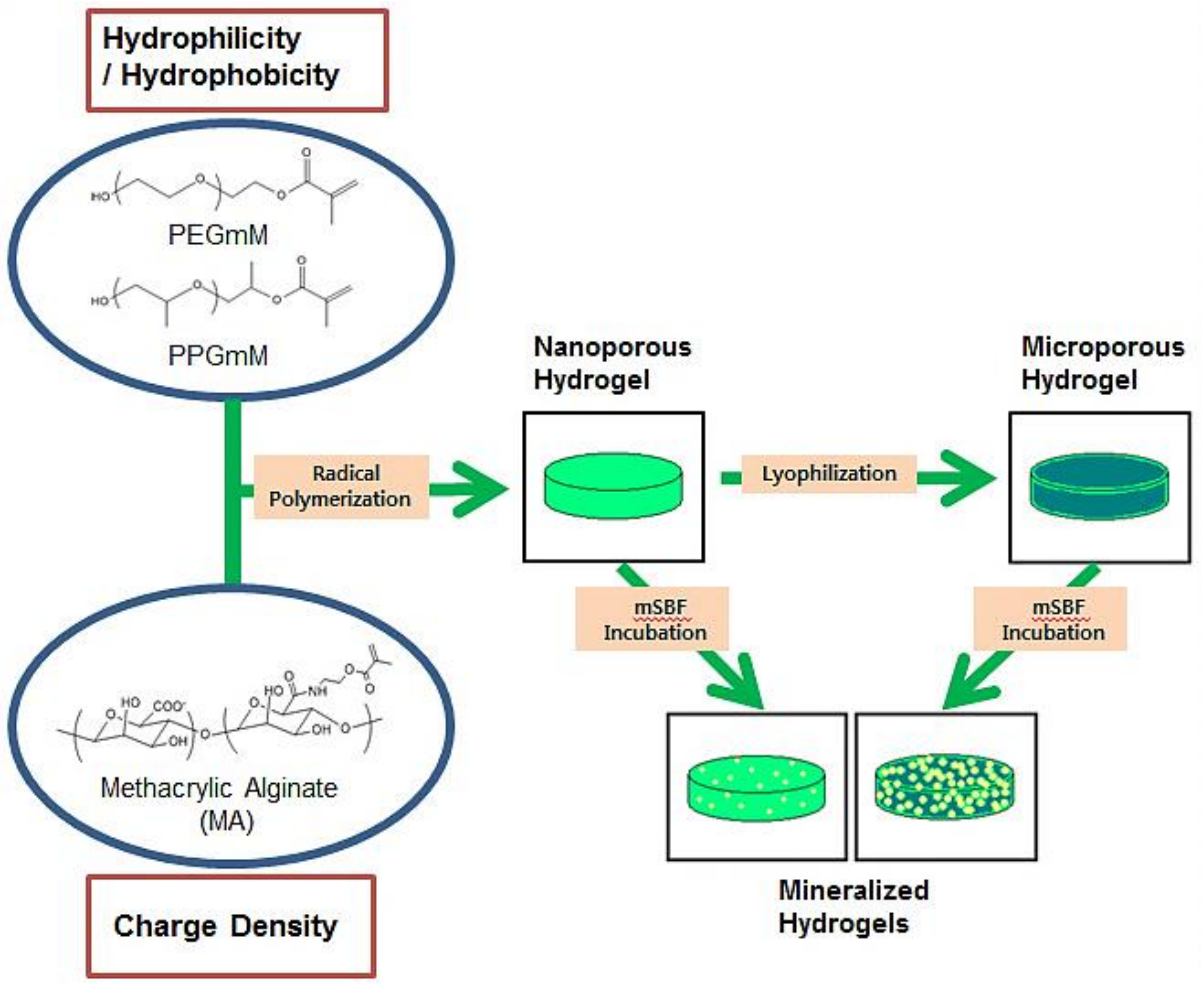

Figure 6.1 Poly(propylene glycol) monomethacylate (PPGmM) and poly(ethylene glycol) monomethacrylate (PEGmM) were chemically cross-linked to form hydrogels, with MA acting as a cross-linker. The ratio of PPGmM and PEGmM were varied to modulate hydrophobicity, while the amount of MA was varied to control the charge density. The resulting hydrogels (nanoporous hydrogels) and those lyophilized to present micro-sized pores (microporous hydrogels) were incubated in modified simulating body fluid (mSBF) to induce mineralization.

Table 6.1 Composition of hydrogels varied with the mass fraction of methacrylic alginate (MA) (Φ_{MA}) (a) and the mass fraction of poly(propylene glycrol) monomethacrylate (PPGmM) (Φ_{PPGmM}) (b). Lyophilization increased the hydrogel pore diameter scale from nanometers (ξ_{nano}) to micrometers (ξ_{micro}). In (a), the ratio of Φ_{PPGmM} and Φ_{PEGmM} was kept constant while increasing Φ_{MA} from 0.007 to 0.04, which increased the charge density (C_{gel}) from 0.7 to 1.6 ($\times 10^{-6}$ C m^{-3}). In (b), Φ_{MA} was kept constant at 0.04 (C_{gel} of 1.6 $\times$ 10^{-6} C m^{-3}) while increasing Φ_{PPGmM} from 0 to 0.72. Water diffusivity of the microporous hydrogel (D_{micro}) was decreased with Φ_{PPGmM}, specifically for microporous hydrogels. Introducing micro-sized pores into nanoporous hydrogels significantly increased water diffusivity of the gel matrix.

(a)

Φ_{PPGmM}	Φ_{PEGmM}	Φ_{MA}	C_{gel} ($\times 10^{-6}$ C m^{-3})	ξ_{nano} (**nm**)	ξ_{micro} (**μm**)	E_0 (kPa)
0.4965	0.4965	0.007	0.7	11.3 ± 0.7	32.4 ± 4.3	< 1*
0.493	0.493	0.014	1.0	14.7 ± 0.9	28.5 ± 6.2	< 1*
0.486	0.486	0.028	1.3	18.1 ± 1.1	25.4 ± 4.3	2.0 ± 1.2
0.48	0.48	0.04	1.6	21.5 ± 1.3	27.4 ± 7.4	2.4 ± 0.9

* Below detection limit

(b)

Φ_{PPGmM}	Φ_{PEGmM}	Φ_{MA}	D_{nano} ($\times 10^{-9}$ m^2 h^{-1})	D_{micro} ($\times 10^{-9}$ m^2 h^{-1})	ξ_{nano} (**nm**)	ξ_{micro} (**μm**)	E_0 (kPa)
0	0.96	0.04	3.5 ± 5	36 ± 6	23.4 ± 5.2	30.6 ± 4.6	3.5 ± 1.2
0.24	0.72	0.04	4.7 ± 4	23 ± 1.5	22.4 ± 3.8	25.4 ± 5.2	3.4 ± 1.4
0.48	0.48	0.04	7.5 ± 3	12 ± 5	21.5 ± 1.3	27.4 ± 7.4	2.4 ± 0.9
0.72	0.24	0.04	0.9 ± 3	4.6 ± 6	17.4 ± 5.2	24.5 ± 5.3	2.6 ± 0.3

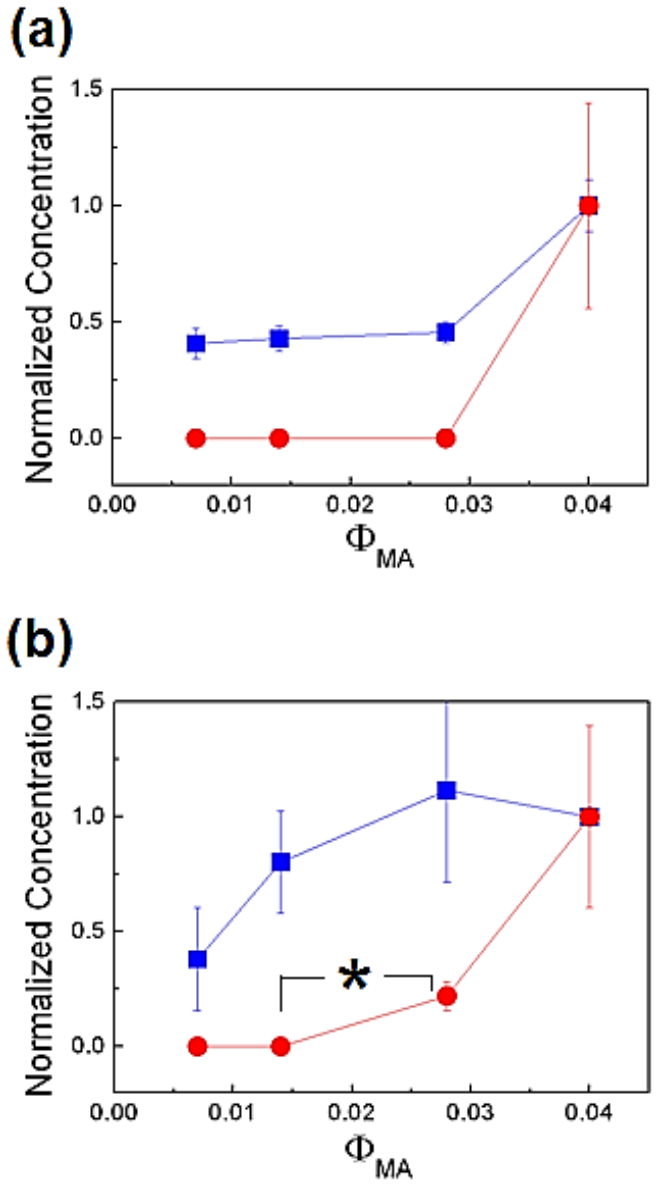

Figure 6.2 Concentrations of calcium (■) and phosphate (●) in the hydrogels increased with Φ_{MA} for both nanoporous (a) and microporous (b) hydrogels. The ratio of Φ_{PPGmM} and Φ_{PEGmM} was kept constant. Calcium and phosphate concentrations in (a) and (b) were normalized with those for the hydrogel formed at the highest Φ_{MA} at 0.04. (*$p<0.05$)

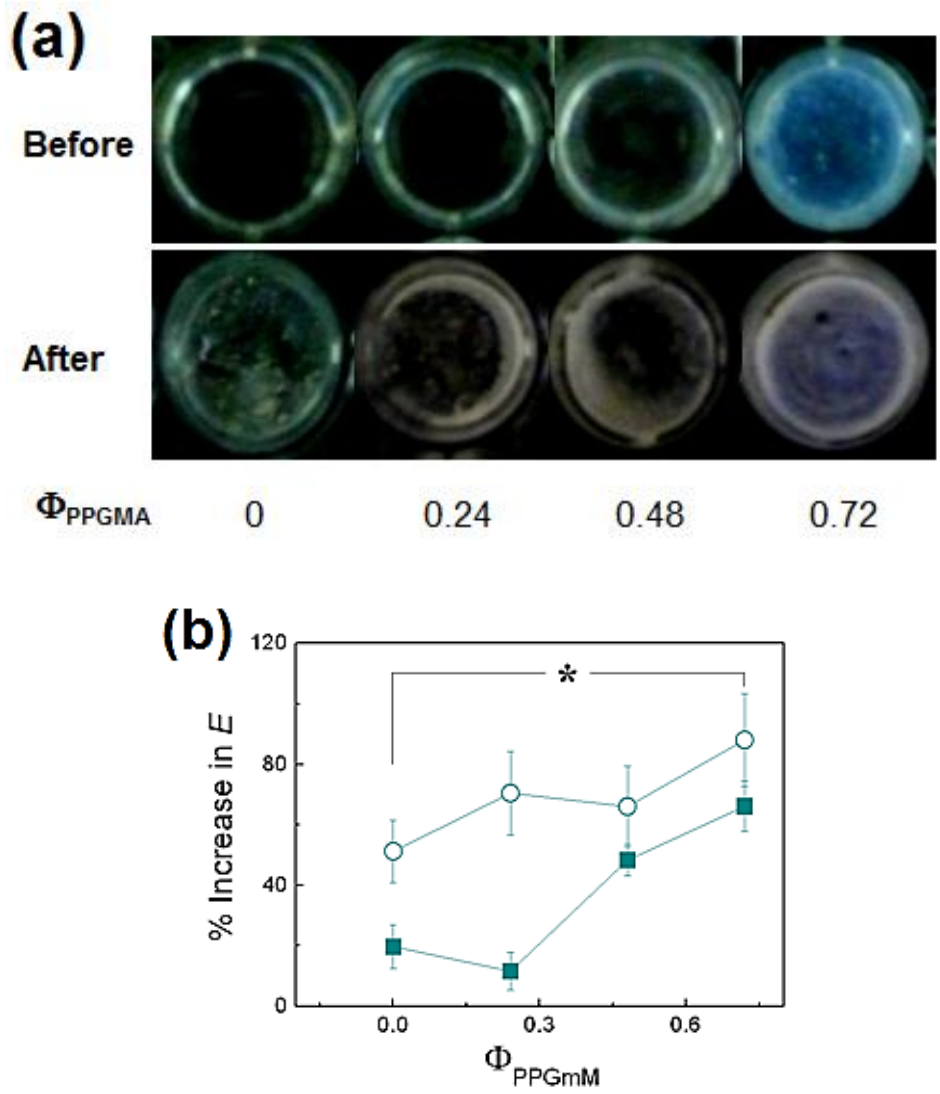

Figure 6.3 (a) Incubating hydrogels consisting of PEGmM, PPGmM, and MA in mSBF increased the opaqueness depending on the Φ_{PPGmM}. (b) Incubation of hydrogels in the mSBF also increased the elastic modulus (E) of the hydrogel matrices, and the degree of increase in the elastic modulus became significant with Φ_{PPGmM} for both nanoporous (■) and microporous (○) hydrogel. The degree of increase in E was quantified by normalizing E of the gel matrix measured after incubation in mSBF with the initial E measured prior to the incubation. (*$p<0.05$)

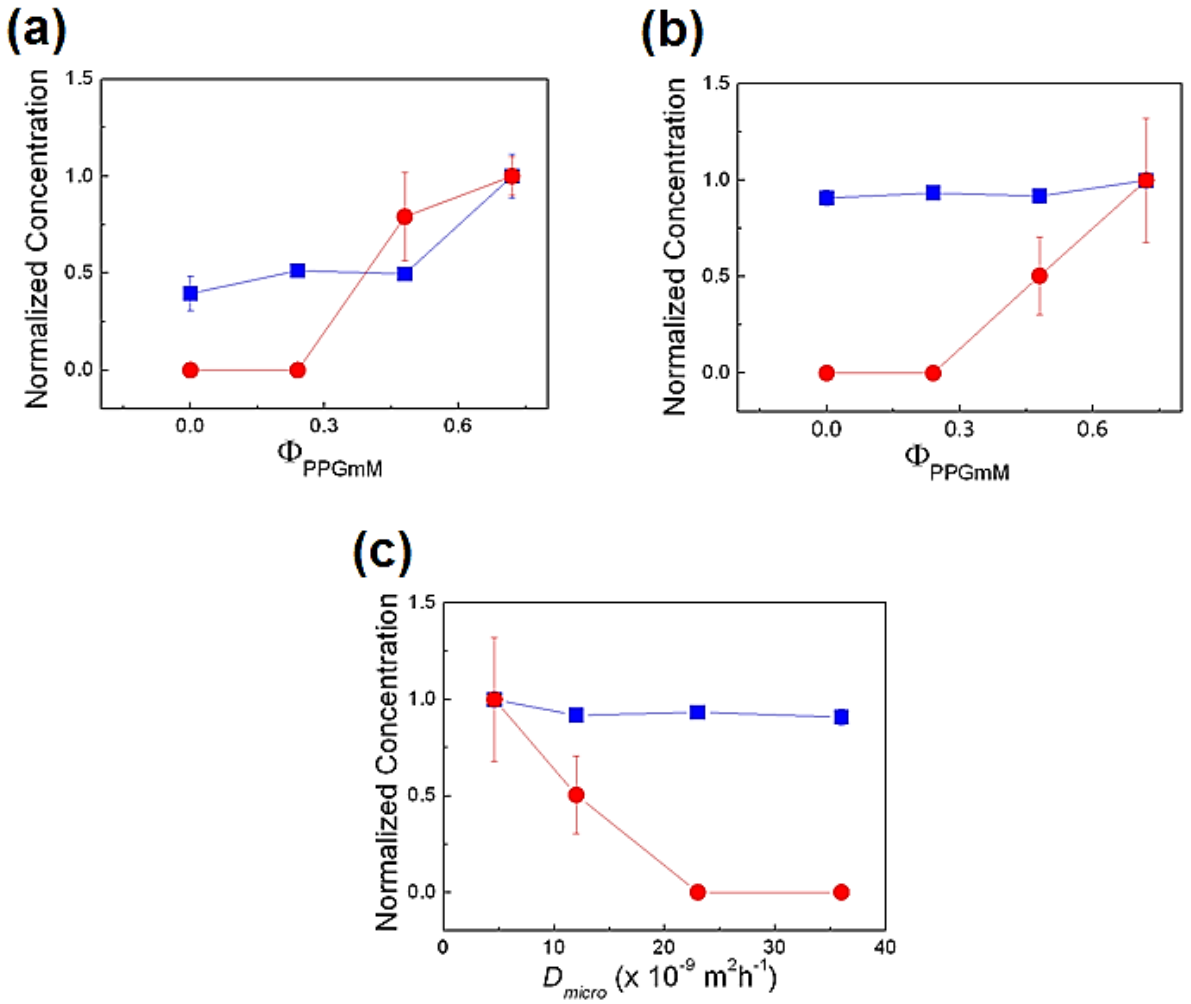

Figure 6.4 Increasing Φ_{PPGmM} of the nanoporous hydrogel (a) and the microporous hydrogel (b) at the constant Φ_{MA} of 0.04 resulted in the increase of the phosphate concentration (■), but it made minimal change in the calcium concentration (●). The calcium and phosphate concentrations of the microporous hydrogel were further related to the diffusivity (D_{micro}) of the hydrogel (c). Calcium and phosphate concentrations in (a) and (b) were normalized with those for the hydrogel formed at the highest Φ_{PPGmM} (at 0.72).

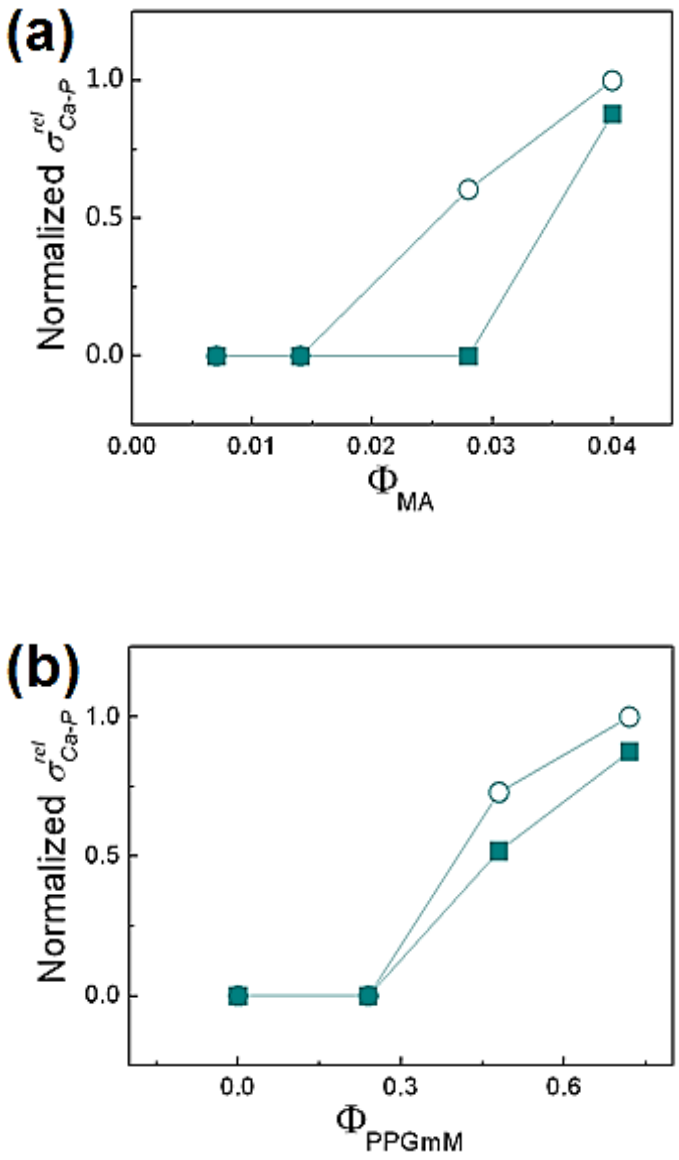

Figure 6.5 Normalized relative supersaturation with respect to apatite, σ^{rel}_{Ca-P}, for the nanoporous (■) and microporous (○) hydrogels increased with Φ_{MA} at a constant ratio of Φ_{PPGmM} and Φ_{PEGmM} (a) or with Φ_{PPGmM} at a constant Φ_{MA} of 0.04 (b).

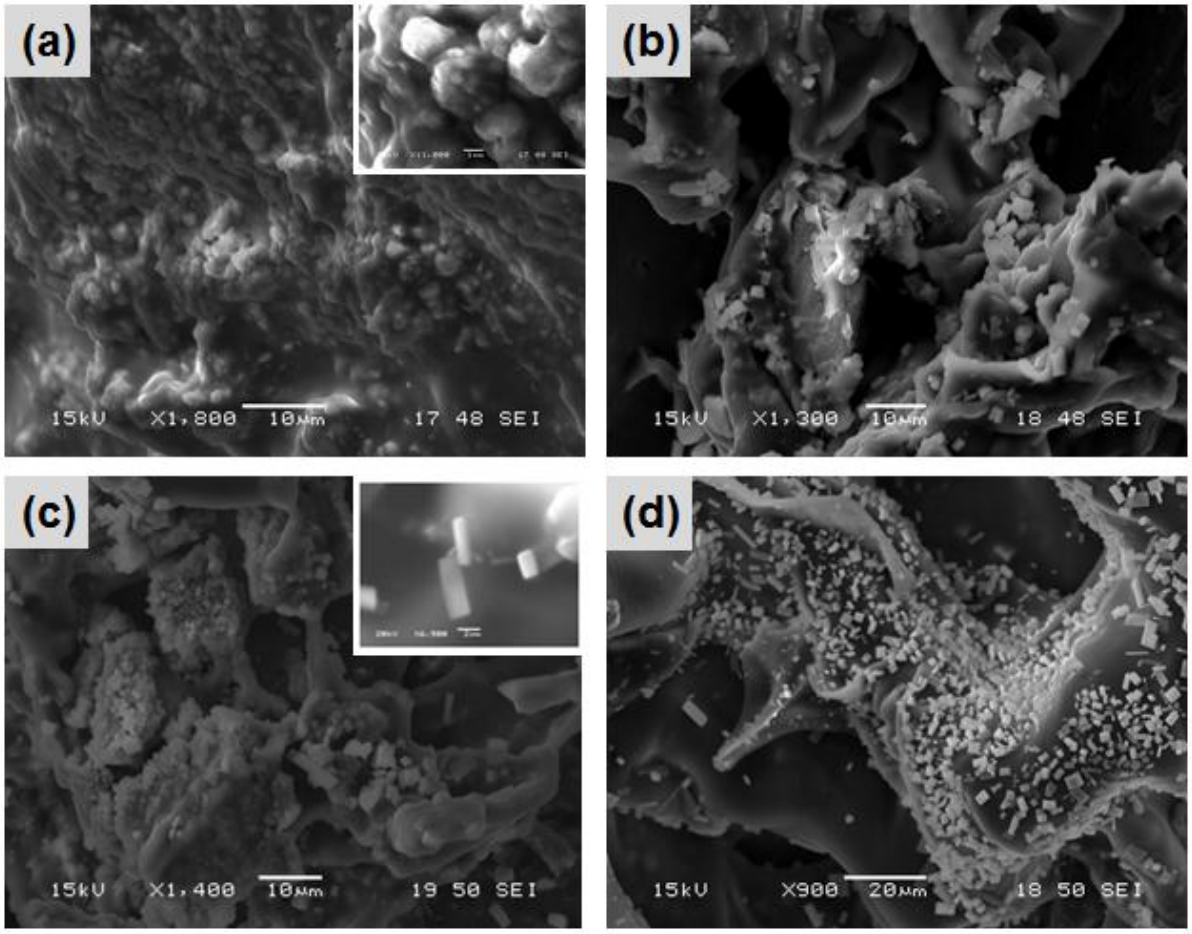

Figure 6.6 Scanning electron microscopic (SEM) images of mineralized hydrogels. The microporous hydrogel at the highest Φ_{PPGmM} of 0.72 presented extensive deposition of spherulitic minerals (a), whereas there were fewer spherulitic minerals at the lowest Φ_{PPGmM} of 0 (b). The inset in (a) shows the magnified view of spherulitic mineral particles. In contrast, the nanoporous hydrogels at the highest Φ_{PPGmM} of 0.72 presented extensive deposition of rhombohedral minerals (c), whereas the hydrogel with the lowest Φ_{PPGmM} of 0 presented fewer rhombohedral minerals (d). The inset in (c) shows the magnified view of rhombohedral mineral particles.

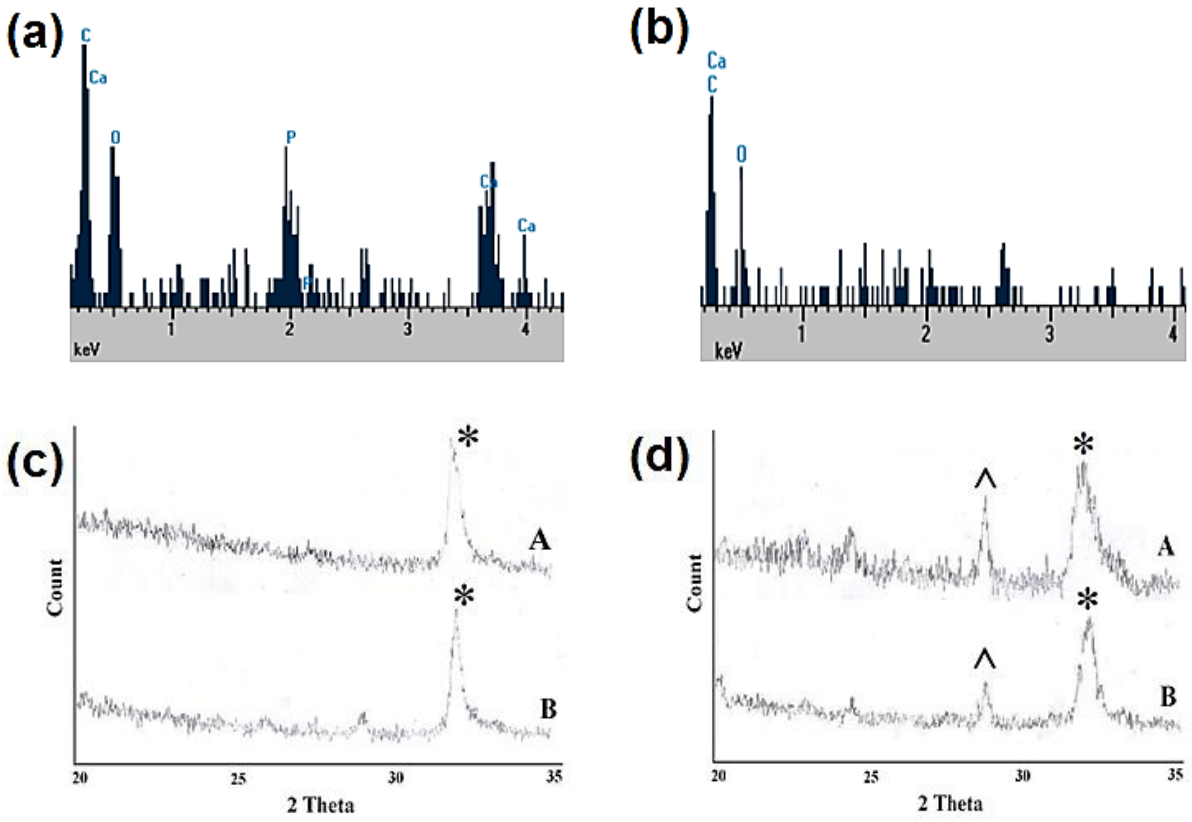

Figure 6.7 Energy-dispersive X-ray (EDX) analysis of spherulitic minerals (a) and rhombohedral minerals (b). Spherulitic minerals show the presence of calcium and phosphate with a Ca/P ratio of 1.7, indicative of apatite. Rhombohedral minerals did not show phosphorous peaks. X-ray diffraction (XRD) spectra for microporous (c) and nanoporous (d) hydrogels. Spectrum A represents the mineralized hydrogel at the highest Φ_{PPGmM} of 0.72, whereas spectrum B represents the mineralized hydrogel at the lowest Φ_{PPGmM} of 0. The peak representing apatite, at 32°, is denoted with *. The peak representing calcite, at 29°, is denoted with ^.

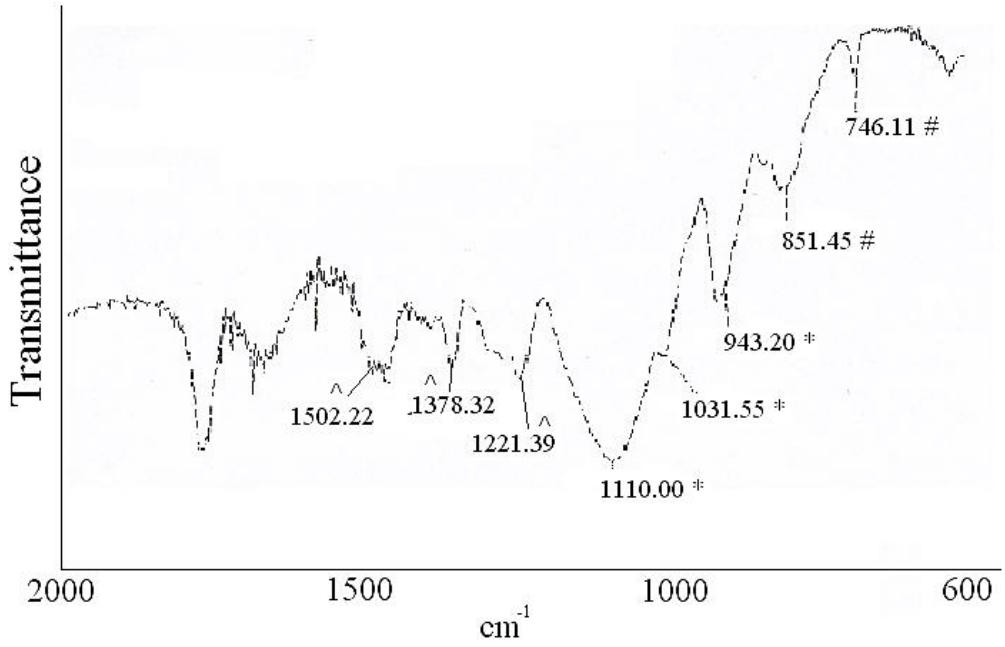

Figure 6.8 Representative Fourier-transform infrared (FT-IR) spectrum of a mineralized microporous hydrogel with Φ_{PPGmM} of 0.72. The spectrum displays the characteristic peaks for apatite (denoted with *). Furthermore, the peaks associated with the carbonate substitution of apatite (denoted with ^) were also shown. Peaks associated with calcite (denoted with #) are also detected.

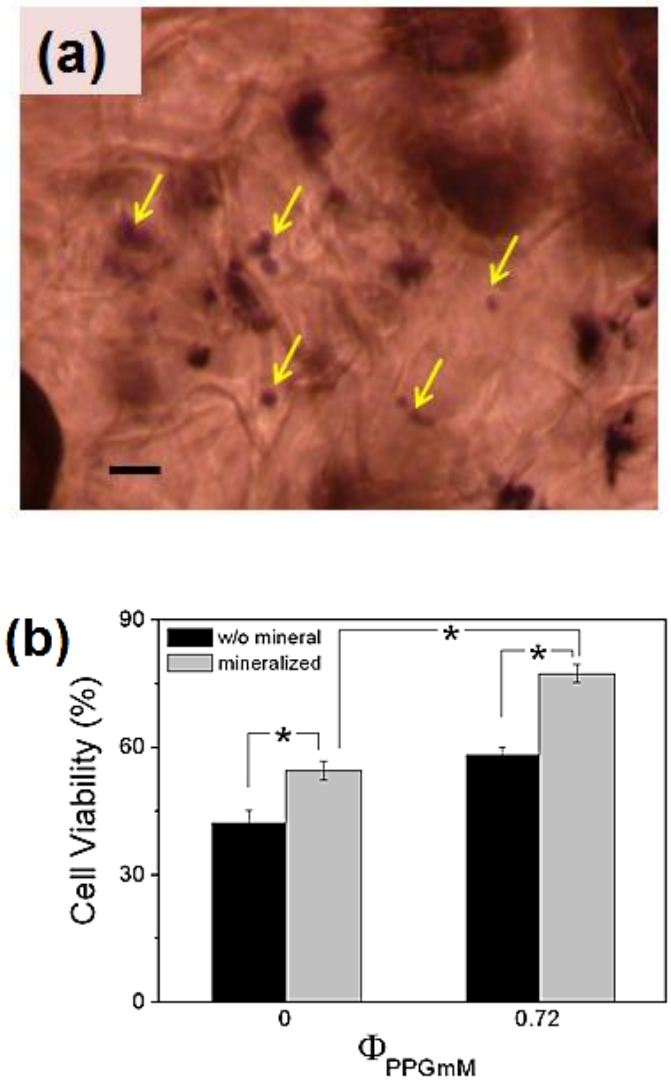

Figure 6.9 (a) The viability of mesenchymal stem cells incorporated into microporous hydrogels were determined by MTT assay, in which viable cells are stained purple by MTT (arrow). (b) The fraction of viable cells was higher in the mineralized hydrogel containing the higher Φ_{PPGmM}. The viability was measured 3 days after the cells were loaded into the hydrogels. (*$p<0.05$)

Chapter 7 Conclusion and Future Works

7.1 Conclusion

In this research, hydrogel system which allows independent control of stiffness from permeability was developed for its applications in 3D cell culture and cell transplantation therapy. The hydrogel system was created by the assembly of three modules that serve individual and distinctive roles, and eventually contribute to the overall hydrogel properties.

First, presenting hydrophilic pendant chains into a hydrogel system allowed control of hydrogel stiffness over a broad range, while limiting the change in permeability. Decreasing cross-linking density of hydrogel system resulted in decreasing hydrogel stiffness, but the decrease in permeability could be effectively minimized by increasing the number of hydrophilic pendant chains which acted as a barrier against diffusion. Viability and growth factor expression of cells encapsulated in the hydrogels with varying stiffness were dependent on the hydrogel stiffness, as they showed biphasic dependency on the stiffness. On the other hand, in a conventional hydrogel system in which stiffness and permeability are inversely coupled, the cell phenotypes were subject to both stiffness and permeability.

Second, methacrylic alginate (MA) was synthesized by conjugating methacrylic functional groups onto alginate. MA could be incorporated into a hydrogel system by co-polymerization with other gel-forming molecules. MA improved the mechanical stiffness of the hydrogel while limiting the change in permeability, due to the stiff molecular structure of alginate contributing to the overall hydrogel stiffness, and multiple hydrophilic functional groups promoting diffusion of surrounding fluid. Extended molecular structure of alginate further prevented swelling by

polymeric chain relaxation for hydrogels with lower cross-linking density. The presence of alginate also improved the viability of encapsulated cells, likely from the ability of alginate to prolong the presence of bioactive molecules within the hydrogel system.

Third, multivalent polymeric protein linker was created by nucleophilic addition of polysuccinimide (PSI). PSI, which consists of a series of succinimidyl ring moieties, allows nucleophilic addition of amine-based molecules to form polyaspartamide. Here, amine-based nucleophile containing functional groups reactive to a desired material was conjugated to PSI to form polyaspartamide linker. A portion of unreacted succinimidyl groups of the polyaspartamide linker would allow conjugation of protein molecules which also contain amine groups. The polyaspartamide linkers have two major advantages over conventional small molecule linkers: multivalency of reactive groups towards both protein and material, and versatility.

The three modules described above were assembled into the overall hydrogel system, and their properties and unique advantages synergistically contributed to the hydrogel structure which allows control of stiffness decoupled from permeability and also presents bioactive molecules to derive desired cell behaviors. Incorporating methacrylic alginate into hydrogels with varying fraction of polymeric pendant chains allowed the control of hydrogel stiffness in the same range at much lower total polymer concentration, while limiting the change in permeability. Modulations of degree of methacrylic substitution and concentration of methacrylic alginate further controlled the range of hydrogel stiffness, while the ability of pendant polymeric chains to decouple the stiffness from permeability was well retained. Polyaspartamide linker was used to conjugate a cell-responsive bioactive protein into the hydrogel system by co-polymerization to

induce desired cell behavior, without affecting the mechanical properties. Mesenchymal stem cells were encapsulated into the hydrogels, and it was determined that their cellular phenotypes, viability and growth factor expression, were shown to have biphasic dependence on the hydrogel stiffness.

Additionally, physical properties of hydrogels, hydrophobicity/hydophilicity, porosity and charge density, in order to control biomineralization within the hydrogels for applications in bone tissue engineering. Hydrophobicity/hydrophilicity was modulated by varying the ratio of hydrophilic poly(ethylene glycol) (PEG) and hydrophobic poly(propylene glycol) (PPG). Porosity of hydrogel was expanded from nanometer to micrometer scale by lyophilization. Charge density was modulated by varying the amount of methacrylic alginate which contains negatively charged carboxylate. Increasing hydrophobicity, charge density and introducing micrometer-sized pores promoted the formation of carbonated hydroxyapatite which is the major type of mineral found in bone.

7.2 Future Works

This research has been focused on creating polymer systems used to fabricate hydrogels, with the properties that allow the control of stiffness while limiting permeability, and link cell-responsive protein into a hydrogel system independently without affecting the mechanical properties. Although the results of this research demonstrate the novelty, functionality, and applicability of the hydrogel system in studying the effects of hydrogel properties on cell functions in three dimensions, I suggest these results should be further validated and strengthened by additional biological studies.

First, exploring various cell types would provide further insights into the effects of hydrogel properties on cell functions. For example, the different cell types may behave differently in response to the same hydrogel properties. Alternatively, the same cell types that are derived from different sources may also behave differently to hydrogel properties as well. Providing different cell-responsive proteins into the hydrogels may also mediate various cellular responses.

Second, although VEGF expression was determined in this research, expressions of other growth factors and cytokines by encapsulated cells should be thoroughly examined to evaluate the therapeutic efficacy of the cells. Mesenchymal stem cells are well known to constitutively express a wide variety of growth factors and cytokines, thus rendering their therapeutic effects. Depending on the applications, it is necessary to focus on different types of soluble factors. Thus, exploring the effects of hydrogel mechanical properties on these soluble factors would provide a more complete evaluation of the cells' therapeutic potentials within the hydrogel system.

Third, it would be interesting to compare the cell phenotypes obtained from 3D cell culture in

the hydrogel system with those obtained on 2D hydrogel surface. Conventionally, much of the biological studies have been conducted by culturing cells on surface, although the cells are surrounded within 3D matrices. Thus comparison study between cells cultured on hydrogel surface (2D) and within hydrogel (3D) at the same range of hydrogel stiffness would reveal the differential effects of stiffness on cells at different dimensions.

Finally, proteomic analyses of protein expressions related to the intracellular signaling pathways and cellular phenotypes such as viability, proliferation and expressions of soluble factors would provide deeper fundamental understanding of the role of matrix properties in tuning cellular activities. Identification of the factors responsible for controlling the phenotypes would open up the possibility of further manipulation of cells to maximize their therapeutic potentials.

References

(1) Jiang, Y. H.; Jahagirdar, B. N.; Reinhardt, R. L.; Schwartz, R. E.; Keene, C. D.; Ortiz-Gonzalez, X. R.; Reyes, M.; Lenvik, T.; Lund, T.; Blackstad, M.; Du, J. B.; Aldrich, S.; Lisberg, A.; Low, W. C.; Largaespada, D. A.; Verfaillie, C. M. *Nature* **2002**, *418*, 41.

(2) Zuk, P. A.; Zhu, M.; Mizuno, H.; Huang, J.; Futrell, J. W.; Katz, A. J.; Benhaim, P.; Lorenz, H. P.; Hedrick, M. H. *Tissue Eng.* **2001**, *7*, 211.

(3) Pittenger, M. F.; Mackay, A. M.; Beck, S. C.; Jaiswal, R. K.; Douglas, R.; Mosca, J. D.; Moorman, M. A.; Simonetti, D. W.; Craig, S.; Marshak, D. R. *Science* **1999**, *284*, 143.

(4) Deans, R. J.; Moseley, A. B. *Exp. Hematol.* **2000**, *28*, 875.

(5) Kinnaird, T.; Stabile, E.; Burnett, M. S.; Lee, C. W.; Barr, S.; Fuchs, S.; Epstein, S. E. *Circ. Res.* **2004**, *94*, 678.

(6) Schmidt, J. J.; Rowley, J.; Kong, H. J. *J. Biomed. Mater. Res. Part A* **2008**, *87A*, 1113.

(7) Bae, M.-S.; Park, Y. J.; Mooney, D. J.; Lee, K. Y. *Macromol. Res.* **2007**, *15*, 469.

(8) Discher, D. E.; Mooney, D. J.; Zandstra, P. W. *Science* **2009**, *324*, 1673.

(9) Wang, N.; Tytell, J. D.; Ingber, D. E. *Nat. Rev. Mol. Cell Biol.* **2009**, *10*, 75.

(10) Geiger, B.; Spatz, J. P.; Bershadsky, A. D. *Nat. Rev. Mol. Cell Biol.* **2009**, *10*, 21.

(11) Eckes, B.; Zweers, M. C.; Zhang, Z. G.; Hallinger, R.; Mauch, C.; Aumailley, M.; Krieg, T. *J. Investig. Dermatol. Symp. Proc.* **2006**, *11*, 66.

(12) Anseth, K. S.; Bowman, C. N.; Brannon-Peppas, L. *Biomaterials* **1996**, *17*, 1647.

(13) Roach, H. I. *Cell Biol. Int.* **1994**, *18*, 617.

(14) Murphy, W. L.; Hsiong, S.; Richardson, T. P.; Simmons, C. A.; Mooney, D. J. *Biomaterials* **2005**, *26*, 303.

(15) Murphy, W. L.; Mooney, D. J. *J. Am. Chem. Soc.* **2002**, *124*, 1910.

(16) Sasaki, S.; Yataki, K.; Maeda, H. *Langmuir* **1998**, *14*, 796.

(17) Jen, A. C.; Wake, M. C.; Mikos, A. G. *Biotechnol. Bioeng.* **1996**, *50*, 357.

(18) Nguyen, K. T.; West, J. L. *Biomaterials* **2002**, *23*, 4307.

(19) Drury, J. L.; Mooney, D. J. *Biomaterials* **2003**, *24*, 4337.

(20) Lee, K. Y.; Mooney, D. J. *Chem. Rev.* **2001**, *101*, 1869.

(21) Benoit, D. S. W.; Schwartz, M. P.; Durney, A. R.; Anseth, K. S. *Nat Mater* **2008**, *7*, 816.

(22) Weber, L. M.; Hayda, K. N.; Haskins, K.; Anseth, K. S. *Biomaterials* **2007**, *28*, 3004.

(23) Peyton, S. R.; Raub, C. B.; Keschrumrus, V. P.; Putnam, A. J. *Biomaterials* **2006**, *27*, 4881.

(24) Batorsky, A.; Liao, J.; Lund, A. W.; Plopper, G. E.; Stegemann, J. P. *Biotechnol. Bioeng.* **2005**, *92*, 492.

(25) Brandl, F.; Sommer, F.; Goepferich, A. *Biomaterials* **2007**, *28*, 134.

(26) Tibbitt, M. W.; Anseth, K. S. *Biotechnol. Bioeng.* **2009**, *103*, 655.

(27) Cukierman, E.; Pankov, R.; Yamada, K. M. *Curr. Opin. Cell Biol.* **2002**, *14*, 633.

(28) Gunn, J. W.; Turner, S. D.; Mann, B. K. *J. Biomed. Mater. Res. Part A* **2005**, *72A*, 91.

(29) Bott, K.; Upton, Z.; Schrobback, K.; Ehrbar, M.; Hubbell, J. A.; Lutolf, M. P.; Rizzi, S. C. *Biomaterials* **2010**, *31*, 8454.

(30) Li, R. H.; Altreuter, D. H.; Gentile, F. T. *Biotechnol. Bioeng.* **1996**, *50*, 365.

(31) Karande, T. S.; Ong, J. L.; Agrawal, C. M. *Ann. Biomed. Eng.* **2004**, *32*, 1728.

(32) Yamada, K. M.; Cukierman, E. *Cell* **2007**, *130*, 601.

(33) Cruise, G. M.; Scharp, D. S.; Hubbell, J. A. *Biomaterials* **1998**, *19*, 1287.

(34) Weber, L. M.; Lopez, C. G.; Anseth, K. S. *J. Biomed. Mater. Res. Part A* **2009**, *90A*, 720.

(35) Anseth, K. S.; Metters, A. T.; Bryant, S. J.; Martens, P. J.; Elisseeff, J. H.; Bowman, C. N. *J. Controlled Release* **2002**, *78*, 199.

(36) Kalyanasundaram, K.; Thomas, J. K. *J. Am. Chem. Soc.* **1977**, *99*, 2039.

(37) Glushko, V.; Thaler, M. S. R.; Karp, C. D. *Arch. Biochem. Biophys.* **1981**, *210*, 33.

(38) Maeda, Y.; Taniguchi, N.; Ikeda, I. *Macromol. Rapid Commun.* **2001**, *22*, 1390.

(39) Chu, C.; Schmidt, J. J.; Carnes, K.; Zhang, Z.; Kong, H. J.; Hofmann, M.-C. *Tissue Eng. Part A* **2009**, *15*, 255.

(40) Tunyogi-Csapo, M.; Koreny, T.; Vermes, C.; Galante, J. O.; Jacobs, J. J.; Glant, T. T. *J. Orthop. Res.* **2007**, *25*, 1378.

(41) Broker, B. J.; Chakrabarti, R.; Blynman, T.; Roesler, J.; Wang, M. B.; Srivatsan, E. S. *Arch. Otolaryngol. Head Neck Surg.* **1999**, *125*, 676.

(42) Kessler, D.; Dethlefsen, S.; Haase, I.; Plomann, M.; Hirche, F.; Krieg, T.; Eckes, B. *J. Biol. Chem.* **2001**, *276*, 36575.

(43) Grugel, S.; Finkenzeller, G.; Weindel, K.; Barleon, B.; Marmé, D. *J. Biol. Chem.* **1995**, *270*, 25915.

(44) Wang, D.; Huang, H.-J. S.; Kazlauskas, A.; Cavenee, W. K. *Cancer Res.* **1999**, *59*, 1464.

(45) Liu, Y.; Huglin, M. B. *Polymer* **1995**, *36*, 1715.

(46) Qu, X.; Wirs, A.; Albertsson, A. C. *Polymer* **2000**, *41*, 4589.

(47) Hou, Y.; Schoener, C. A.; Regan, K. R.; Munoz-Pinto, D.; Hahn, M. S.; Grunlan, M. A. *Biomacromolecules* **2010**, *11*, 648.

(48) Lee, W.; Cho, N.-J.; Xiong, A.; Glenn, J. S.; Frank, C. W. *Proc. Natl. Acad. Sci. U.S.A.* **2010**, *107*, 20709.

(49) Huebsch, N.; Arany, P. R.; Mao, A. S.; Shvartsman, D.; Ali, O. A.; Bencherif, S. A.; Rivera-Feliciano, J.; Mooney, D. J. *Nat. Mater.* **2010**, *9*, 518.

(50) Klein, E. A.; Yin, L.; Kothapalli, D.; Castagnino, P.; Byfield, F. J.; Xu, T.; Levental, I.; Hawthorne, E.; Janmey, P. A.; Assoian, R. K. *Curr. Biol.* **2009**, *19*, 1511.

(51) Lutolf, M. P.; Lauer-Fields, J. L.; Schmoekel, H. G.; Metters, A. T.; Weber, F. E.; Fields, G. B.; Hubbell, J. A. *Proc. Natl. Acad. Sci. U.S.A.* **2003**, *100*, 5413.

(52) Cha, C.; Kohman, R. E.; Kong, H. *Adv. Funct. Mater.* **2009**, *19*, 3056.

(53) Cha, C.; Kim, S. Y.; Cao, L.; Kong, H. *Biomaterials* **2010**, *31*, 4864.

(54) Soumpasis, D. M. *Biophys. J.* **1983**, *41*, 95.

(55) Brandl, F.; Kastner, F.; Gschwind, R. M.; Blunk, T.; Teßar, J.; Göferich, A. *J. Controlled Release* **2010**, *142*, 221.

(56) Vermonden, T.; Jena, S. S.; Barriet, D.; Censi, R.; van der Gucht, J.; Hennink, W. E.; Siegel, R. A. *Macromolecules* **2009**, *43*, 782.

(57) Ratner, B. D.; Hoffman, A. S. *In hydrogels for medical and related applications*; American Chemical Society: Washington, D. C., 1976.

(58) Nielsen, L. E.; Landel, R. F. *Mechanical properties of polymer and composites*; Marcel Dekker: New York, 1994.

(59) Bajpai, S. K. *J. Appl. Polym. Sci.* **2001**, *80*, 2782.

(60) De, S. K.; Aluru, N. R.; Johnson, B.; Crone, W. C.; Beebe, D. J.; Moore, J. *J. Microelectromech. Syst.* **2002**, *11*, 544.

(61) Yanagishita, M. *Acta Pathol. Jpn.* **1993**, *43*, 283.

(62) Scott, J. E. *Pathol. Biol.* **2001**, *49*, 284.

(63) Jeon, O.; Bouhadir, K. H.; Mansour, J. M.; Alsberg, E. *Biomaterials* **2009**, *30*, 2724.

(64) George, K. A.; Wentrup-Byrne, E.; Hill, D. J. T.; Whittaker, A. K. *Biomacromolecules* **2004**, *5*, 1194.

(65) Quijada-Garrido, I.; Prior-Cabanillas, A.; Garrido, L.; Barrales-Rienda, J. M. *Macromolecules* **2005**, *38*, 7434.

(66) Ostroha, J.; Pong, M.; Lowman, A.; Dan, N. *Biomaterials* **2004**, *25*, 4345.

(67) Bouhadir, K. H.; Hausman, D. S.; Mooney, D. J. *Polymer* **1999**, *40*, 3575.

(68) Bruneel, D.; Schacht, E. *Polymer* **1993**, *34*, 2628.

(69) Poe, G. D.; McCormick, C. L. *J. Polym. Sci. Pol. Chem.* **2004**, *42*, 2520.

(70) Poe, G. D.; Jarrett, W. L.; Scales, C. W.; McCormick, C. L. *Macromolecules* **2004**, *37*, 2603.

(71) Riess, G. *Prog. Polym. Sci.* **2003**, *28*, 1107.

(72) Tanford, C. *The hydrophobic effect - Formation of micelles and biological membranes*; Wiley Interscience: New York, 1973.

(73) Yiu, C. K. Y.; King, N. M.; Carrilho, M. R. O.; Sauro, S.; Rueggeberg, F. A.; Prati, C.; Carvalho, R. M.; Pashley, D. H.; Tay, F. R. *Biomaterials* **2006**, *27*, 1695.

(74) Canal, T.; Peppas, N. A. *J. Biomed. Mater. Res.* **1989**, *23*, 1183.

(75) Flessner, M. F. *Perit. Dial. Int.* **2001**, *21*, S24.

(76) Kong, H. J.; Smith, M. K.; Mooney, D. J. *Biomaterials* **2003**, *24*, 4023.

(77) Lee, K. Y.; Kong, H. J.; Larson, R. G.; Mooney, D. J. *Adv. Mater.* **2003**, *15*, 1828.

(78) Bulpitt, P.; Aeschlimann, D. *J. Biomed. Mater. Res.* **1999**, *47*, 152.

(79) Zimm, B. H. *J. Chem. Phys.* **1948**, *16*, 1093.

(80) Ramakrishnan, S.; Fuchs, M.; Schweizer, K. S.; Zukoski, C. F. *Langmuir* **2002**, *18*, 1082.

(81) Lambeth, R. H.; Ramakrishnan, S.; Mueller, R.; Poziemski, J. P.; Miguel, G. S.; Markoski, L. J.; Zukoski, C. F.; Moore, J. S. *Langmuir* **2006**, *22*, 6352.

(82) Beaucage, G.; Rane, S.; Sukumaran, S.; Satkowski, M. M.; Schechtman, L. A.; Doi, Y. *Macromolecules* **1997**, *30*, 4158.

(83) Kong, H. J.; Alsberg, E.; Kaigler, D.; Lee, K. Y.; Mooney, D. J. *Adv. Mater.* **2004**, *16*, 1917.

(84) Kong, H. J.; Kaigler, D.; Kim, K.; Mooney, D. J. *Biomacromolecules* **2004**, *5*, 1720.

(85) Skoog, D. A.; West, D. M.; Holler, F. J.; Crouch, S. R. *Fundamentals of Analytical Chemistry. 8th ed.*; Brooks/Cole: Belmont, CA, 2004.

(86) Dario, P.; Carrozza, M. C.; Benvenuto, A.; A., M. *J. Micromech. Microeng.* **2000**, *10*, 235.

(87) Grayson, A. C. R.; Shawgo, R. S.; Johnson, A. M.; Flynn, N. T.; Yawen, L. I.; Cima, M. J.; Langer, R. *Proc. IEEE* **2004**, *92*, 6.

(88) Shin, H.; Jo, S.; Mikos, A. G. *Biomaterials* **2003**, *24*, 4353.

(89) Dario, P.; Carrozza, M. C.; Benvenuto, A.; A., M. *J. Micromech. Microeng.* **2000**, *10*, 235.

(90) Hubbell, J. A. *Curr. Opin. Biotechnol.* **1999**, *10*, 123.

(91) Sakiyama-Elbert, S.; Hubbell, J. *Ann. Rev. Mater. Res.* **2001**, *31*, 183.

(92) Pelham, R. J.; Wang, Y.-l. *Proc. Natl. Acad. Sci. U.S.A.* **1997**, *94*, 13661.

(93) Lee, H. J.; Lee, J.-S.; Chansakul, T.; Yu, C.; Elisseeff, J. H.; Yu, S. M. *Biomaterials* **2006**, *27*, 5268.

(94) Madison, L. D.; Rosenzweig, S. A.; Jamieson, J. D. *J. Biol. Chem.* **1984**, *259*, 14818.

(95) Jin, L.; Horgan, A.; Levicky, R. *Langmuir* **2003**, *19*, 6968.

(96) Kang, H. S.; Yang, S. R.; Kim, J.-D.; Han, S.-H.; Chang, I.-S. *Langmuir* **2001**, *17*, 7501.

(97) Craparo, E. F.; Cavallaro, G.; Bondi, M. L.; Mandracchia, D.; Giammona, G. *Biomacromolecules* **2006**, *7*, 3083.

(98) Tomida, M.; Nakato, T.; Matsunami, S.; Kakuchi, T. *Polymer* **1997**, *38*, 4733.

(99) Habeeb, A. F. S. A. *Anal. Biochem.* **1966**, *14*, 328.

(100) Inerowicz, H. D.; Howell, S.; Regnier, F. E.; Reifenberger, R. *Langmuir* **2002**, *18*, 5263.

(101) Gooding, J. J.; Mearns, F.; Yang, W.; Liu, J. *Electroanalysis* **2003**, *15*, 81.

(102) Green, R. J.; Frazier, R. A.; Shakesheff, K. M.; Davies, M. C.; Roberts, C. J.; Tendler, S. J. B. *Biomaterials* **2000**, *21*, 1823.

(103) Ellman, G. L. *Arch. Biochem. Biophys.* **1959**, *82*, 70.

(104) Yang, S.; Saif, T. *Rev. Sci. Instrum.* **2005**, *76*, 044301.

(105) Yang, S.; Saif, T. *Exp. Cell Res.* **2005**, *305*, 42.

(106) Yershov, G.; Barsky, V.; Belgovskiy, A.; Kirillov, E.; Kreindlin, E.; Ivanov, I.; Parinov, S.; Guschin, D.; Drobishev, A.; Dubiley, S.; Mirzabekov, A. *Proc. Natl. Acad. Sci. U.S.A.* **1996**, *93*, 4913.

(107) Palmer, T. D.; Takahashi, J.; Gage, F. H. *Mol. Cell. Neurosci.* **1997**, *8*, 389.

(108) Sathish, V.; Thompson, M. A.; Bailey, J. P.; Pabelick, C. M.; Prakash, Y. S.; Sieck, G. C. *Am. J. Physiol. - Lung Cell. Mol. Physiol.* **2009**, *297*, L26.

(109) Cha, C.; Jeong, J. H.; Shim, J.; Kong, H. *Acta Biomater.* **2011**, *7*, 3719.

(110) Vuori, K.; Ruoslahti, E. *J. Biol. Chem.* **1993**, *268*, 21459.

(111) Niemeyer, P.; Krause, U.; Fellenberg, J.; Kasten, P.; Seckinger, A.; Ho, A. D.; Simank, H. G. *Cells Tissues Organs* **2004**, *177*, 68.

(112) Kim, H. J.; Kim, U.-J.; Kim, H. S.; Li, C.; Wada, M.; Leisk, G. G.; Kaplan, D. L. *Bone* **2008**, *42*, 1226.

(113) Kretlow, J. D.; Mikos, A. G. *Tissue Eng.* **2007**, *13*, 927.

(114) Gao, Y. F.; Koumoto, K. *Cryst. Growth Des.* **2005**, *5*, 1983.

(115) Weiner, S.; Addadi, L. *J. Mater. Chem.* **1997**, *7*, 689.

(116) Sarikaya, M. *Proc. Natl. Acad. Sci. U. S. A.* **1999**, *96*, 14183.

(117) Addadi, L.; Weiner, S. *Proc. Natl. Acad. Sci. U. S. A.* **1985**, *82*, 4110.

(118) Falini, G.; Fermani, S. *Tissue Eng.* **2004**, *10*, 1.

(119) Song, J.; Malathong, V.; Bertozzi, C. R. *J. Am. Chem. Soc.* **2005**, *127*, 3366.

(120) Huo, Q. S.; Margolese, D. I.; Ciesla, U.; Feng, P. Y.; Gier, T. E.; Sieger, P.; Leon, R.; Petroff, P. M.; Schuth, F.; Stucky, G. D. *Nature* **1994**, *368*, 317.

(121) Hartgerink, J. D.; Beniash, E.; Stupp, S. I. *Science* **2001**, *294*, 1684.

(122) Kirkham, J.; Brookes, S. J.; Shore, R. C.; Wood, S. R.; Smith, D. A.; Zhang, J.; Chen, H. F.; Robinson, C. *Curr. Opin. Colloid Interface Sci.* **2002**, *7*, 124.

(123) Tanck, E.; van Driel, W. D.; Hagen, J. W.; Burger, E. H.; Blankevoort, L.; Huiskes, R. *J. Biomech.* **1999**, *32*, 153.

(124) Calvert, P.; Rieke, P. *Chem. Mater.* **1996**, *8*, 1715.

(125) Meinel, L.; Karageorgiou, V.; Fajardo, R.; Snyder, B.; Shinde-Patil, V.; Zichner, L.; Kaplan, D.; Langer, R.; Vunjak-Novakovic, G. *Ann. Biomed. Eng.* **2004**, *32*, 112.

(126) Phadke, A.; Zhang, C.; Hwang, Y.; Vecchio, K.; Varghese, S. *Biomacromolecules* **2010**, *11*, 2060.

(127) Kim, C. W.; Kim, S. E.; Kim, Y. W.; Lee, H. J.; Choi, H. W.; Chang, J. H.; Choi, J.; Kim, K. J.; Shim, K. B.; Jeong, Y.; Lee, S. C. *J. Mater. Res.* **2009**, *24*, 50.

(128) Shapiro, L.; Cohen, S. *Biomaterials* **1997**, *18*, 583.

(129) Perez, P.; Plieva, F.; Gallardo, A.; San Roman, J.; Aguilar, M. R.; Morfin, I.; Ehrburger-Dolle, F.; Bley, F.; Mikhalovsky, S.; Galaev, I. Y.; Mattiasson, B. *Biomacromolecules* **2008**, *9*, 66.

(130) Zhao, Q.; Sun, J.; Ling, Q.; Zhou, Q. *Langmuir* **2009**, *25*, 3249.

(131) Astilleros, J. M.; Pina, C. M.; Fernandez-Diaz, L.; Putnis, A. *Geochim. Cosmochim. Acta* **2003**, *67*, 1601.

(132) Nancollas, G. H.; Mohan, M. S. *Arch. Oral Biol.* **1970**, *15*, 731.

(133) Ishikawa, K.; Eanes, E. D.; Tung, M. S. *J. Dent. Res.* **1994**, *73*, 1462.

(134) Koutsoukos, P. G.; Nancollas, G. H. *J. Cryst. Growth* **1981**, *55*, 369.

(135) Wang, H. B.; Lee, J. K.; Moursi, A.; Lannutti, J. J. *J. Biomed. Mater. Res. Part A* **2003**, *67A*, 599.

(136) Ślósarczyk, A.; Paszkiewicz, Z.; Paluszkiewicz, C. *J. Mol. Struct.* **2005**, *744-747*, 657.

(137) Falini, G.; Albeck, S.; Weiner, S.; Addadi, L. *Science* **1996**, *271*, 67.

(138) Stepkowska, E. T.; Pérez-Rodríguez, J. L.; Sayagués, M. J.; Martínez-Blanes, J. M. *J. Therm. Anal. Calorim.* **2003**, *73*, 247.

(139) Nancollas, G. H.; Tomazic, B. *J. Phys. Chem.* **1974**, *78*, 2218.

(140) Li, H. Y.; Xin, H. L.; Muller, D. A.; Estroff, L. A. *Science* **2009**, *326*, 1244.

(141) Augst, A. D.; Kong, H. J.; Mooney, D. J. *Macromol. Biosci.* **2006**, *6*, 623.

(142) Song, J.; Saiz, E.; Bertozzi, C. R. *J. Am. Chem. Soc.* **2003**, *125*, 1236.

(143) Watanabe, J.; Akashi, M. *Cryst. Growth Des.* **2008**, *8*, 478.

(144) Liu, G.; Zhao, D.; Tomsia, A. P.; Minor, A. M.; Song, X.; Saiz, E. *J. Am. Chem. Soc.* **2009**, *131*, 9937.

(145) Lowenstam, H. A.; Weiner, S. *On Biomineralization*; Oxford University Press: New York, 1989.

(146) Kawaguchi, S.; Imai, G.; Suzuki, J.; Miyahara, A.; Kitano, T.; Ito, K. *Polymer* **1997**, *38*, 2885.

(147) Amsden, B.; Turner, N. *Biotechnol. Bioeng.* **1999**, *65*, 605.

(148) Gainaru, C.; Hiller, W.; Böhmer, R. *Macromolecules* **2010**, *43*, 1907.

(149) Strand, K. A.; Boee, A.; Dalberg, P. S.; Sikkeland, T.; Smidsroed, O. *Macromolecules* **1982**, *15*, 570.

(150) Franson, N. M.; Peppas, N. A. *J. Appl. Polym. Sci.* **1983**, *28*, 1299.

(151) Lee, W. F.; Yeh, Y. C. *Eur. Polym. J.* **2005**, *41*, 2488.

(152) Valverde, P.; Zhang, J.; Fix, A.; Zhu, J.; Ma, W. L.; Tu, Q. S.; Chen, J. *J. Bone Miner. Res.* **2008**, *23*, 1775.

(153) Williams, K. J.; Picou, A. A.; Kish, S. L.; Giraldo, A. M.; Godke, R. A.; Bondioli, K. R. *Cells Tissues Organs* **2008**, *188*, 251.